universität wien

# MASTERARBEIT | MASTER'S THESIS

Titel | Title

Novel derivatives of clofarabine-based organometallics

verfasst von | submitted by

Judith Wutschitz BSc

angestrebter akademischer Grad | in partial fulfilment of the requirements for the degree of

Master of Science (MSc)

Wien | Vienna, 2024

| | |
|---|---|
| Studienkennzahl lt. Studienblatt \| Degree programme code as it appears on the student record sheet: | UA 066 862 |
| Studienrichtung lt. Studienblatt \| Degree programme as it appears on the student record sheet: | Masterstudium Chemie |
| Betreut von \| Supervisor: | o. Univ.-Prof. i.R. Dr. Dr. Bernhard Keppler |
| Mitbetreut von \| Co-Supervisor: | Dipl.-Ing. Dr. Wolfgang Kandioller |

# Acknowledgements

I would like to extend my sincere gratitude to o. Univ.-Prof. Dr. Dr. Bernhard Keppler for granting me the opportunity to be part of his research group in the field of bioinorganic chemistry within the Institute of Inorganic Chemistry.

A special thanks goes to Dipl.-Ing. Dr. Wolfgang Kandioller for his exceptional supervision, motivation, and guidance throughout my master's thesis.

I am also deeply appreciative of the NMR, MS, and microanalytical laboratory teams at the University of Vienna for their invaluable assistance in sample analysis.

A huge thank you to my Lab 6 colleagues – Alex and Paul – not only for helping me find solutions to the challenges I faced but also for creating a wonderful atmosphere filled with laughter and great music.

I also wish to thank all the other members of the Faculty of Inorganic Chemistry for their continuous support.

I want to give a special thanks to my parents, whose unwavering emotional and financial support made this journey possible. Their guidance has been a cornerstone in my life and I am deeply grateful for everything they've done.

A heartfelt thanks also goes to my sister, Anna, who has always been there for me. Her constant presence, whether through her advice or simply lending an ear, has been invaluable. I couldn't have asked for a better sister to accompany me through this experience.

Finally, to my friends, both within and beyond the faculty, your friendship and support over the years have meant the world to me. I truly could not have done this without you.

# Abstract

Cancer remains a leading cause of death worldwide, driving the need for novel therapeutic strategies. This thesis explores the development of new cancer treatments, focusing on clofarabine-bearing organometallic compounds. Clofarabine, a bioactive ligand, was incorporated into ruthenium complexes, with the goal of evaluating their potential as anticancer agents. Precursor ruthenium complexes were synthesized and subjected to ligand exchange reactions, first with an adenine derivative as a model ligand and later with clofarabine itself.

This work shows that two of the eight tested ligands, oxalate and maltolate, formed stable ruthenium complexes with the adenine model. However, due to purification challenges, only the corresponding oxalate complex was synthesized with clofarabine. The syntheses were conducted through a series of reactions, including microwave-assisted methods. Characterization via NMR spectroscopy and mass spectrometry confirmed the formation of these complexes. Stability tests using UV/vis spectroscopy showed that the two oxalate complexes remained stable in aqueous solution for at least 24 hours, a crucial factor for potential biological applications.

These results expand the understanding of organometallic ruthenium complexes and at the same time emphasizing the need for optimized purification methods. In the future, achieving higher purity of the compounds would be essential for conducting biological tests, such as evaluating their effectiveness against cancer cell lines.

# Zusammenfassung

Krebs ist nach wie vor eine der häufigsten Todesursachen weltweit, was den Bedarf an neuen therapeutischen Strategien erhöht. Diese Arbeit untersucht die Entwicklung neuer Krebstherapien, wobei der Schwerpunkt auf Clofarabin-haltigen metallorganischen Verbindungen liegt. Clofarabin, ein bioaktiver Ligand, der in die Rutheniumkomplexe eingebaut wurde, um deren Potenzial als Krebsmittel zu untersuchen. Dabei wurden Vorläufer-Rutheniumkomplexe synthetisiert und Ligandenaustauschreaktionen durchgeführt, zunächst mit einem Adeninderivat als Modellliganden und später mit Clofarabin selbst.

Es wird gezeigt, dass zwei der acht getesteten Liganden, Oxalat und Maltolat, stabile Rutheniumkomplexe mit dem Adeninmodell bilden. Da es jedoch Herausforderungen bei der Aufreinigung gab, konnte nur der entsprechende Oxalatkomplex mit Clofarabin synthetisiert werden. Die Synthesen wurden durch eine Reihe von Reaktionen, unter anderem mithilfe von Mikrowellenmethoden, durchgeführt. Die Charakterisierung der Verbindungen mittels NMR-Spektroskopie und Massenspektrometrie bestätigte die Bildung dieser Komplexe. In Stabilitätstests, die mithilfe von UV/vis-Spektroskopie durchgeführt wurden, zeigte sich, dass die zwei Oxalatkomplexe in wässriger Lösung über mindestens 24 Stunden stabil blieben, was für biologische Anwendungen von großer Bedeutung ist.

Diese Ergebnisse erweitern das Verständnis von metallorganischen Rutheniumkomplexen und heben gleichzeitig die Notwendigkeit verbesserter Aufreinigungsverfahren hervor. In Zukunft wäre eine höhere Reinheit der Verbindungen unerlässlich, um biologische Tests, wie die Untersuchung ihrer Wirksamkeit gegen Krebszelllinien, durchführen zu können.

# Abbreviations

| | |
|---|---|
| **ACN** | acetonitrile |
| **calcd.** | calculated |
| **cbdca** | 1,1-Cyclobutanedicarboxylic acid |
| **CML** | chronic myeloid leukemia |
| **COSY** | correlated spectroscopy |
| **CPT** | camptothecin |
| **CVD** | cardiovascular disease |
| **d** | doublet |
| **DACH** | (1R,2R)-Cyclohexane-1,2-diamine, (trans-1,2-diaminocyclohexane) |
| **DCM** | dichloromethane |
| **dd** | doublet of doublets of doublets |
| **ddd** | doublet of doublets |
| **DMSO** | dimethylsulfoxide |
| **DMSO-d6** | deuterated dimethyl sulfoxide |
| **DNA** | deoxyribonucleic acid |
| **dt** | doublet of triplets |
| **EA** | elemental analysis |
| **eq.** | equivalents |
| **ESI** | electrospray ionization |
| ***Et al.*** | et alii – and others |
| **FDA** | Food and Drug Administration |
| **GRP78** | 78 kDa glucose-regulated protein |
| **hept** | heptet |
| **HMBC** | heteronuclear hultiple bonds coherence |
| **HR-MS** | high resolution mass spectrometry |
| **HSQC** | heteronuclear single quantum coherence |
| ***J*** | coupling constant |
| **m** | multiplet |
| **MPLC** | medium-pressure liquid chromatography |
| **NCD** | non-communicable diseases |
| **NMR** | nuclear magnetic resonance |
| **PBS** | phosphate-buffered saline |
| **pH** | potential of hydrogen |
| **PTA** | 1,3,5-Triaza-7-phosphaadamantane |
| **q** | quartet |
| **RAED** | ruthenium arene ethylendiamine |
| **RAPTA** | ruthenium arene PTA |
| **RNA** | ribonucleic acid |
| **ROS** | reactive oxygen species |
| **RR** | ribonucleotide reductase |
| **s** | singulet |
| **SCLC** | small cell lung cancer |
| **t** | triplet |
| **TOP1** | topoisomerase 1 |
| **UV/vis** | ultraviolet/visible |
| **VA** | vinca alkaloid |

# Contents

# 1 Introduction

Cancer is a general term used to refer to a large group of diseases that can affect all areas of the body. Malignant tumors and neoplasms are other terms used. One hallmark of cancer is the fast development of abnormal cells that grow beyond their normal proportions, allowing them to invade nearby areas of the body and spread to other organs.[1]

## 1.1 Incidences and Mortality

Based on mortality data, four out of every ten deaths from non-communicable diseases (NCDs), are caused by cardiovascular diseases (CVDs) while three are due to cancer.[2] This makes cancer one of the leading causes of death worldwide alongside CVDs.[3] In 70 out of 127 countries, the leading cause of death are CVDs, while in the other 57 countries cancer holds that position. Based on estimations it is expected that cancer will overtake CVDs as the leading cause of death in the future.[4]

In 2022 alone, approximately 20 million new cancer cases were reported worldwide, leading to 9.7 million deaths. The most common type of cancer among males is trachea, bronchus and lung cancer, followed by prostate and colorectal cancer. Most females are diagnosed with breast, trachea, bronchus and lung or colorectal cancer (Figure 1).[5,6]

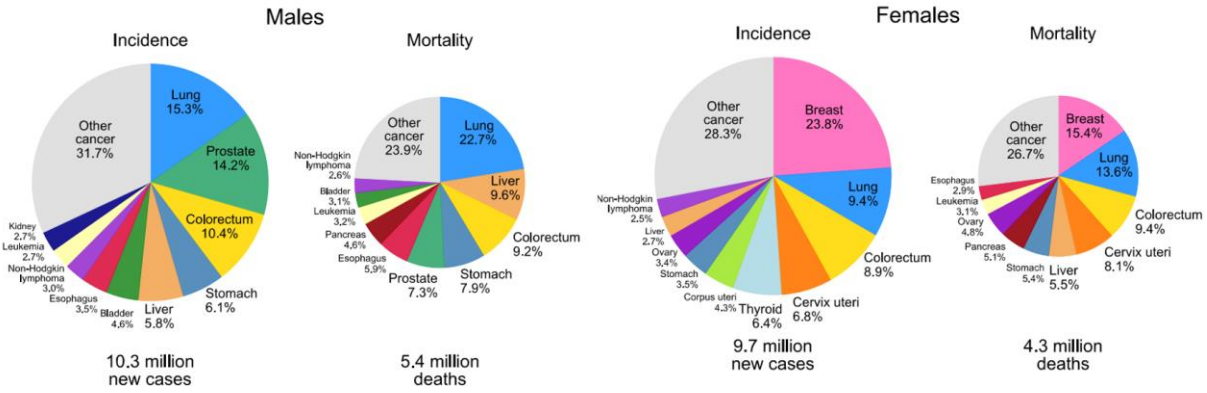


*Figure 1: Distribution of cases and deaths for ten most common cancers (2022) for males and females.[6]*

## 1.2 Hallmarks of Cancer

In spite of the diversity of cancer types, research has discovered a set of underlying principles that determine how cancer develops and progresses. These features, known as the “hallmarks of cancer”, were first described by Hanahan and Weinberg and provide a framework for understanding how cancer cells gain the ability to grow uncontrollably and escape normal cellular control.[7,8] The original hallmarks of cancer (2000) include evading apoptosis, self-sufficiency in growth signals, insensitivity to anti-growth signals, tissue invasion & metastasis, limitless replicative potential and sustained angiogenesis. These properties indicate the ability of cancer cells to overcome the body's natural defense mechanisms against uncontrolled cell growth.[7] Over time, new factors have been continuously added, since 2022 there are eight core traits and two enabling characteristics. In order to better capture the complexity of the disease, another four hallmarks may be added to this framework (Figure 2).[8] Understanding these common traits could enable a more logical and systematic approach to cancer research and treatment.[7] With the increasing knowledge of the characteristics of cancer, numerous treatment approaches have been developed to fight the disease more effectively.

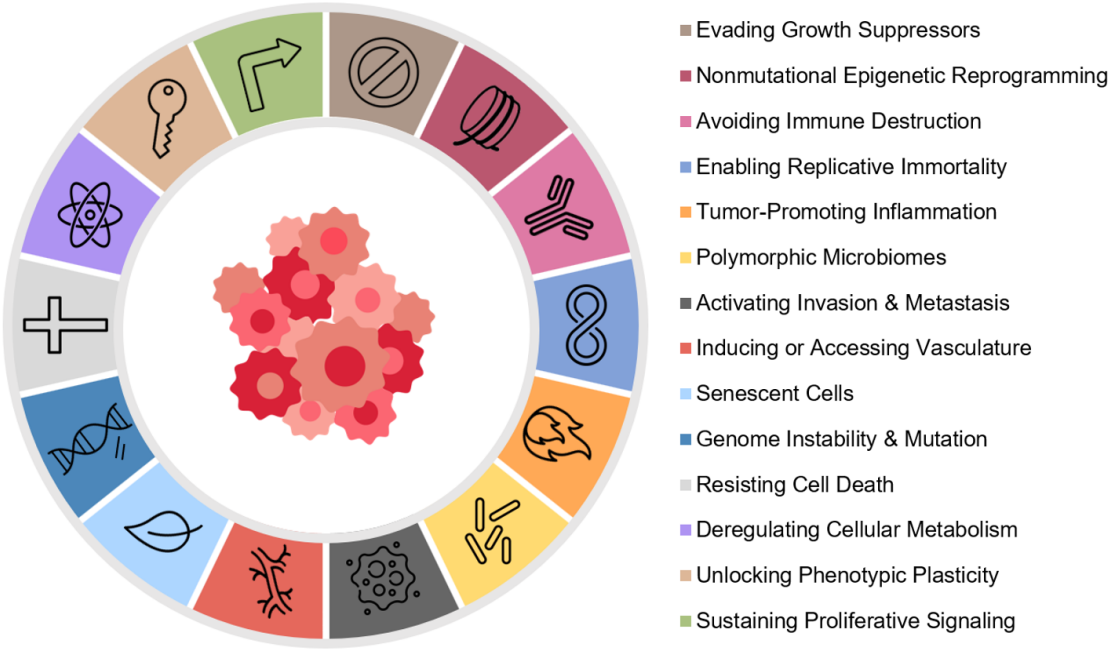


*Figure 2: Hallmarks of cancer – new additions.*
*Adapted from Hanahan, D. Hallmarks of Cancer: New Dimensions.* Cancer Discov. ***2022***, 12 *(1), 31–46 and Hallmarks of Cancer. Rockland Immunochemicals.*[8,9].

## 1.3 Cancer Treatment

Different types of cancer treatments include surgery, radiation therapy, chemotherapy, targeted therapy, immunotherapy and others.[10] The different types of treatments can be used both individually and in combination with each other.

**Radiation therapy** uses high doses of radiation to destroy cancer cells and reduce the size of tumors. At high doses, radiotherapy either destroys the cancer cells or slows their growth by damaging their DNA. Cancer cells with irreparable DNA damage either stop reproducing or undergo cell death (apoptosis). During this cell death, these damaged cells are broken down and cleared from the body.[11]

**Immunotherapy** is a form of cancer treatment in which the body's own immune system is used to prevent, control and eliminate cancer. There are different types of cancer immunotherapies, including targeted antibodies, cancer vaccines, adoptive cell transfer, tumor-infecting viruses, checkpoint inhibitors, cytokines and adjuvants. An immunotherapy is a type of biotherapy as it uses materials from living organisms to fight disease.[12]

**Targeted therapy** uses drugs that specifically target cancer cells while leaving normal cells unaffected. Cancer cells often have mutations that distinguish them from normal cells and allow them to grow and divide rapidly. The environment in which cancer develops can vary, with certain proteins or enzymes promoting the growth of cancer cells. Targeted drugs block these proteins or enzymes, interrupting the signals that promote cancer cell growth or cause the cells to self-destruct.[13]

**Chemotherapy** is one of the most important types of cancer treatment alongside surgery and radiotherapy. It involves the treatment of malignant tumors with chemotherapeutic agents or cytostatics, which intervene in the cancer cells' reproduction cycle. The chemotherapeutic agents are administered in the form of infusions, injections or tablets.[14] Not only are they used to treat malignant diseases, cytostatics are also used for the long-term treatment of transplant recipients and patients with rheumatological and autoimmune diseases.[15] There are different types of cytostatic drugs, which are briefly described in the following paragraphs.

Alkylating agents are substances that react with electron-rich donor atoms in biological molecules by forming covalent bonds. These agents are typically divided into two types: ones that react with biological molecules directly and ones that form reactive intermediates, which then react with the biological molecules.[16] They primarily work by inhibiting the transcription of DNA into RNA, thereby stopping protein synthesis. Alkylating agents replace

hydrogen atoms in the DNA with alkyl groups. As a result, cross-links are formed within the DNA chain, leading to cytotoxic, mutagenic and carcinogenic effects. This effect occurs in all cells, but alkylating agents mainly affect fast-dividing cells lacking time for DNA repair. These are not only cancer cells but also reproductive and endothelial cells, resulting in the common side effects (bone marrow depression, nausea, vomiting).[17,18] The final result of the alkylating process is the misreading of the DNA code and the inhibition of DNA, RNA and protein synthesis as well as the induction of programmed cell death in fast proliferating tumor cells.[17] Different types of alkylating agents include nitrogen mustards, aziridines and epoxides, alkyl sulfonates or nitrosoureas (Figure 3).[18,19]

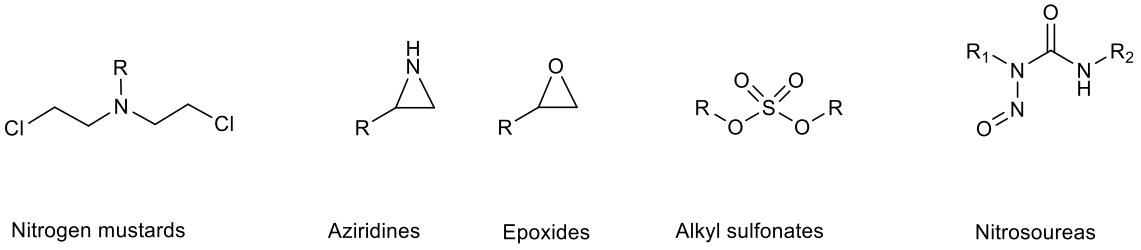


*Figure 3: Structures of different types of alkylating agents.[20,21]*

Anticancer antibiotics are chemicals with anticancer effects produced by microorganisms. These are mainly peptides and anthraquinones that have an inhibitory effect on the uncontrolled proliferation, aggressive growth and metastasis of malignant cancers. The classification of anticancer antibiotics mainly includes anthracyclines, mitomycin, bleomycin, actinomycin, guanorycin and enediyne.[22] Among them, some have an anthracyclic plane, which can be inserted between DNA base pairs and tightly bound to DNA, becoming an obstacle to the spatial structure of DNA, thus inhibiting DNA and RNA synthesis.[23] Along with the cytotoxic effects, they can also inhibit the activity of nuclear topoisomerase and interfere with the DNA breakage reaction caused by topoisomerase, leading to DNA double- and single-strand breakage.[24]

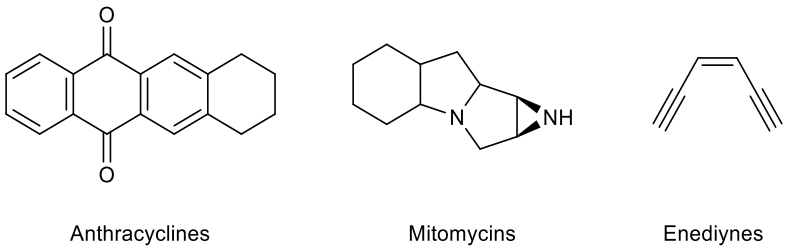


*Figure 4: Base structures of different types of anticancer antibiotics.*

Antimetabolites usually function as structural analogs of DNA or RNA components. Such molecules are inserted instead of nucleotides during replication, inhibiting the process and ultimately leading to cell death.[25] Most of the antimetabolites currently in use are purine and pyrimidine analogs, fourteen of which are FDA-approved for cancer treatment. Among the clinically important antimetabolites are decitabine, nelarabine, clofarabine and capecitabine (Figure 5).[25,26]

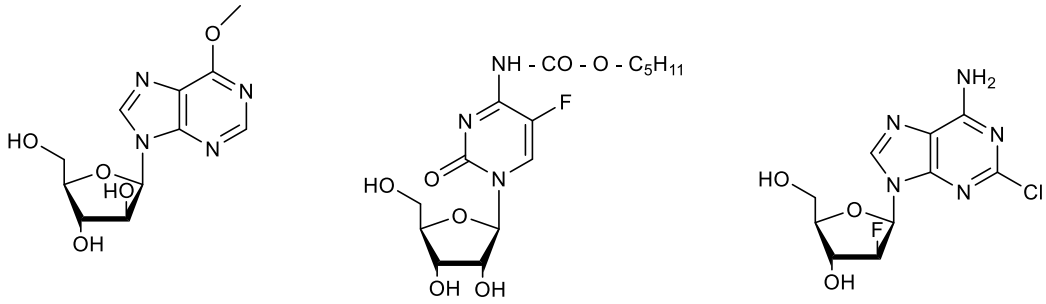


*Figure 5: Structures of antimetabolites nelarabine, capecitabine and clofarabine.*

Plant-derived anticancer agents

- Vinca alkaloids (VAs) are phytochemicals that occur naturally in the Cape periwinkle (*Catharanthus roseus*). Known anti-cancer compounds include vinorelbine, vindesine, vincristine and vinblastine (Figure 6). The mode of action of VAs is to bind to specific sites on microtubulin heterodimers, thereby stopping the actively dividing cell in metaphase. Currently, VAs are used in the treatment of blood, breast, liver and lung cancer.[27–29]

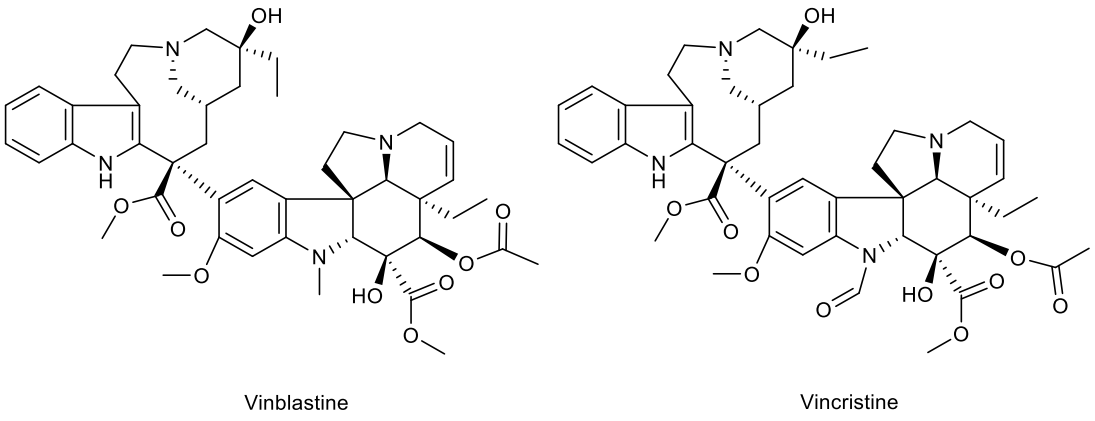


*Figure 6: Structures of the vinca alkaloids vinblastine and vincristine.*

- Taxanes are extracted from the inner bark of the Pacific yew (*Taxus brevifolia*) and are classified as polycyclic diterpenoids. They mainly act by disrupting the formation of microtubules, an essential component of both mitotic spindles and axonal structures of nerves, and stopping cell division. Taxanes include paclitaxel and docetaxel (Figure 7) and are used for treatment of early and metastatic breast cancer.[25,30]

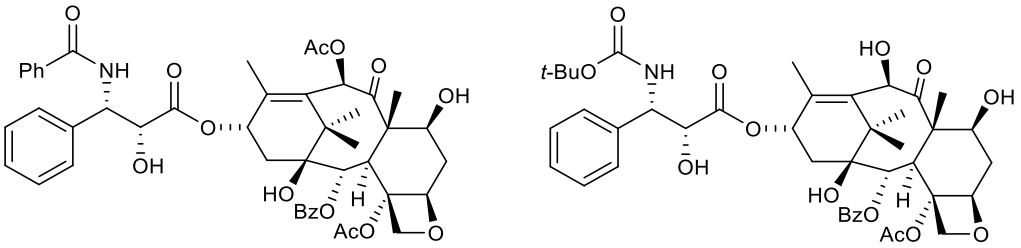


*Figure 7: Structures of Paclitaxel and Docetaxel.[31]*

- Camptothecin (CPT) and its derivatives (Figure 8) form an alkaloid class of chemical compounds. These compounds have shown antitumor activity in both *in vitro* systems and mouse leukemia models. The mode of action of CPT is based on the inhibition of topoisomerase 1 (TOP 1), which is known to be expressed in higher amounts in cancer cells compared to normal tissue. The formation of the TOP 1-CPT complex leads to irreversible strand breaks in the DNA and ultimately leads to cell death.[32]

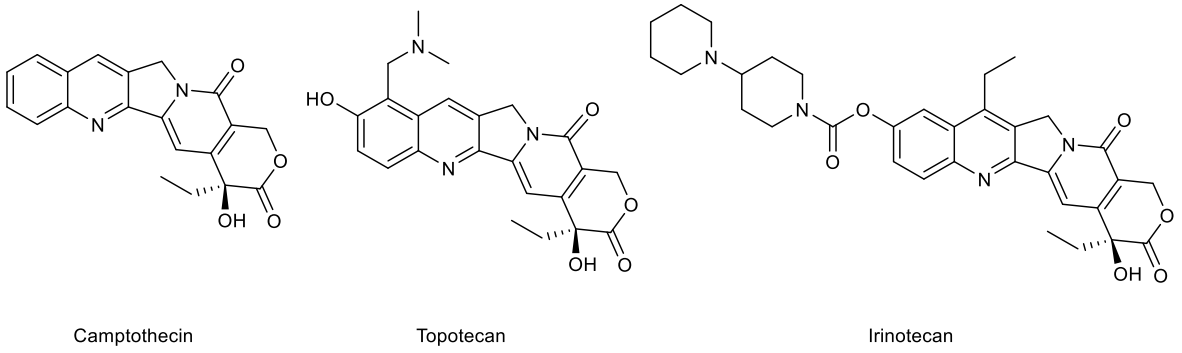


*Figure 8: Structures of camptothecin, topotecan and irinotecan.*

In addition to the cytostatic agents described above, there are others such as mitosis or topoisomerase inhibitors, as well as platinum and other metal complexes.[33] The latter are described in greater detail in the following chapters.

## 1.4 Platinum Anticancer Agents

Over the past 30 years, platinum-based drugs, particularly cisplatin and carboplatin, have been the cornerstone of treatment for various types of cancer.[34] The following sections describe the approved platinum complexes (Figure 10) in cancer therapy in more detail.

**Cisplatin** is the first metal-based cytostatic drug to be used successfully in chemotherapy worldwide since its approval by the FDA in 1978.[35] The mode of action of cisplatin (Figure 9) can be described as follows: Once a cisplatin molecule reaches a cell, preferably a tumor cell, it enters the cytoplasm by either passive diffusion through the cell membrane or active transport. As a result of the lower chloride ion concentration in the cytoplasm, reactive aquaplatin(II) complexes can form. These complexes can subsequently react with DNA bases, primarily with the N-7 of guanine. After an initial monofunctional binding, most cisplatin-DNA adducts form cross-links within the same DNA strand ("intrastrand crosslink").[36]

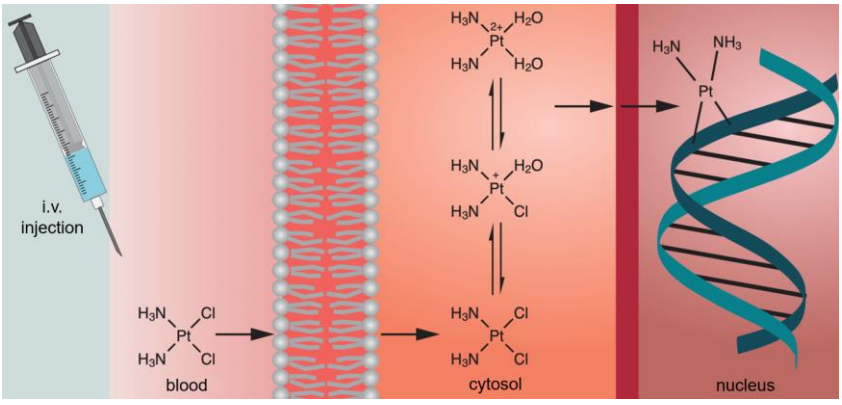


*Figure 9: Cisplatin mode of action.[36]*

Since cisplatin treatment can target both tumor and healthy cells, the therapy can cause serious side effects including nephrotoxicity (which is responsible for dose limitation), neurotoxicity or ototoxicity. In response, research was carried out into alternative, novel platinum complexes which led to the development of such complexes as therapeutic agents.[35,37]

**Carboplatin** was one of the first cisplatin analogs. In contrast to cisplatin, which has two chlorides as leaving moieties, carboplatin has a 1,1-cyclobutanedicarboxylate ligand. Cisplatin achieved better therapeutic results in general, but also showed higher toxicity. Carboplatin, on the other hand, had a more favorable toxicity profile because of its chelating ligand. Patients tolerate carboplatin better and it can be used in significantly higher doses than cisplatin. Since its approval in 1986, the drug has been used to treat ovarian carcinoma, lung, head and neck cancers.[38–40]

**Oxaliplatin** was the first drug approved to overcome cisplatin resistance. Oxaliplatin was first synthesized by Kidani et al. and shows stronger antitumor activity against various colorectal cancer cell lines compared to cisplatin and carboplatin. In oxaliplatin, a bidentate ligand, (1R,2R)-cyclohexane-1,2-diamine (R,R-DACH), replaces the two ammine ligands of cisplatin, which probably contributes to its efficacy in overcoming cisplatin resistance due to different DNA adduct formation. Oxaliplatin, which was approved in France in 1996 and subsequently in all of Europe in 1999 and the USA in 2002, is used in combination with other chemotherapeutic agents for the treatment of colorectal cancer and non-small cell lung cancer. The oxalate scaffold of oxaliplatin reduces its reactivity, limiting toxic side effects to peripheral sensory neuropathy. Its DACH ligand, which is more lipophilic, improves passive uptake and may allow different cellular entry routes compared to cisplatin and carboplatin.[38,40,41]

**Nedaplatin** is a platinum derivative with significant antineoplastic activity, meaning it inhibits the growth and spread of cancerous cells.[42] Since 1995 it has been used in the treatment of head, neck, lung, testicular and gynecologic cancers in Japan. It has a ring structure in which glycolate is bound to platinum via a bidentate ligand and forms reactive complexes that induce DNA cross-linking and apoptosis. Compared to cisplatin, nedaplatin shows better antitumor activity and significantly lower nephrotoxicity, neurotoxicity and gastrointestinal toxicity while being ten times more soluble in water.[38,40,41,43]

**Lobaplatin** is a diastereomeric mixture of platinum(II) complexes with lactic acid as leaving group and 1,2-bis(aminomethyl)cyclobutane as stable ligand. Lobaplatin interacts with DNA and influences the expression of an oncogene in cells that is associated with oncogenesis, apoptosis and cell proliferation.[44] Lobaplatin is currently approved for the treatment of chronic myeloid leukemia (CML), unresectable metastatic breast cancer and small cell lung cancer (SCLC) in China. The nephrotoxicity, neurotoxicity and ototoxicity are lower, but the hematotoxic effects are severe. Its dose-limiting toxicity is thrombocytopenia.[45]

**Heptaplatin** consists of malonate as a chelating leaving group and of 2-(1-methylethyl)-1,3-dioxolane-4,5-dimethanamine as stable ligand. It is currently approved in the Republic of

Korea for the treatment of gastric cancer.[41] The advantages of this drug include high solution stability, no notable toxicity and potent anti-cancer effect against cis-platinum-resistant cells.[40,46]

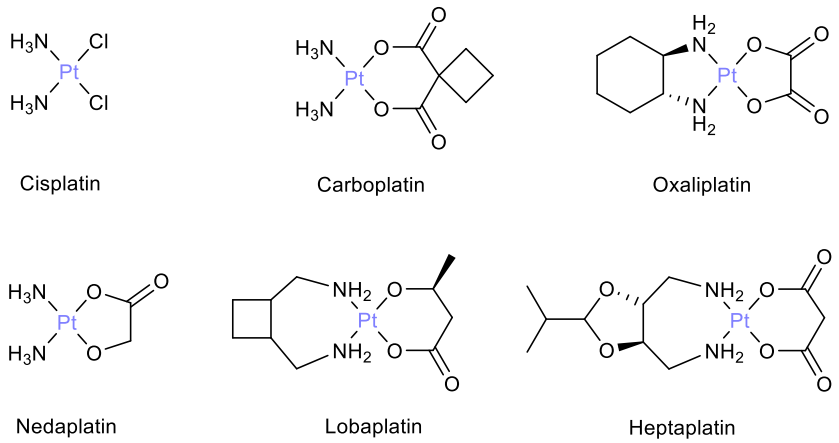


*Figure 10: Structures of worldwide approved (top) and regionally approved (bottom) platinum (II) complex for cancer treatment.*

## 1.5 Non-platinum Anticancer Agents

**Gallium**(III)'s chemical behavior is similar to that of Iron(III), but Ga(III) cannot be reduced under physiological conditions, while Fe(III) is easily reduced to Fe(II). This offers therapeutic potential for gallium(III). The compounds KP46 (tris-(8-quinolinolato)gallium(III), Figure 11a) and gallium tris-maltolate (Figure 11b) were investigated in clinical trials. Their mechanism of action is related to the inhibition of ribonucleotide reductase (RR).[47,48] Among the two, KP 46 is an orally administered anti-cancer and bone-protective drug being tested in patients with advanced solid tumors with bone involvement.[49]

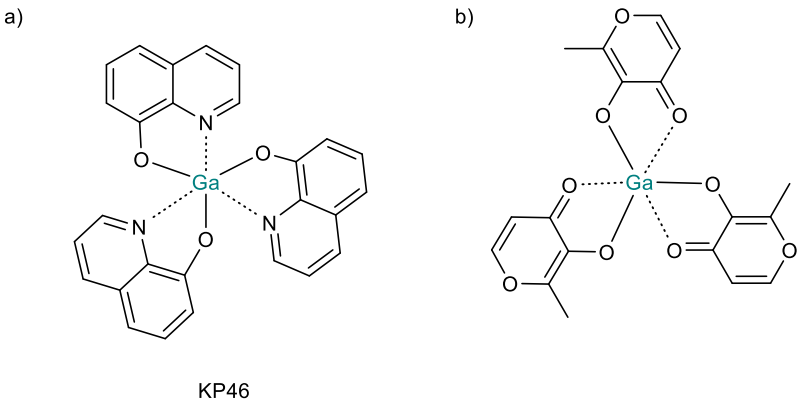


*Figure 11: Structure of gallium-based anticancer drugs in clinical trials.*

One **titanium** complex, known as budotitane, was the second transition metal complex to undergo clinical trials as an anticancer agent, following cisplatin (Figure 12)[50]. It belongs to the class of bis(β-diketonato) metal complexes, which has demonstrated antitumor activity since reports first emerged in 1982.[51,52]

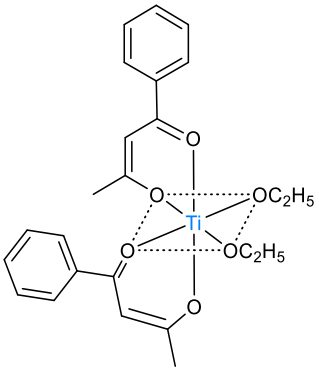


Budotitane

*Figure 12: Structure of budotitane.*

**Gold** compounds such as auranofin (Figure 13), which was used as an antirheumatic agent, and its analogs have been studied for their tumor inhibiting effects since 1986. It was discovered that many gold(I) thiolates can inhibit tumor growth and metastasis in various cancer models *in vitro* and demonstrated promising results *in vivo*, particularly against P388 leukemia in mice. Some compounds exhibited cytotoxicity comparable to or even greater than cisplatin, with lower toxicity.[53,54]

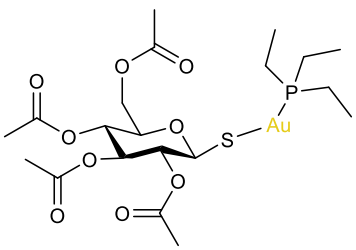


Auranofin

*Figure 13: Structure of gold(I) thiolate auranofin.*

**Ruthenium** based compounds (Figure 14) are being investigated as less toxic alternatives to platinum-based cancer treatments, with several ruthenium(II) and ruthenium(III) complexes showing promising results.[38] Particularly noteworthy are NAMI-A, KP1019 and KP1339, which have proven effective in preclinical studies and are already being tested in clinical trials.[55]

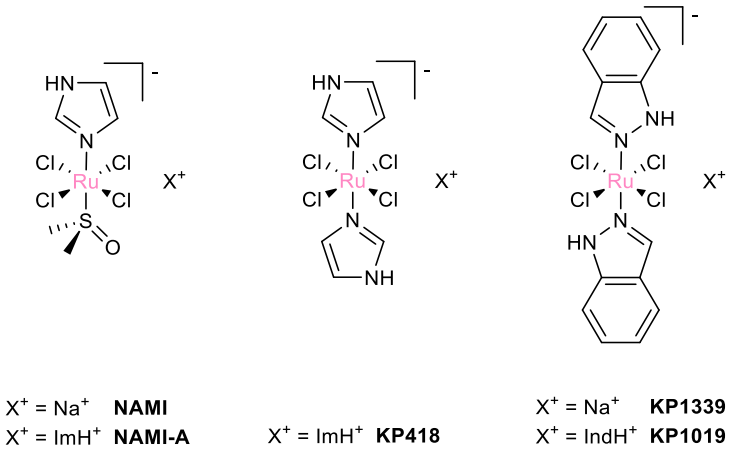


*Figure 14: Structure of ruthenium-based anticancer compounds.*

NAMI-A is a ruthenium(III) prodrug that selectively targets lung metastases without attacking the primary tumor cells like cisplatin. It inhibits the growth of cancer cells by shutting down the cell cycle, altering the morphology of the cell membrane and reducing invasion. NAMI-A also has strong anti-angiogenic properties by inhibiting the formation of blood vessels.[56] It is converted to an active form in the body, where it binds to serum proteins and can be reduced to a more reactive form, although it remains predominantly in its Ru(III) state. This conversion and the corresponding activity are influenced by the pH of the environment, with the drug behaving differently under physiological conditions than under acidic conditions.[57]

KP1019 was introduced as an improvement to its predecessor KP418 to improve its therapeutic profile. It showed promising anti-cancer activity with fewer side effects and demonstrated good efficacy in preclinical studies.[58,59] The mechanism of action is postulated to consist of KP1019 binding to serum proteins and possibly DNA, leading to cancer cell death.[60] A Phase I clinical trial of KP1019 showed disease stabilization in various cancer types with minimal toxicities, but the maximum tolerated dose could not be determined due to solubility issues.[59]

KP1339/BOLD-100 was developed as a more soluble version of KP1019 by replacing the indazolium cation with a sodium cation.[61] It exhibits stable oxidation states in tissues. In addition, it has a multimodal mechanism of action (Figure 15) by downregulating GRP78, a protein associated with cancer metastasis, and recovers chemosensitivity in cancer resistant cells.[62–65] The compound also induces reactive oxygen species (ROS), causing DNA damage and cell cycle arrest.[65] In clinical trials, KP1339 was well tolerated with modest side effects and showed promise for use in combination therapy. In colorectal cancer and neuroendocrine tumors, it proved effective as a single agent, with some patients achieving extended disease stability.[59] Additionally, BOLD-100 acts as an anti-Warburg drug, disrupting glycolysis by depleting lactate and pyruvate, which is associated with resistance to the ruthenium-based therapy. The metabolic changes, including acetyl-CoA production, were linked to both lipid metabolism and epigenetic regulation, which play a key role in resistance development.[66]

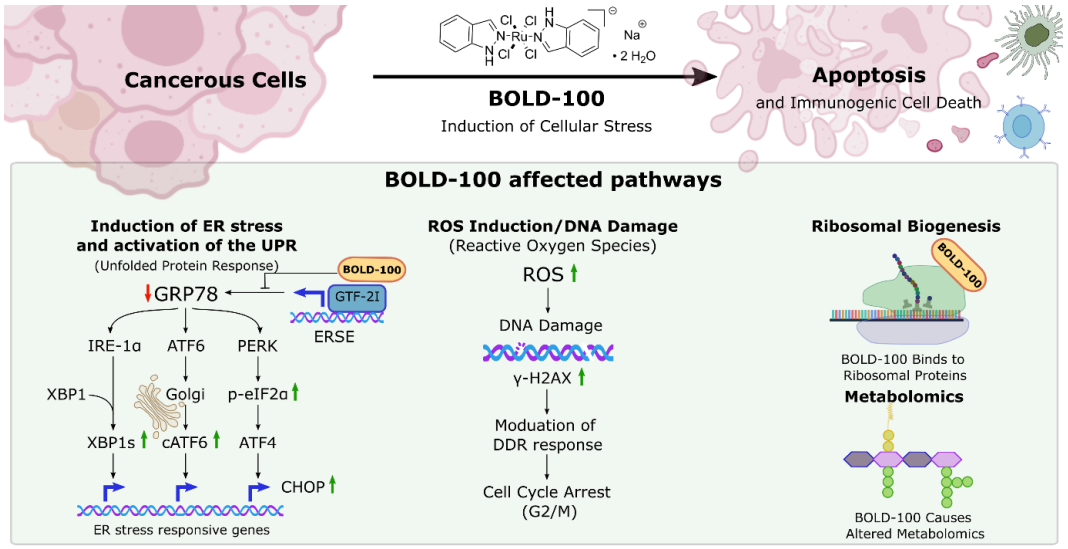


*Figure 15: KP1339/BOLD-100 mechanism of action.*

### 1.5.1 Organometallic Therapeutics

Organometallic compounds, defined as metal complexes that have at least one direct covalent metal-carbon bond, are traditionally used in catalysis or biosensorics but are lately also finding application in medicinal chemistry. They recently have emerged as promising candidates for anticancer metallodrugs. Organometallic compounds exhibit great structural diversity, are kinetically stable, usually uncharged, relatively lipophilic, and their metal atoms are in a low oxidation state. These properties open up many possibilities for the development

of new types of drugs. The main classes of organometallic compounds include metallocenes, metal-arenes, metal-carbenes and metal-carbonyls with carbon monoxide as ligand (Figure 16).[67]

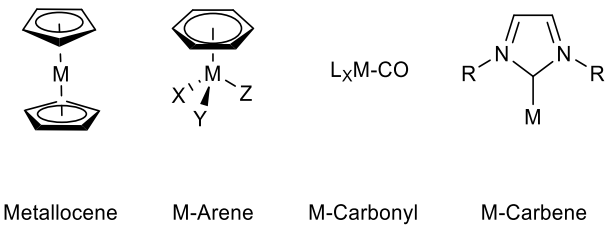


*Figure 16: Typical classes of organometallic compounds used in medicinal chemistry summarized.*

The investigation of ruthenium(II) drugs began with the research into the mechanism of "activation by reduction" of ruthenium(III) compounds.[68] More recently, organometallic ruthenium(II) arene compounds have been developed, offering a new type of metallodrug different from traditional coordination compounds used in clinical studies.[69] These ruthenium(II) arene compounds, which are also known as “piano-stool” complexes, are stabilized in the +2 oxidation state by a $\eta^6$-coordinated arene ligand. In a typical half sandwich piano-stool complex [($\eta^6$-arene)M(X)(Y)(Z] (see Figure 16 M-Arene) the arene forms the seat and the ligands represent the legs of the stool.[69–71]

Two subfamilies of Ru(II) arene compounds, the RAPTA and the RAED family, have been studied extensively (Figure 17). In the RAPTA family ([Ru($\eta^6$-arene)(PTA)$Cl_2$], PTA = 1,3,5-triaza-7-phosphaadamantane), the PTA ligand offers a certain level of water solubility (depending on the type of arene ligand), which facilitates administration and transportation in the body.[72,73] However, RAPTA compounds with modified arene ligands were found to be low toxic to cancer cells and completely non-toxic to healthy cells. However, they are effective *in vivo* by reducing lung metastases in mice with mammary carcinoma, although it has minimal effects on primary tumors.[74]

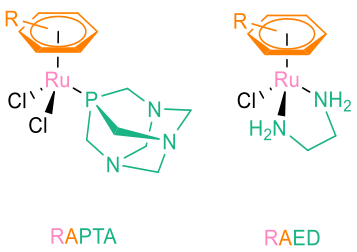


*Figure 17: Structure of RAPTA and RAED complexes.*

## 1.6 Bioactive Ligands

Many drugs face problems in clinical trials, such as poor bioavailability, low efficacy and severe side effects.[75] Synthetic modification of drugs to overcome these problems can be very challenging. An alternative approach is to use metal complexes as chaperones for drug delivery. This method is more straightforward and can improve the pharmacokinetics and pharmacodynamics of the drug.[76] Metal complexes can enhance solubility of drugs, especially for those with poor aqueous solubility, by coordinating with positively charged metals.[76,77] This strategy also helps to reduce the negative charge of the drug, when present, which improves cellular uptake. Transition metals are ideal for controlled drug release, as their bonds can respond to environmental changes like pH or redox status, minimizing systemic toxicity. In addition, metal complexes can enhance biological activity by providing multiple mechanisms for targeting diseases, potentially increasing efficacy and overcoming drug resistance.[76]

Ideally, bioactive ligands coordinate selectively at metal centers, but complications such as the formation of binding isomers can occur. To overcome these, ligands are often modified for targeted anticancer activity. Research efforts focus on five design strategies (Figure 18): direct coordination (i), ligand derivatization (ii), structural mimicry of bioactive molecules (iii), metal complexes as prodrugs (iv), and bioactive ligands as tumor targeting vectors (v).[78]

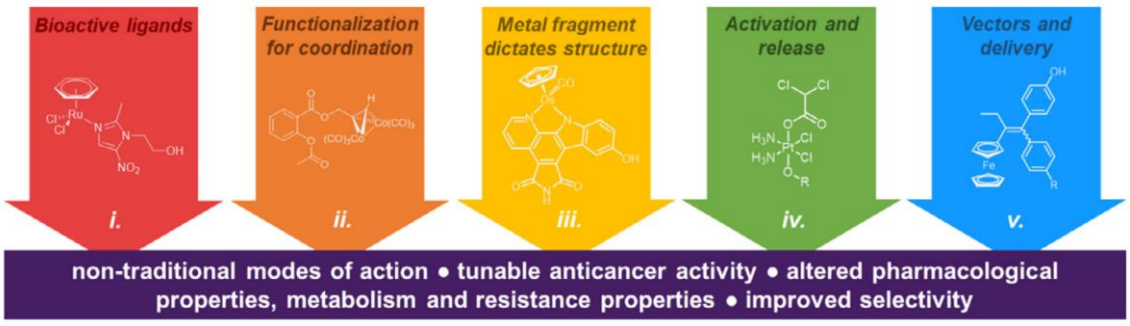


*Figure 18: Design concepts for bioactive scaffolds in metallodrugs.[78]*

To further illustrate the application of bioactive ligands in cancer treatment, one example is clofarabine ((2R,3R,4S,5R)-5-(6-amino-2-chloropurin-9-yl)-4-fluoro2(hydroxymethyl)oxolan -3-ol), a second-generation purine nucleoside analog.[79] As previously stated in section 1.3, it is considered an antimetabolite and is approved by the FDA for the treatment of cancer.

The anti-cancer effect of clofarabine is based on three main mechanisms: Inhibition of DNA synthesis, inhibition of ribonucleotide reductase and induction of apoptosis (Figure 19).[80,81]

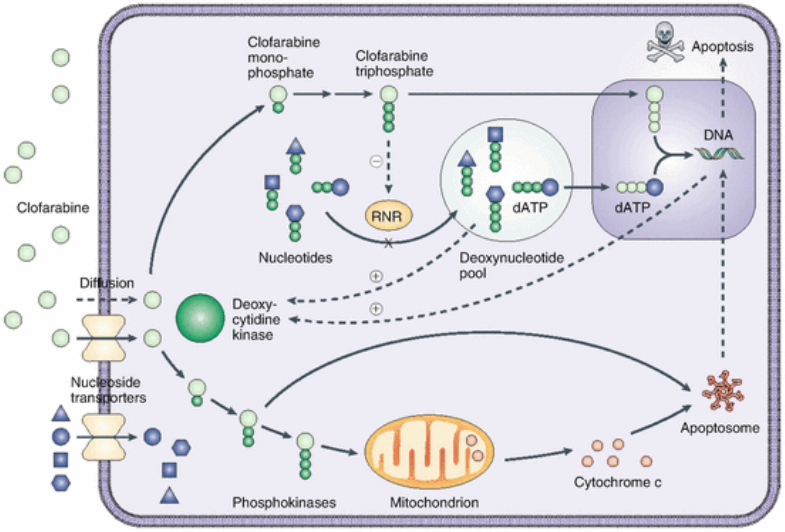


*Figure 19: Mechanisms of action for clofarabine.*[80]

# 2 Aim and Objective

The aim of this thesis was to synthesize new clofarabine-bearing organometallic cancer compounds with various mono and bidentate ligands by ligand exchange of a precursor complex (Scheme 1).

Initially, the ligand exchange was tested with an adenine derivative as a clofarabine model. After successful synthesis of the adenine derivate complex, including purification, the bioactive clofarabine was coordinated to the organometallic moiety.

For this purpose, the ruthenium dimer and the adenine derivative were synthesized first. Complexation to the precursor complexes was then carried out with the adenine derivative (**a**) and clofarabine (**b**) respectively.

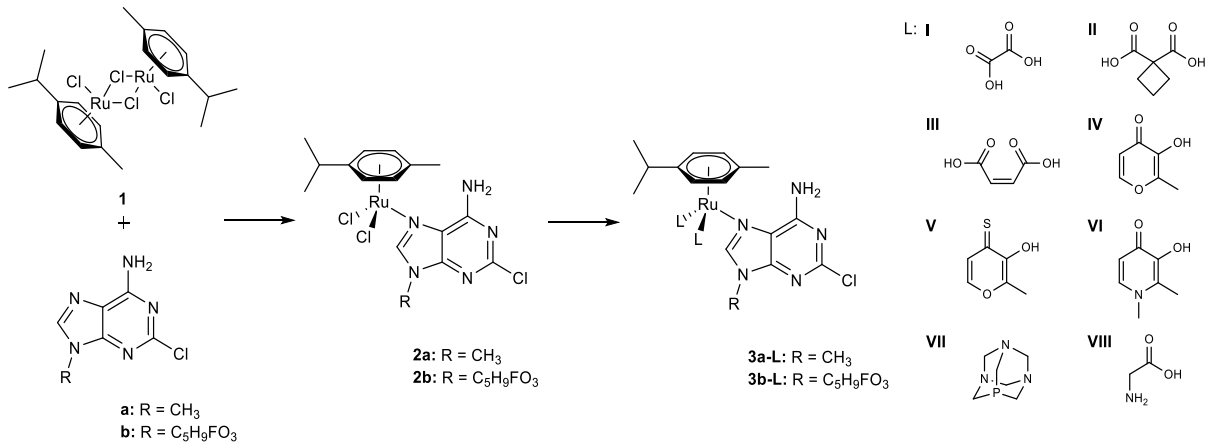


*Scheme 1: General scheme for the planned syntheses of the thesis.*

The compounds are characterized by NMR spectroscopy, elemental analysis, mass spectrometry and solubility in aqueous medium. The stability of these complexes is determined by UV/vis spectrometry over 24 hours.

# 3 Results and Discussion

## 3.1 Syntheses

The following paragraphs describe the syntheses of the compounds which were performed during the thesis. The synthesis of ligand **a** and the ruthenium dimer are well-established procedures.[82,83] The precursor syntheses were conducted using the same methods as those employed by a previous master's student. The novel syntheses involve ligand exchange reactions, where one or two chlorine atoms in the precursor complexes are substituted with ligands **I-VIII**, the synthesis of which was the primary objective of this work.

**Ligand Synthesis**

Ligands **a** and **b** (clofarabine) were used for coordination with the metal dimer. For this purpose, ligand **a** was synthesized, while clofarabine was obtained from commercial suppliers.

2-Chloro-9-methyl-9H-purin-6-amine: **a**

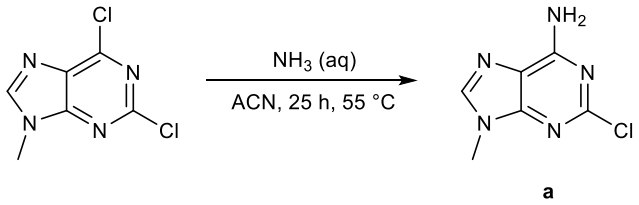


**a**

*Scheme 2: Synthesis of 2-chloro-9-methyl-9H-purin-6-amine.*

The reaction shown in Scheme 2 was performed according to Jörg *et al*.[82] In this reaction, 2,6-dichloro-9-methly-9H-purine (1 eq.) was dissolved in acetonitrile and reacted with an excess of aqueous ammonia (7.5 eq.). The reaction involved a nucleophilic substitution in which the chloride at position 6 was replaced by an amine group. The isolated white solid was obtained in excellent yield (94%).

**Dimer Synthesis**

Bis[dichlorido(η$^6$-*p*-cymene)ruthenium(II)]: **1**

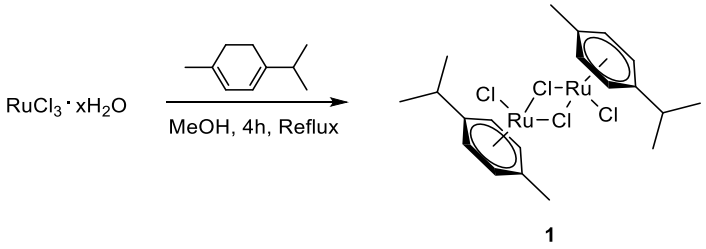


**1**

*Scheme 3: Synthesis of ruthenium p-cymene dimer.*

Ruthenium(III) chloride hydrate (1 eq.) and α-terpinene (5 eq.) were refluxed in methanol. Thereby Ru(III) was reduced to Ru(II) and α-terpinene was oxidized to *para*-cymene (Scheme 3). After washing with ether and drying, the red solid was obtained in fair yield (69%).

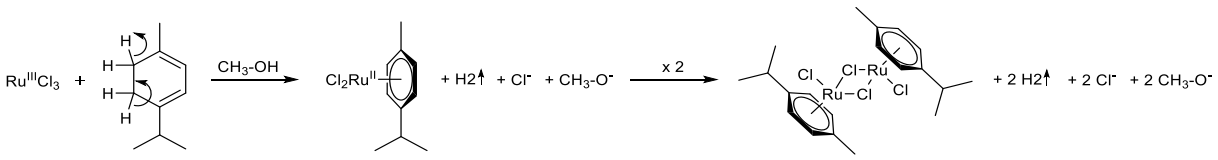


*Scheme 4: Mechanism of the dimer formation.*

In the redox reaction shown in Scheme 4, Ru(III)$Cl_3$ serves as the oxidizing agent, which is reduced to Ru(II) while oxidizing α-terpinene to form the aromatic ligand *p*-cymene. The aromatization of α-terpinene releases two electrons per molecule, resulting in a total of four electrons per ruthenium dimer. Half of these electrons are used to reduce ruthenium, while the other two reduce hydrogen protons to generate elemental hydrogen. This emphasizes the crucial role of protic solvents in this synthesis. The formation of $H_2$ clearly drives the reaction equilibrium towards the desired product, the ruthenium dichloride *p*-cymene dimer.

**Precursor Complex Syntheses**

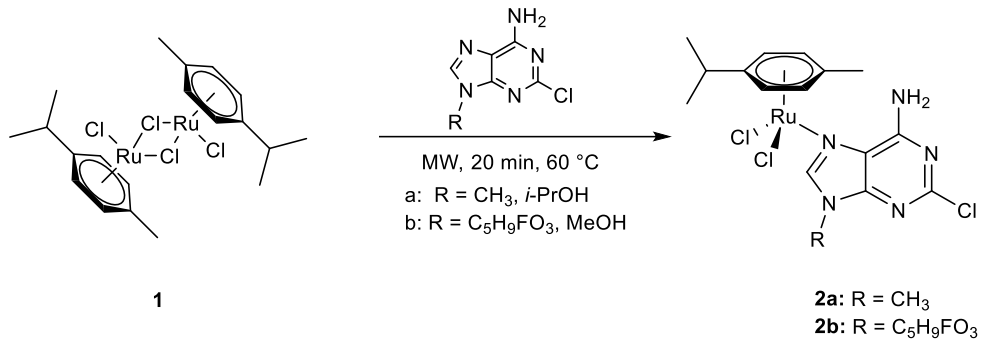


*Scheme 5: General procedure for the precursor complex syntheses.*

The metal dimer and the respective adenine derivative in alcohol were reacted under microwave conditions to the desired precursor complexes (Scheme 5). These were obtained in very good to excellent yields (84 – 98%).

[Dichlorido(2-chloro-9-methyl-9H-purin-6-amine-κ$N^7$)(η$^6$-*p*-cymene)ruthenium(II)]: **2a**

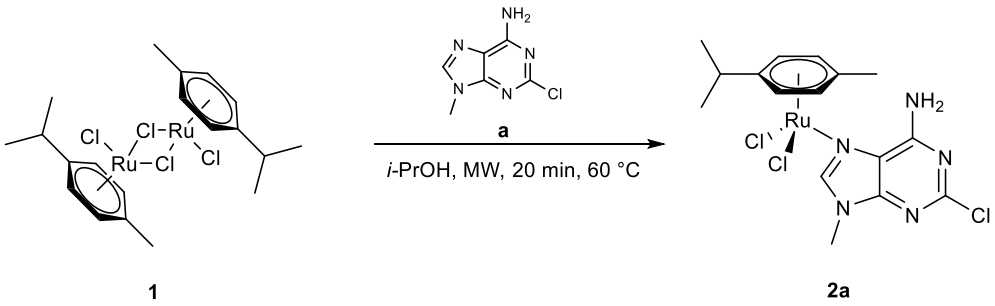


[Ru(*p*-cym)$Cl_2$]$_2$ **1** (1 eq.) and 2-chloro-9-methyl-9H-purin-6-amine **2** (2 eq.) were dissolved in isopropanol and then reacted under microwave conditions. After purification the orange solid was obtained in good, or even up to very good yields (70 – 84%).

[Dichlorido((2R,3R,4S,5R)-5-(6-amino-2-chloropurin-9-yl)-4-fluoro-2(hydroxymethyl) oxolan-3-ol-κ$N^7$)(η$^6$-*p*-cymene)ruthenium(II)]: **2b**

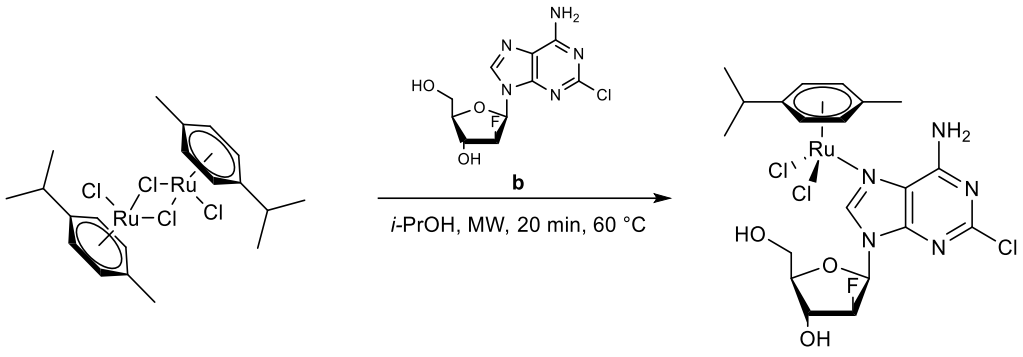


**1** **2b**

[Ru(*p*-cym)$Cl_2$]$_2$ **1** (1 eq.) and clofarabine **b** (2 eq.) were dissolved in methanol and reacted in the microwave. This resulted in the formation of an orange solid with excellent yields from 97 up to 98%.

**Novel Complex Syntheses**

In the following syntheses, one or two chloro ligands were exchanged. If the synthesis and purification with the adenine model ligand (**a**) was successful, the complex was also synthesized using clofarabine (**b**).

[Oxalato-κ*O*$^1$,κ*O*$^2$(2-chloro-9-methyl-9H-purin-6-amine-κ*N*$^7$)(η$^6$-*p*-cymene)ruthenium(II)]: **3a-l**


**2a** **3a-l**

[Dichlorido(2-chloro-9-methyl-9H-purin-6-amine-κ*N*$^7$)(η$^6$-*p*-cymene)ruthenium(II)] **2a** (1 eq.) and $AgNO_3$ (2 eq.) were reacted with sodium oxalate in methanol and stirred under exclusion of light. After workup and drying, the product was obtained as a yellow solid in very good yield (83%). The formation of the complex was confirmed by NMR measurements. Unfortunately, attempts to purify the complex using MPLC were unsuccessful. Instead, purification could only be achieved through precipitation, which unfortunately led to insufficient purity in elemental analysis.

[Oxalato-κ$O^1$,κ$O^2$((2R,3R,4S,5R)-5-(6-amino-2-chloropurin-9-yl)-4-fluoro-2(hydroxy-methyl)oxolan-3-ol- κ$N^7$)(η$^6$-*p*-cymene)ruthenium(II)]: **3b-l**

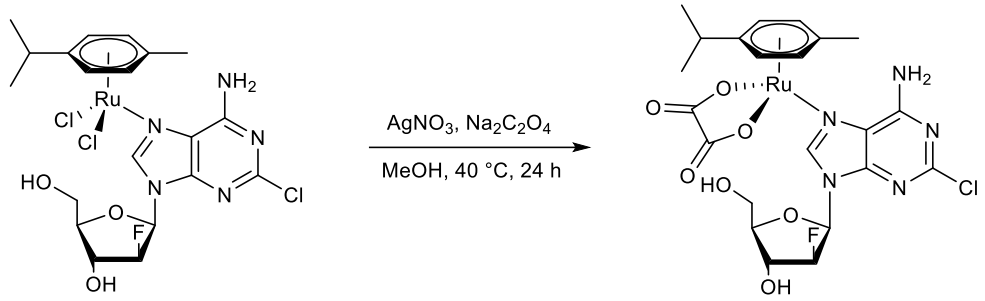


**2b** **3b-l**

[Dichlorido((2R,3R,4S,5R)-5-(6-amino-2-chloropurin-9-yl)-4-fluoro-2(hydroxymethyl) oxolan-3-ol-κ$N^7$)(η$^6$-*p*-cymene)ruthenium(II)] **2b** (1 eq.) and $AgNO_3$ (2 eq.) were reacted with sodium oxalate in methanol under the exclusion of light. After workup, the product was isolated as a yellow solid in excellent yield (90%). NMR analyses confirmed the formation of the complex. Unfortunately, attempts to purify the complex by MPLC were unsuccessful. Only precipitation was able to achieve purification, but this did not lead to elemental-analysis purity.

[1,1-Cyclobutanedicarboxylato-κ$O^1$,κ$O^2$(2-chloro-9-methyl-9H-purin-6-amine-κ$N^7$)(η$^6$-*p*-cymene)ruthenium(II)]: **3a-II**

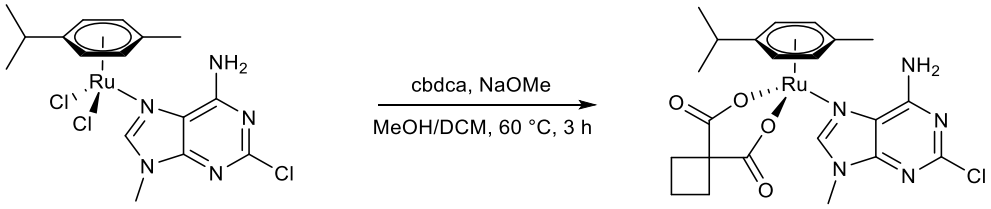


**2a** **3a-II**

1,1-Cyclobutanedicarboxylic acid (cbdca) (1 eq.) and sodium methoxide (2.2 eq.) were dissolved in methanol and reacted with [dichlorido(2-chloro-9-methyl-9H-purin-6-amine-κ$N^7$)(η$^6$-*p*-cymene)ruthenium(II)] **2a** (0.9 eq.). The $^1$H-NMR spectrum after reaction indicated that the desired complex was not formed. Instead, a mixture of complexes was detected.

[Maleato-κ*O*$^1$,κ*O*$^2$(2-chloro-9-methyl-9H-purin-6-amine-κ*N*$^7$)(η$^6$-*p*-cymene)ruthenium(II)]: **3a-III**

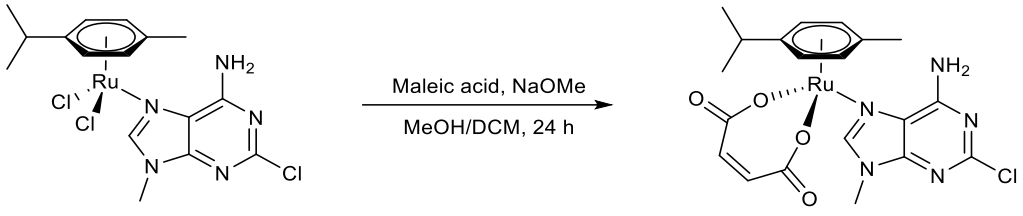


**2a** **3a-III**

Maleic acid (1 eq.) and sodium methoxide (2.2 eq.) were dissolved in methanol. [Dichlorido(2-chloro-9-methyl-9H-purin-6-amine-κ*N*$^7$)(η$^6$-*p*-cymene)ruthenium(II)] **2a** (0.9 eq.) was suspended in DCM and then added dropwise to the maleate solution. Based on the recorded $^1$H spectrum, there was no indication that the complex was formed. The likely reason is that the formation of a seven-membered ring with maleic acid as a ligand is unfavorable due to ring strain and its flexibility and electronic properties may lead to weak or unstable coordination, preventing the formation of the desired complex.

[Maltolato-κ*O*$^1$,κ*O*$^2$(2-chloro-9-methyl-9H-purin-6-amine-κ*N*$^7$)(η$^6$-*p*-cymene)ruthenium(II)]: **3a-IV**

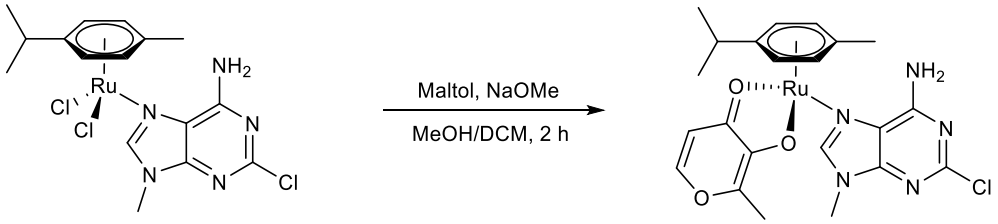


**2a** **3a-IV**

Maltol (1 eq.) and sodium methoxide (1.1 eq.) were dissolved in methanol. [Dichlorido(2-chloro-9-methyl-9H-purin-6-amine-κ*N*$^7$)(η$^6$-*p*-cymene)ruthenium(II)] **2a** (0.9 eq.) was suspended in DCM and then gradually added to the maltol solution. Although the complex synthesis was successful according to $^1$H-NMR), various purification approaches such as MPLC or precipitation with different solvents proved ineffective. This was likely due to the instability of the product, which could not withstand these purification conditions.

[Thiomaltolato-κ*O*,κ*S*(2-chloro-9-methyl-9H-purin-6-amine-κ*N*$^7$)(η$^6$-p-cymene) ruthenium(II)]: **3a-V**

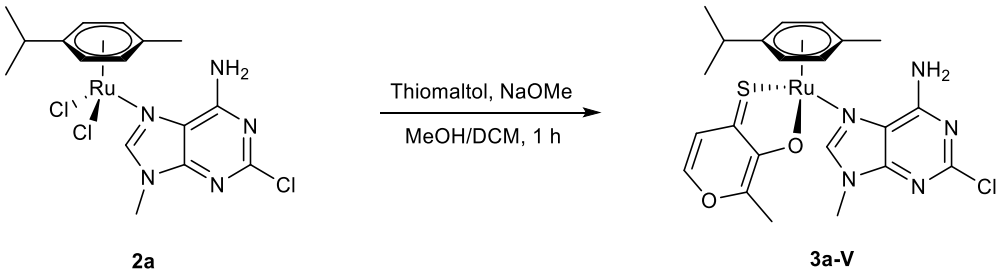


**2a** **3a-V**

Thiomaltol (1 eq.) and sodium methoxide (1.1 eq.) were dissolved in dry methanol. [Dichlorido(2-chloro-9-methyl-9H-purin-6-amine-κ*N*$^7$)(η$^6$-*p*-cymene)ruthenium(II)] **2a** (0.9 eq.) was suspended in dry DCM and subsequently added to the thiomaltol solution dropwise under inert conditions. There was no evidence of complex formation with thiomaltol according to the recorded $^1$H-NMR spectrum, likely due to the trans effect of the coordinated Sulphur atom of thiomaltol weakening the bond of the coordinated purine ligand.

[3-Hydroxy-1,2-dimethyl-4(1H)-pyridonato-κ*O*$^1$,κ*O*$^2$(2-chloro-9-methyl-9H-purin-6-amine-κ*N*$^7$)(η$^6$-p-cymene)ruthenium(II)]: **3a-VI**

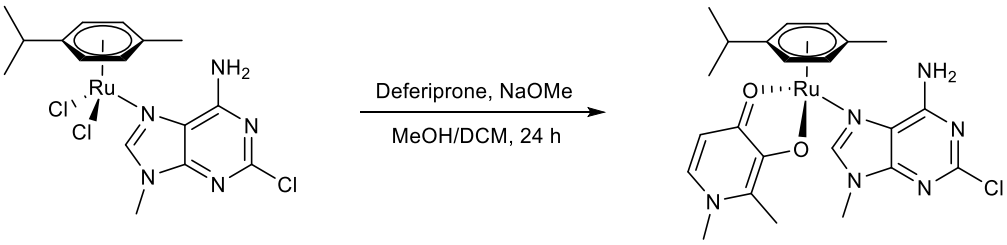


**2a** **3a-VI**

Deferiprone (1 eq.) and sodium methoxide (1.1 eq.) were dissolved in methanol. [Dichlorido(2-chloro-9-methyl-9H-purin-6-amine-κ*N*$^7$)(η$^6$-*p*-cymene)ruthenium(II)] **2a** (0.9 eq.) was suspended in DCM and then added dropwise to the deferiprone solution. According to the analyzed $^1$H-NMR spectrum, there were no signs indicating the formation of the desired complex.

[1,3,5-Triaza-7-phosphaadamantane-κ*P*(2-chloro-9-methyl-9H-purin-6-amine-κ*N*$^7$)(η$^6$-p-cymene)ruthenium(II)]: **3a-VII**

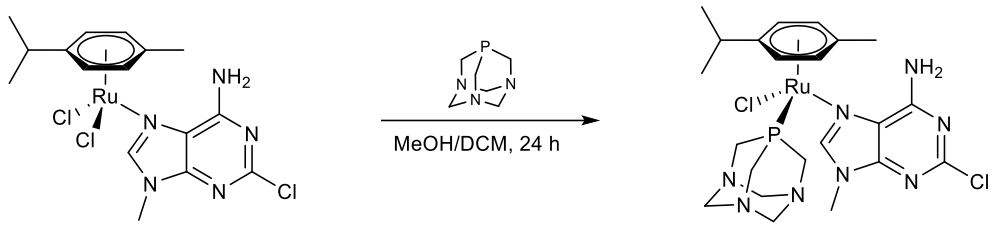


**2a** **3a-VII**

1,3,5-Triaza-7-phosphaadamantane (PTA) (1 eq.) was dissolved in methanol, and [dichlorido(2-chloro-9-methyl-9H-purin-6-amine-κ*N*$^7$)(η$^6$-*p*-cymene)ruthenium(II)] **2a** (0.9 eq.) was suspended in DCM before being added dropwise to the PTA solution. However, the purine ligand detached during the reaction, as seen in the $^1$H NMR, indicating that the formation of the complex was unsuccessful. This result suggests that the adenine ligand was more easily exchanged, indicating that the formation of RAPTA complexes, detailed in chapter 1.5.1, is favored over the desired chloride-PTA exchange.

[Glycinato-κ*O*,κ*N*(2-chloro-9-methyl-9H-purin-6-amine-κ*N*$^7$)(η$^6$-p-cymene)ruthenium(II)]: **3a-VIII**


**2a** **3a-VIII**

Glycine (1 eq.) and sodium methoxide (1.1 eq.) were dissolved in methanol. [Dichlorido(2-chloro-9-methyl-9H-purin-6-amine-κ*N*$^7$)(η$^6$-*p*-cymene)ruthenium(II)] **2a** (0.9 eq.) was suspended in DCM and thereafter added to the deferiprone solution dropwise. The $^1$H-NMR spectrum revealed that the desired complex was not formed. A mixture of different complexes was observed instead.

## 3.2 NMR Characterization

NMR spectroscopy was employed to confirm the formation of the synthesized complexes and to characterize the compounds. Various techniques, including $^{1}$H-NMR, $^{13}$C-NMR, and 2D-NMR methods (COSY, HSQC, and HMBC), were applied for this purpose. The following paragraphs provide a more detailed description of the characterization process of the compounds and complexes for which the synthesis (and purification) was successful.

### 3.2.1 $^{1}$H-NMR

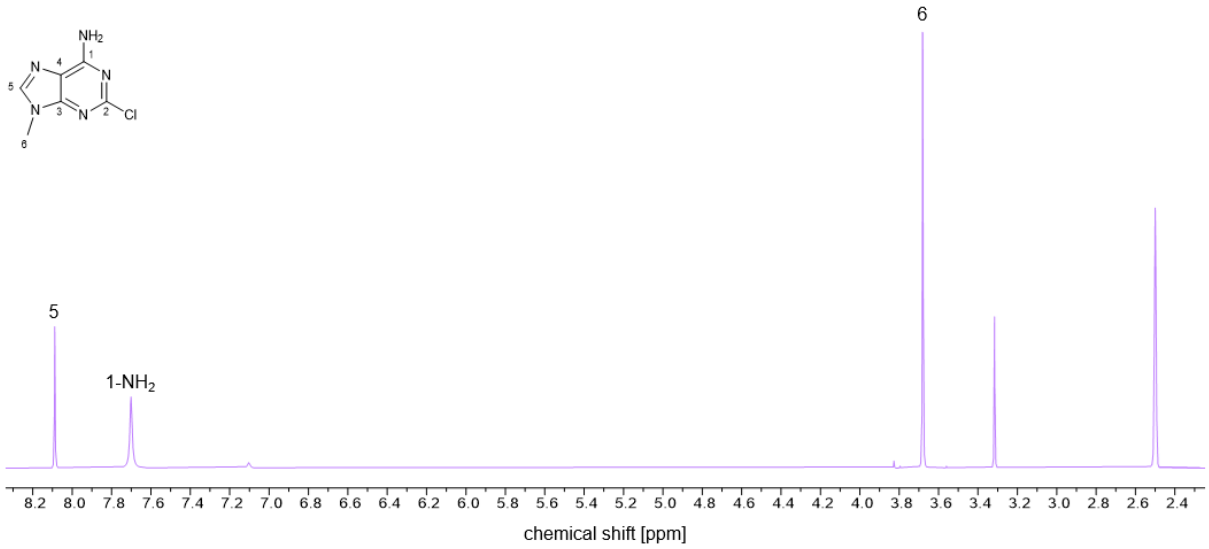


*Figure 20: $^{1}$H-NMR spectrum of compound **a** in DMSO-d$^{6}$.*

The $^{1}$H-NMR spectrum of the adenine derivate **a** (Figure 20) was measured in deuterated DMSO, showing no impurities other than water at 3.31 ppm. The proton 5 (8.09 ppm) and the $NH_2$ protons (7.70 ppm) are shifted downfield due to the proximity to the electron-withdrawing nitrogen atoms. Since the protons of the methyl group (3.68 ppm) are attached to a carbon that is less electronegative than nitrogen or chlorine, they are shifted upfield. All peaks are singlets, indicating that the protons do not have neighboring protons with which they can couple.

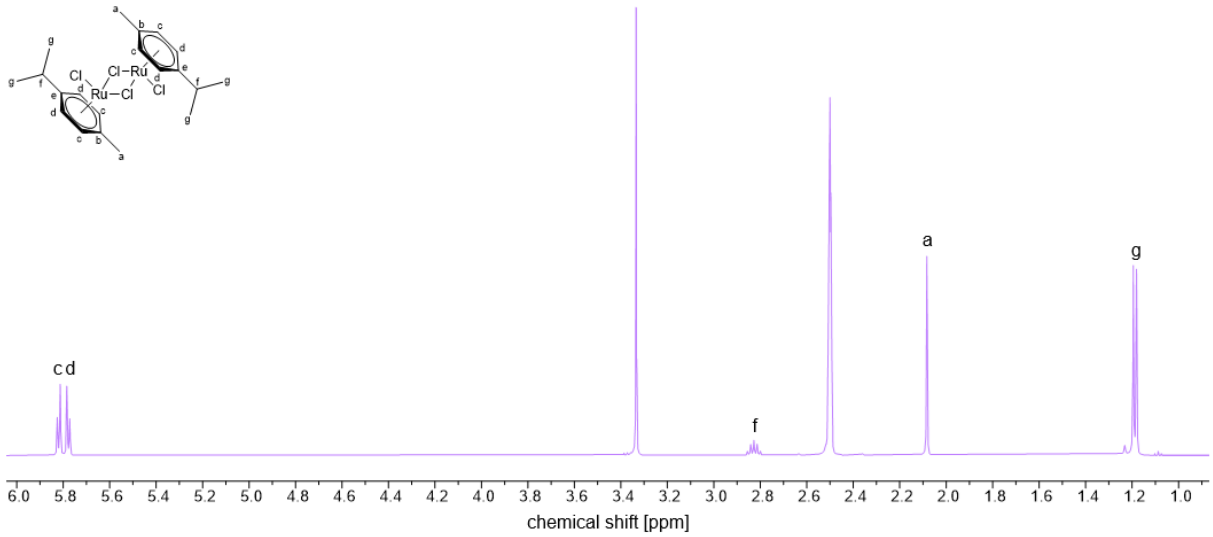


*Figure 21: $^{1}$H-NMR spectrum of compound **1** in DMSO-d$^{6}$.*

The $^{1}$H-NMR spectrum of complex **1** displays distinct peaks corresponding to the protons of the *p*-cymene ligand. The doublets at 5.82 ppm and 5.78 ppm correspond to the four aromatic protons of c and the four protons of d. The heptet at 2.83 ppm is assigned to the proton f coupled to six methyl protons (g). The singlet at 2.08 ppm corresponds to six methyl protons (a) attached to the aromatic ring, and the doublet at 1.19 ppm reflects the twelve methyl protons (g) of the isopropyl groups. The aromatic protons are shifted downfield due to the connection to an aromatic system, whereas the isopropyl and methyl protons resonate upfield.

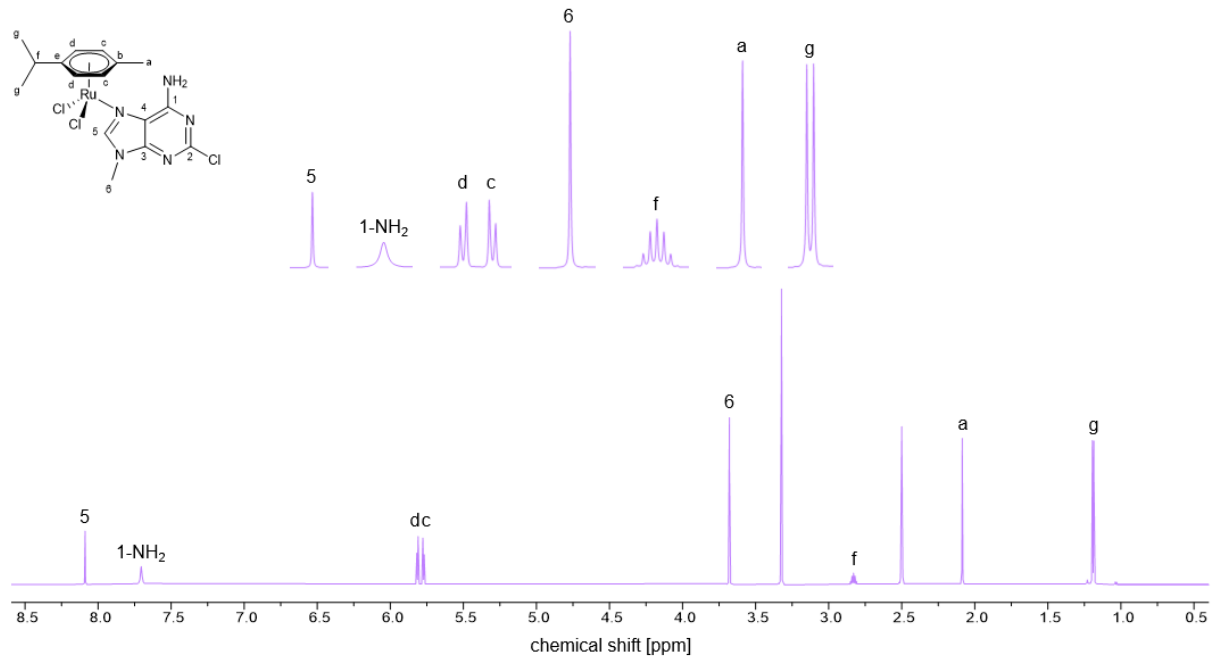


*Figure 22: [1]H-NMR spectrum of complex **2a** in DMSO-d[6].*

The [1]H-NMR spectrum of complex **2a** (Figure 22) reveals that coordination of the adenine ligand to the organometallic fragment does not significantly alter the chemical shifts of the peaks. The aromatic protons of the *p*-cymene system are represented by signals c and d, which each correspond to two protons and appear as doublets around 5.60 ppm. The signal at 2.83 ppm is a heptet, corresponding to one proton (f) which is coupled to two adjacent methyl groups (g). The singlet at 2.09 ppm represents three methyl protons (a), showing a slightly higher chemical shift due to their connection to the aromatic system. The isopropyl groups' methyl protons are observed as a doublet at 1.19 ppm reflecting the presence of six protons (g).

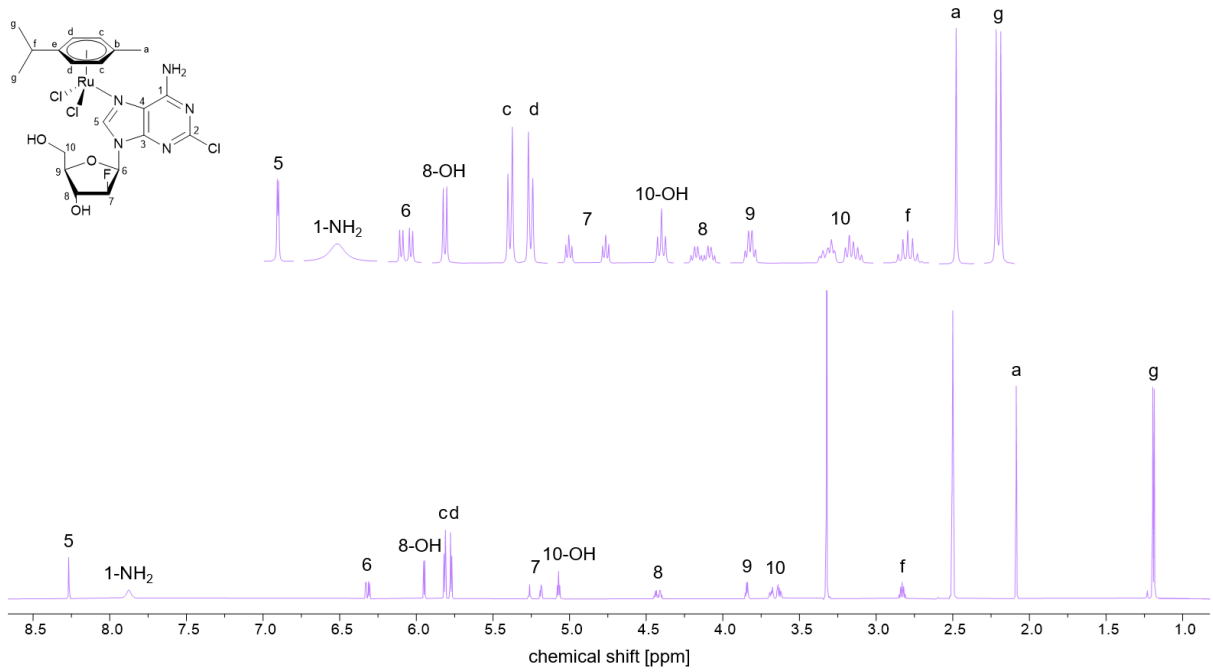


*Figure 23: $^{1}$H-NMR spectrum of complex **2b** in DMSO-d$^{6}$.*

In the spectrum of **2b** (Figure 23), proton 5 appears as a doublet and corresponds to the aromatic CH in the purine core, while the amine group (1-$NH_2$) shows as a singlet. Proton 6 is seen as a doublet of doublets, influenced by the adjacent fluoride on the carbon atom, causing this splitting pattern. Protons 8 and 10, corresponding to the exchangeable OH groups, appear as a doublet and a triplet. The aromatic protons of the *p*-cymene ligand (c and d) show as doublets, each representing two equivalent aromatic protons. These are slightly deshielded due to their position within the arene-metal system. Proton 7 appears as a doublet of triplets due to strong coupling with the fluorine atom, which causes it to shift to a higher ppm value than those typical of alkyl protons. The remaining protons 8, 9 and 10, correspond to the ribose unit and exhibit the anticipated multiplicities. The signals at 2.83 ppm correspond to the heptet of the isopropyl group (f), with coupling to the methyl groups (g), which appear as a doublet at 1.19 ppm, representing six protons. The methyl group attached to the aromatic ring shows as a singlet at 2.09 ppm (a).

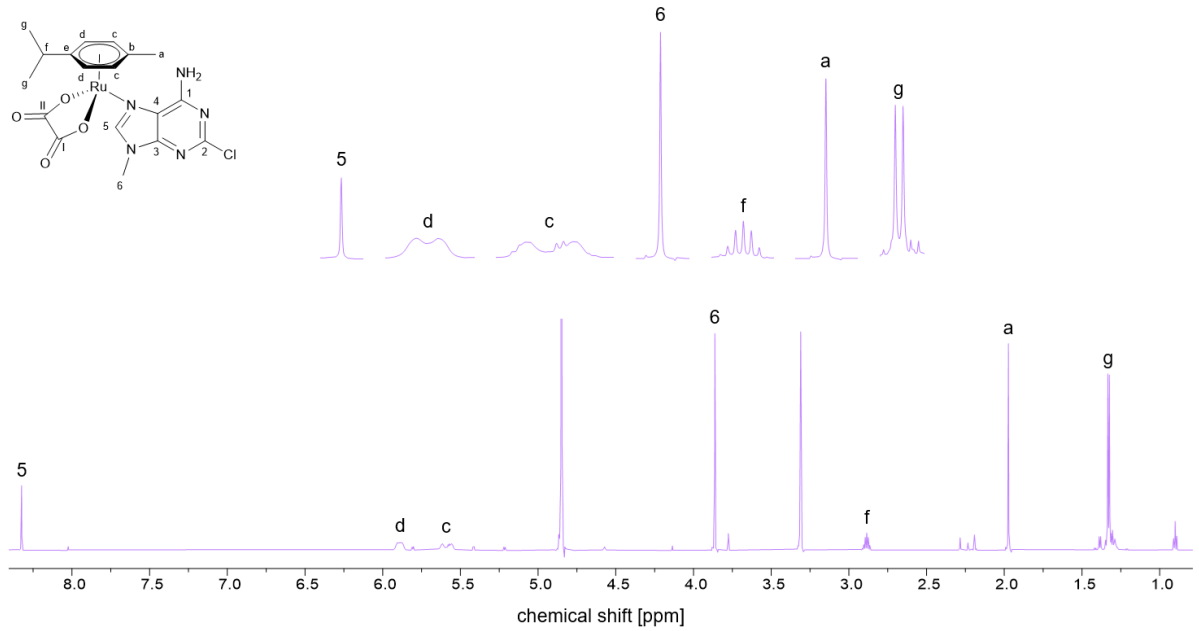


*Figure 24: $^{1}$H-NMR spectrum of complex **3a-I** in MeOD.*

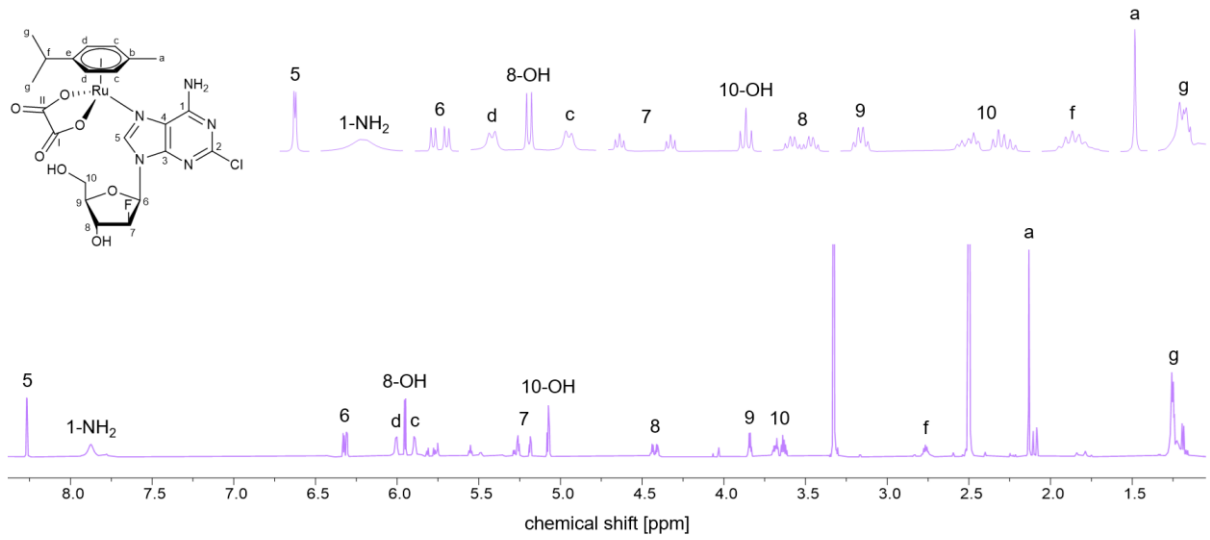


*Figure 25: $^{1}$H-NMR spectrum of complex **3b-I** in DMSO-d$^{6}$.*

In both $^{1}$H-NMR spectra (Figure 24 and Figure 25), following ligand exchange, the signals remain largely unchanged in comparison to the precursor spectra. This consistency is expected, as no new hydrogen atoms are introduced during the ligand exchange. However, due to challenges in purification, the spectra display more impurities.

### 3.2.2 $^{13}$C-NMR

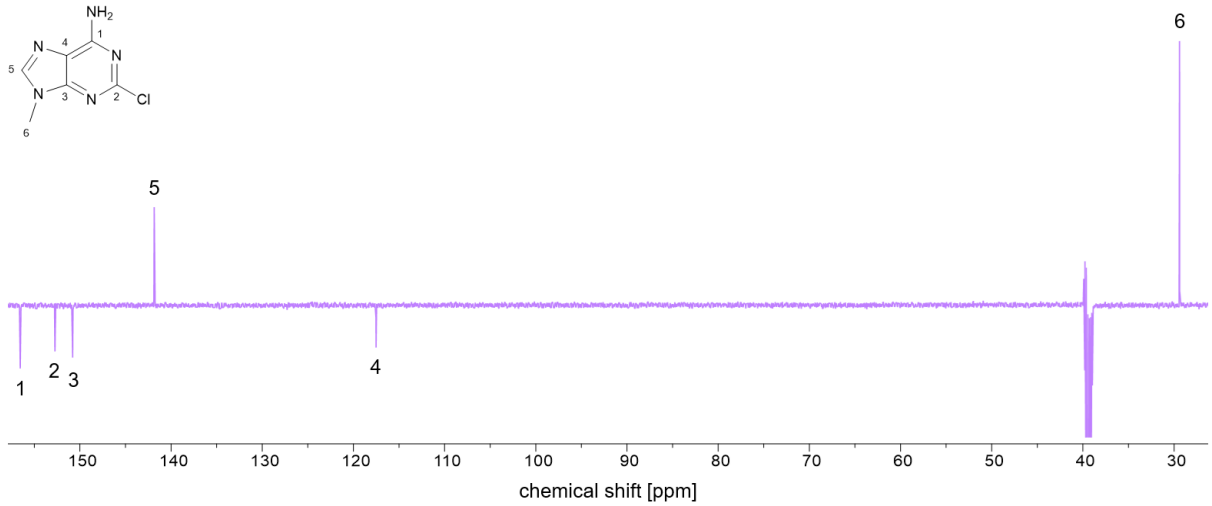


*Figure 26: $^{13}$C-NMR spectrum of compound **a** in DMSO-d$^6$.*

In the $^{13}$C-NMR spectrum of 2-chloro-9-methyl-9H-purin-6-amine (**a**, Figure 26), the quaternary carbon 4 resonates at a lower chemical shift of 117.5 ppm compared to the other quaternary carbons at 1, 2 and 3. This lower shift can be explained by the electronic environment surrounding carbon 4. Because the other quaternary carbons are influenced by more than one electronegative group, such as the chlorine atom or the amine group. The signal at 141.9 ppm corresponds to the CH carbon 5, appearing downfield due to deshielding from the aromatic system as well as the nitrogen atoms. The methyl group, at position 6, attached to the nitrogen resonates at 29.4 ppm.

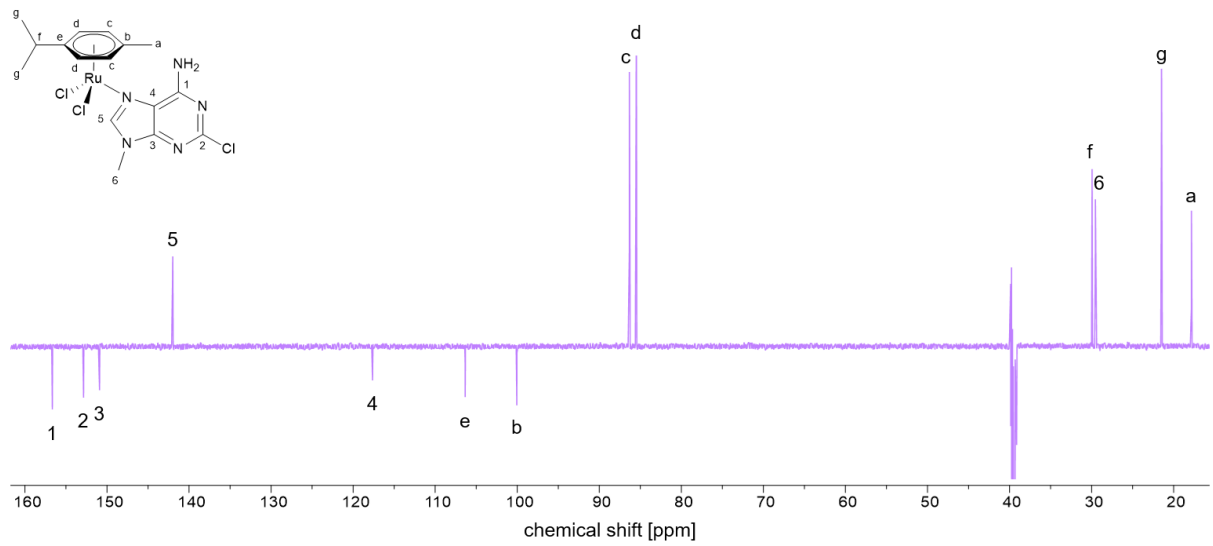


*Figure 27: $^{13}$C-NMR spectrum of complex **2a** in DMSO-d$^6$.*

In the spectrum of the complex **2a** (Figure 27), the quaternary carbons are observed at 156.7 ppm (1), 152.9 ppm (2), 150.9 ppm (3), 117.6 ppm (4), 106.4 ppm (e), and 100.1 ppm (b). These shifts are typical for quaternary carbons in aromatic and conjugated systems. The signals at 142.0 ppm (5), 86.3 ppm (c), 85.5 ppm (d), and 29.9 ppm (f) correspond to CH carbons. The methyl groups resonate at 29.5 ppm (6), 21.5 ppm (g), and 17.8 ppm (a), exhibiting the expected upfield shifts for methyl groups.

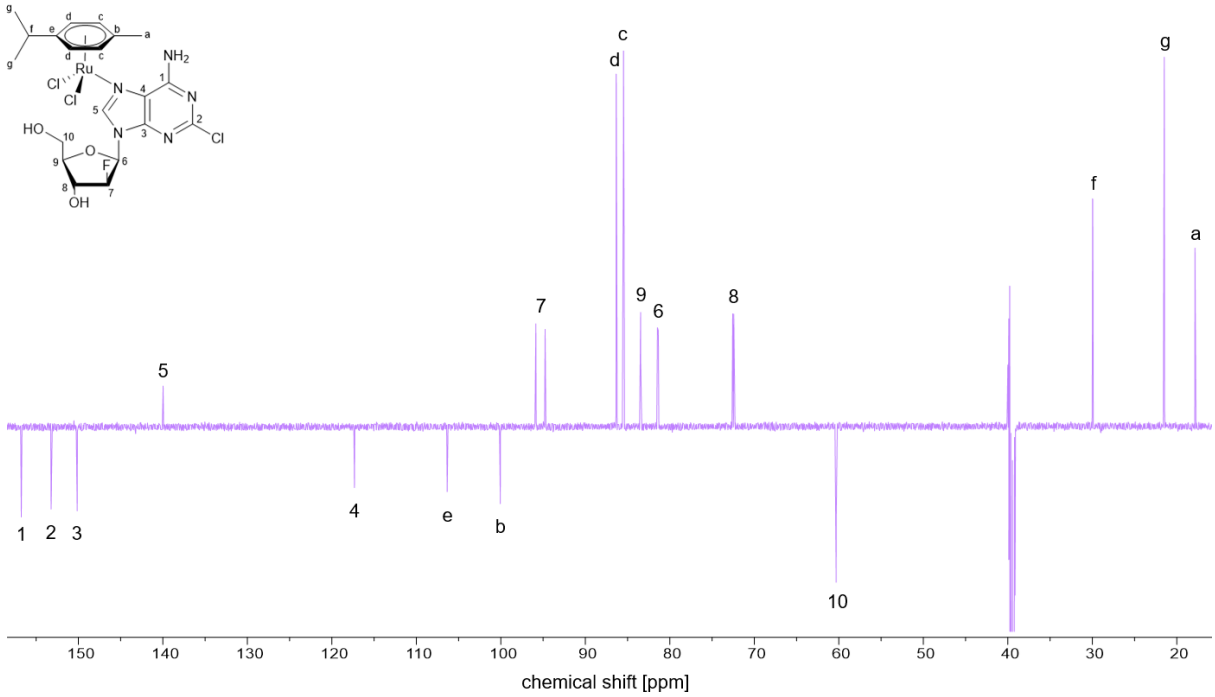


*Figure 28: $^{13}$C-NMR spectrum of compound **2b** in DMSO-d$^6$.*

In the $^{13}$C-NMR spectrum of **2b** (Figure 28), the quaternary carbons are observed at 156.8 ppm (1), 153.2 ppm (2), 150.1 ppm (3), 117.3 ppm (4), 106.4 ppm (e) and 100.1 ppm (b), which is typical for (coordinated) aromatic and conjugated environments. The CH carbons resonate at 140.0 ppm (5), 95.9 ppm and 94.8 ppm (7), 86.3 ppm (d), 85.5 ppm (c), 83.5 ppm (9), 81.4 ppm (6), 72.5 ppm (8), 60.3 ppm (10) and 30.0 ppm (f). The peaks of the methyl groups are observed at 21.5 ppm (g), and 17.8 ppm (a), consistent with typical upfield shifts for such groups.

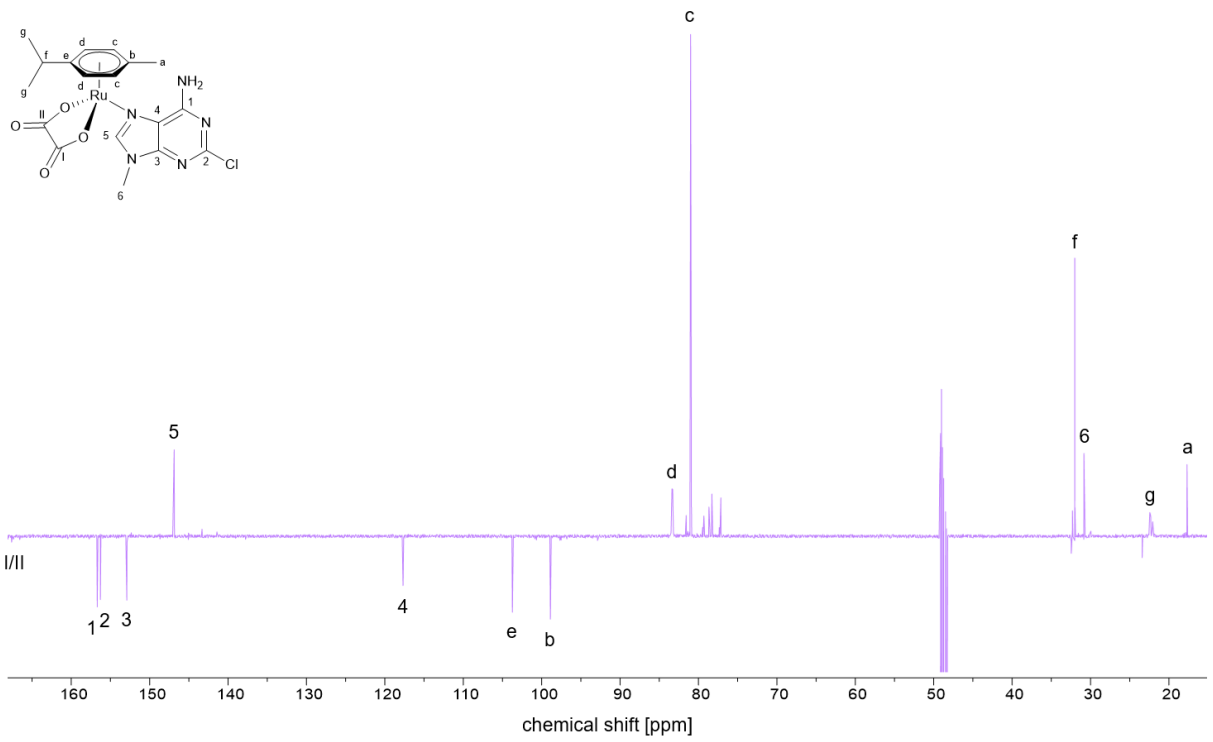


*Figure 29: $^{13}$C-NMR spectrum of compound **3a-I** in DMSO-d$^6$.*

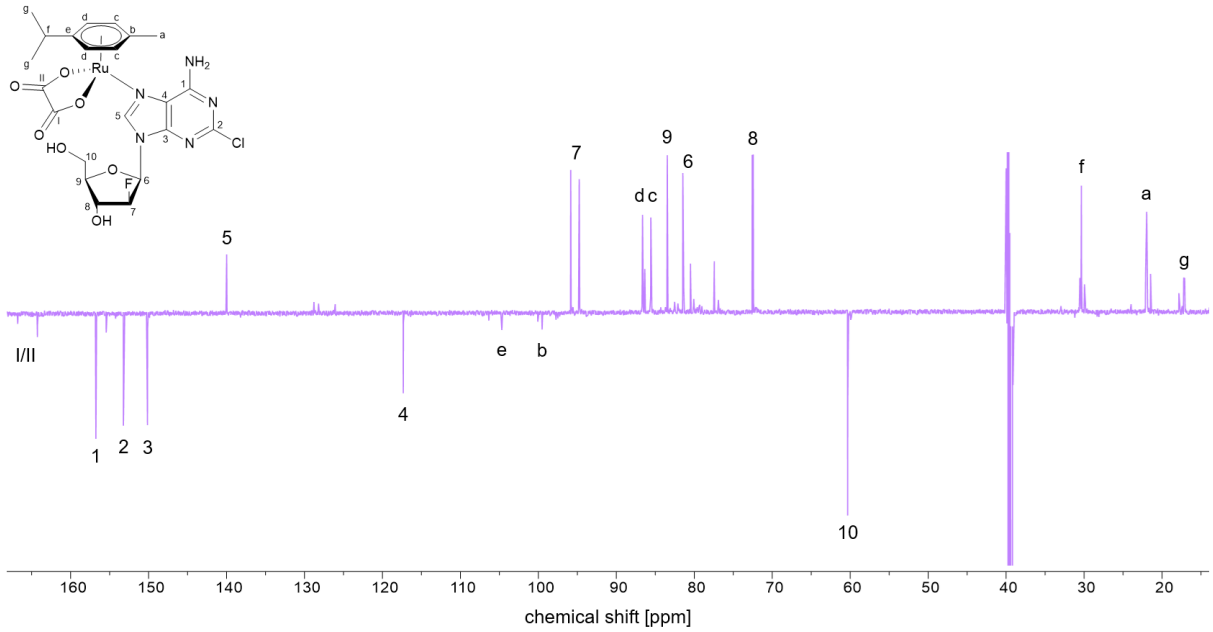


*Figure 30: $^{13}$C-NMR spectrum of compound **3b-I** in DMSO-d$^6$.*

In both $^{13}$C-NMR spectra (Figure 29 and Figure 30), the signals show minimal variation after ligand exchange. The carbon signals from the newly introduced oxalate can be observed at around 160-170 ppm, consistent with expectations. However, the spectra also reveal a higher level of impurities, a result of challenges faced during purification.

## 3.3 Stability UV/vis Measurements

In order to determine the stability of the successfully synthesized complexes in aqueous solutions, UV/vis measurements were conducted. For this purpose, the complexes **3a-l** and **3b-l** were dissolved in PBS (pH 7.4) with 1 % DMSO for as solubilizer. The final concentration of both samples was 40 µmol/L. The maximum absorbance values were measured at 265 nm for complex **3a-l** and at 264 nm for complex **3b-l**, with values ranging from 0.41 to 0.44. The UV/vis measurements were carried in 30-minute intervals over a 24-hour period and covered a wavelength range of 200 - 700 nm. The trends of the maximum absorbance values over time at the respective wavelengths are shown in Figure 31.

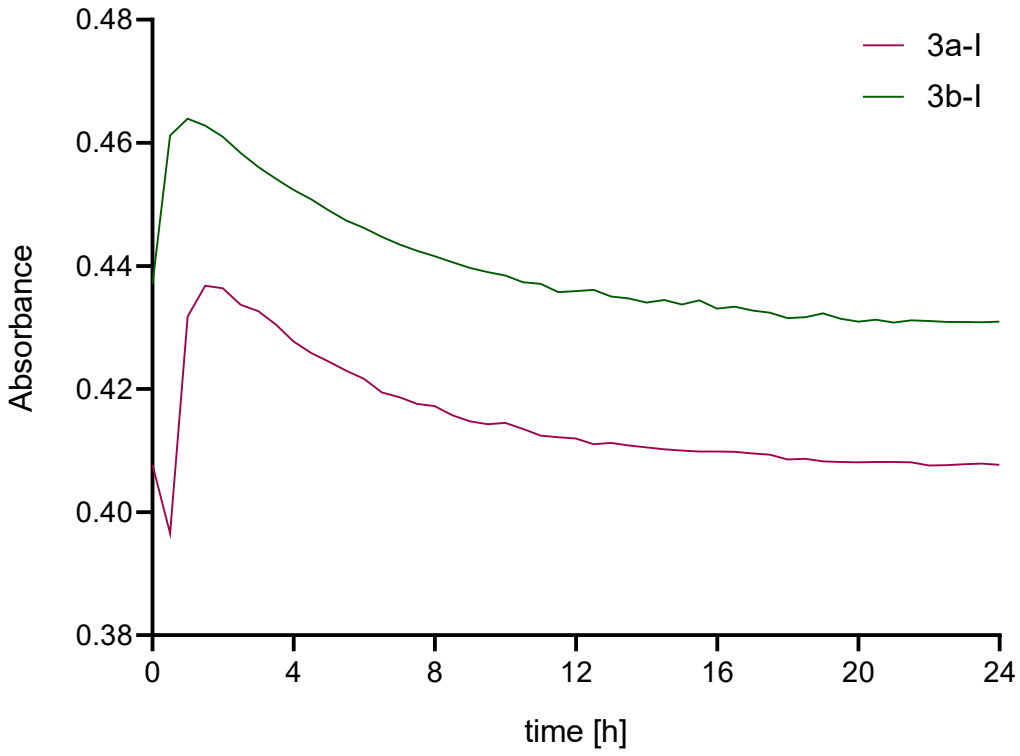


*Figure 31: Absorbance stability over 24 h for complexes **3a-l** and **3b-l** (UV/vis Analysis).*

The results show that both complexes remained stable for at least 24 hours. The 24-hour UV/vis stability data is shown in Figure 32 and Figure 33, where it can be observed that the absorbance for each compound remained essentially constant over time.

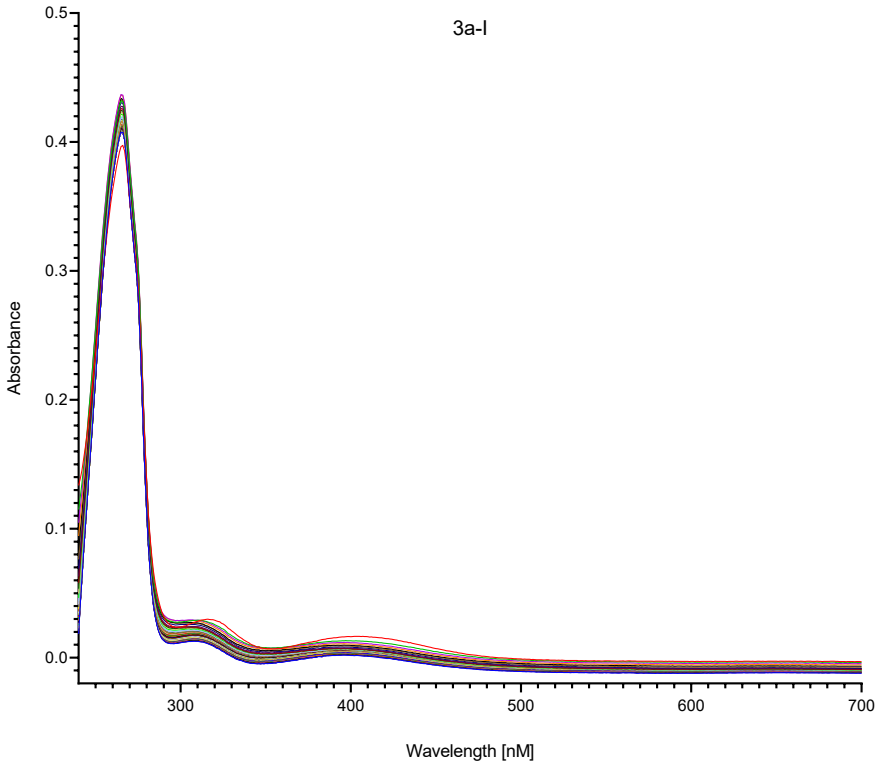


*Figure 32: 24 h UV/vis stability profile of complex **3a-I**.*

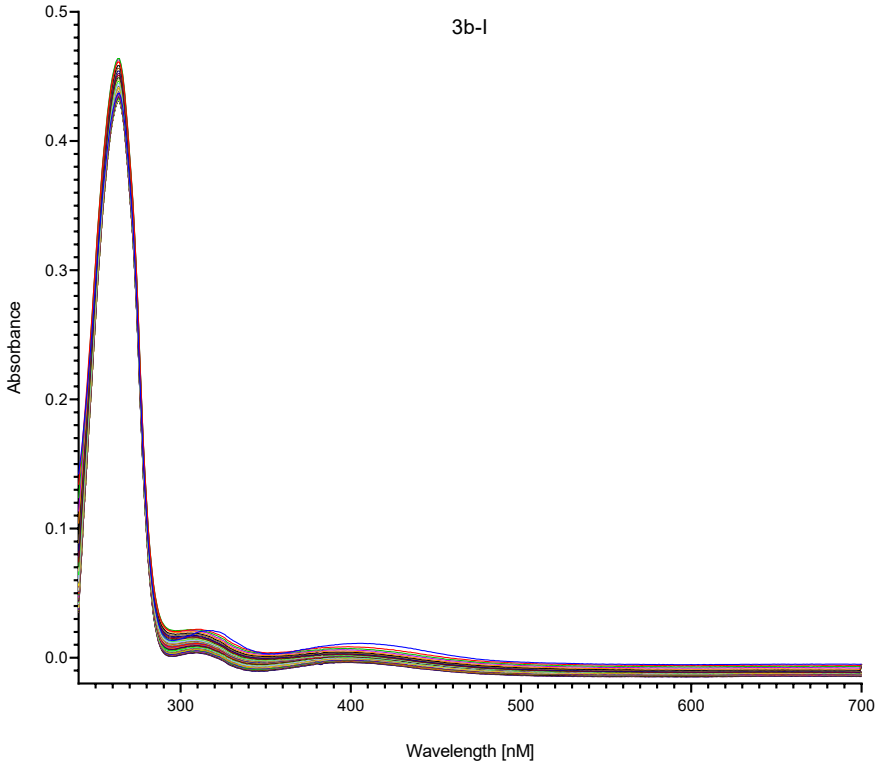


*Figure 33: 24 h UV/vis stability profile of complex **3b-I**.*

## 3.4 Solubility in Aqueous Medium

The solubility of the successfully synthesized complexes **3a-l** and **3b-l** was determined in PBS with 1 % DMSO (pH 7.4). The solubility for both complexes was found to be 50 mg/mL, indicating a favorable solubility profile.

# 4 Experimental

## 4.1 Equipment

Routine NMR spectroscopy measurements were recorded on a Bruker AV NEO 500 spectrometer at 500.10 ($^{1}$H) MHz in DMSO and MeOD. The solvent resonances were used as internal reference for chemical shifts: $^{1}$H (DMSO-$d_6$, 2.50 ppm; MeOD, 3.31 ppm).

Service NMR spectroscopy measurements were conducted using a Bruker AV III HD 700 spectrometer at 700.40 ($^{1}$H) and 176.12 ($^{13}$C) MHz or a Bruker AV III 60 spectrometer at 600.18 ($^{1}$H) and 150.92 ($^{13}$C) MHz in DMSO and MeOD. The solvent resonances served as internal reference for chemical shifts: $^{1}$H (DMSO-$d_6$, 2.50 ppm; MeOD, 3.31 ppm) and $^{13}$C (DMSO-$d_6$, 39.53 ppm; MeOD, 49.03 ppm).

The electrospray ionization mass spectra were measured with a Bruker maXis ESI-QqTOF (electrospray ionization quadrupole–quadrupole time-of-flight) spectrometer in the positive mode using ACN/MeOH/$H_2O$ (49.5:49.5:1) as solvent.

Elemental analyses were performed at the microanalytical laboratory of the University of Vienna with a PerkinElmer 2400 Series II CHNS/O Elemental Analyzer for CHN analyses or Eurovector EA3000 Elemental Analyzer for CHNS analyses.

UV/vis measurements were performed with a Perkin Elmer Lambda 35 photometer with PTP (Peltier Temperature Programmer) and Julabo AWC 100 recirculating cooler.

The synthesis microwave used was a Biotage® Initiator+.

## 4.2 Materials

All solvents were obtained from commercial sources and no additional purification was performed. α-Terpinene (Alfa Aesar, 90+ %), 1,1-Cyclobutanedicarboxylic acid (ACROS, 99 %), clofarabine (BLD pharm, 99.9 %), 2,6-dichloro-9-methly-9H-purine (BLD pharm, 97 %), maltol (SAFC, >99.0 %), maleic (Fluka, 99%), aqueous $NH_3$ (30 - 33 %, Sigma Aldrich, puriss.), 1,3,5-triaza-7-phosphaadamantane (Alfa Aesar, 97+ %), sodium methoxide (TCI, >96 %), sodium oxalate (Fluka, ≥99.5 %) were used without further purification.

## 4.3 Solubility in Aqueous Medium

The solubility of the complexes **3a-l** and **3b-l** was determined in PBS with 1 % DMSO (pH 7.4). In the initial step, the compounds were dissolved in pure DMSO. Specifically, 1 mg of the substance was weighed and DMSO was added in steps of 10 µL. Subsequently, 10 µL of this stock solution was added to 990 µL of PBS.

## 4.4 Syntheses

2-Chloro-9-methyl-9H-purin-6-amine: **a**

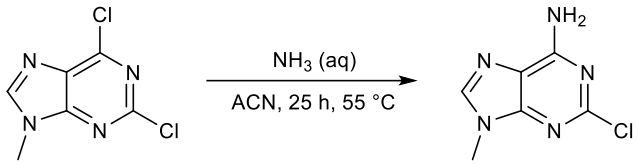


**a**

2,6-Dichloro-9-methyl-9H-purine (0.704 g, 3.5 mmol, 1.0 eq.) was dissolved in 8 mL acetonitrile. Thereafter, aqueous ammonia solution (30 – 33%, 3.25 mL, 2.925 g, 26.7 mmol, 7.5 eq.) was added to the solution and stirred for 5.5 h at 55°C. After that another aliquot of ammonia solution (30 – 33%, 3.25 mL, 2.925 g, 26.7 mmol, 7.5 eq.) was added and stirred for additional 19.5 h at 55°C. Then, the solvent was removed under reduced pressure, the residue was suspended in methanol. The solid was filtered off and dried in vacuum at 50°C. The white solid was obtained in excellent yield (0.591 g, 93%).

$^{1}$H-NMR (600.18 MHz, DMSO d-6) δ = 8.09 (s, 1H, H5), 7.70 (s, 2H, 1-$NH_2$), 3.68 (s, 3H, H6) ppm.

$^{13}$C-NMR (150.92 MHz, DMSO d-6) δ = 156.5 ($C_q$, C1), 152.7 ($C_q$, C2), 150.8 ($C_q$, C3), 141.9 (CH, C5), 117.5 ($C_q$, C4), 29.4 ($CH_3$, C6) ppm.

EA: $C_6H_6N_5Cl$, calcd. C 39.25 H 3.29 N 38.15, found C 39.09 H 3.24 N 37.92 w-%.

HR-MS: calcd. 184.0390, found 184.0383 g/mol [M + $H^+$].

Bis[dichlorido(η$^6$-*p*-cymene)ruthenium(II)]: **1**

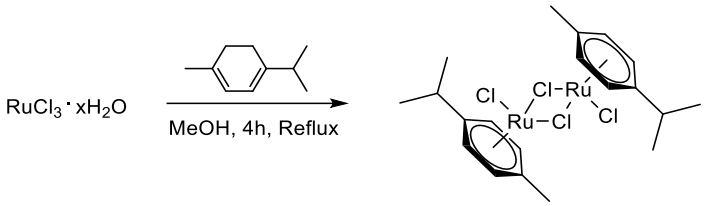


**1**

$RuCl_3 \cdot x\,H_2O$ (1.22 g, 5.88 mmol, 1 eq.) was suspended in 95 mL of methanol. Subsequently, α-terpinene (3.70 mL, 22.81 mmol, 5 eq.) was added. The resulting black mixture was refluxed while stirring for 4 hours, during which the color transitioned from black to red. Following this, the reaction mixture was allowed to cool to room temperature and then reduced to one-third under reduced pressure. Diethyl ether was then added to induce precipitation of the red solid. The crystallization process was finalized by refrigerating the solution at 4 °C overnight. The resulting precipitate was subsequently isolated via filtration and washed with ether. The red solid was acquired with fair yield (1.24 g, 69%).

$^1$H-NMR (500.10 MHz, DMSO d-6) δ = 5.82 (d, *J* = 6.4 Hz, 4H, Hc), 5.78 (d, *J* = 6.4 Hz, 4H, Hd), 2.83 (hept, *J* = 6.7 Hz, 2H, Hf), 2.08 (s, 6H, Ha), 1.19 (d, *J* = 6.9 Hz, 12H, Hg) ppm.

[Dichlorido(2-chloro-9-methyl-9H-purin-6-amine-κ$N^7$)(η$^6$-*p*-cymene)ruthenium(II)]: **2a**

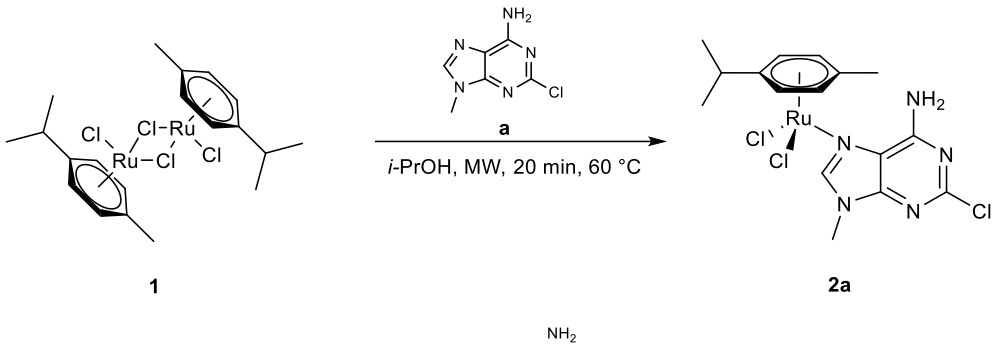


**1** **2a**

$NH_2$

$[Ru(p\text{-cym})Cl_2]_2$ (0.095 g, 0.155 mmol, 1 eq.) and 2-chloro-9-methyl-9H-purin-6-amine (0.055 g, 0.300 mmol, 2 eq.) were suspended in 5 mL 2-propanol. The mixture was reacted under microwave conditions for 20 min at 60 °C. After cooling down, the orange precipitate was filtered off and washed with diethyl ether. The orange solid was dried at 50 °C in vacuum and was obtained in good yield (0.103 g, 70%).

$^1$H-NMR (700.40 MHz, DMSO d-6) δ = 8.09 (s, 1H, H5), 7.70 (s, 2H, 1-$NH_2$), 5.81 (d, *J* = 6.5 Hz, 2H, Hd), 5.77 (d, *J* = 6.5 Hz, 2H, Hc), 3.68 (s, 3H, H6), 2.83 (hept, *J* = 7.0 Hz, 1H, Hf), 2.09 (s, 3H, Ha), 1.19 (d, *J* = 6.9 Hz, 6H, Hg) ppm.

$^{13}$C-NMR (176.12 MHz, DMSO d-6) δ = 156.7 ($C_q$, C1), 152.9 ($C_q$, C2), 150.9 ($C_q$, C3), 142.0 (CH, C5), 117.6 ($C_q$, C4), 106.4 ($C_q$, Ce), 100.1 ($C_q$, Cb), 86.3 (CH, Cc), 85.5 (CH, Cd), 29.9 (CH, Cf), 29.5 ($CH_3$, C6), 21.4 ($CH_3$, Cg), 17.8 ($CH_3$, Ca) ppm.

EA: $C_{16}H_{20}N_5Cl_3Ru$, calcd. C 39.24 H 4.12 N 14.30, found C 38.87 H 4.04 N 14.33 w-%.

HR-MS: calcd. 487.9749, found 487.9755 g/mol [M - $H^+$].

[Dichlorido((2R,3R,4S,5R)-5-(6-amino-2-chloropurin-9-yl)-4-fluoro-2(hydroxymethyl) oxolan-3-ol-κ$N^7$)(η$^6$-*p*-cymene)ruthenium(II)]: **2b**

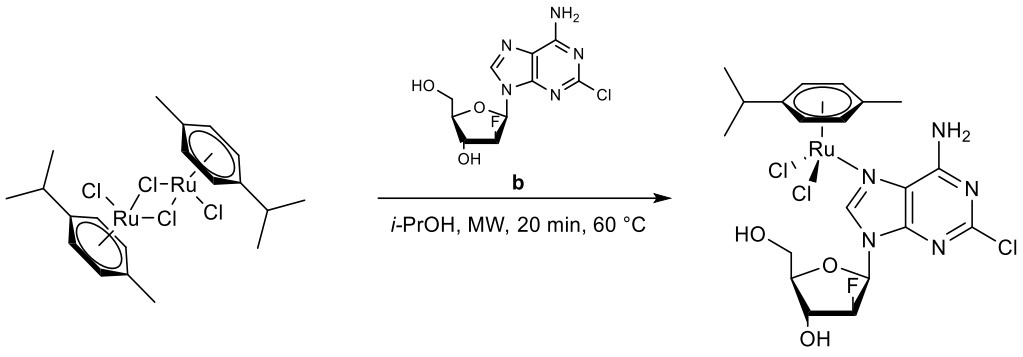


**1** **2b**

[Ru(*p*-cymene)$Cl_2$]$_2$ (0.071 g, 0.116 mmol, 1 eq.) and clofarabine (0.070 g, 0.231 mmol, 2 eq.) were dissolved in 5 mL MeOH. The dark orange mixture was stirred for 20 min at 60 °C under microwave conditions. After cooling to room temperature, the solvent was removed under reduced pressure. The orange solid was dried at 50 °C *in vacuo* and was obtained in excellent yield (0.138 g, 97%).

$^1$H NMR (700.40 MHz, DMSO d-6) δ = 8.27 (d, *J* = 1.9 Hz, 1H, H5), 7.88 (s, 2H, 1-$NH_2$), 6.32 (dd, *J* = 13.8, 4.6 Hz, 1H, H6), 5.95 (d, *J* = 5.2 Hz, 1H, 8-OH), 5.81 (d, *J* = 6.1 Hz, 2H, Hc), 5.77 (d, *J* = 6.3 Hz, 2H, Hd), 5.22 (dt, *J* = 52.7, 4.3 Hz, 1H, H7), 5.07 (t, *J* = 5.7 Hz, 1H, 10-OH), 4.42 (ddd, *J* = 18.9, 9.4, 5.2 Hz, 1H, H8), 3.84 (q, *J* = 4.8 Hz, 1H, H9), 3.72 – 3.60 (m, 2H, H10), 2.83 (hept, *J* = 7.0 Hz, 1H, Hf), 2.09 (s, 3H, Ha), 1.19 (d, *J* = 6.9 Hz, 6H, Hg) ppm.

$^{13}$C NMR (176.12 MHz, DMSO d-6) δ = 156.8 ($C_q$, C1), 153.2 ($C_q$, C2), 150.1 ($C_q$, C3), 140.0(CH, C5), 117.3 ($C_q$, C4), 106.4 ($C_q$, Ce), 100.1 ($C_q$, Cb), 95.9 (CH, C7), 94.8 (CH, C7), 86.3 (CH, Cd), 85.5 (CH, Cc), 83.5 (CH, C9), 81.4 (CH, C6), 72.5 (CH, C8), 60.3 ($CH_2$, C10), 30.0 (Ch, Cf), 21.5 ($CH_3$, Cg), 17.8 ($CH_3$, Ca) ppm.

EA: $C_{20}H_{25}N_5Cl_3O_3FRu \cdot 0.7\ H_2O$, calcd. C 38.59 H 4.27 N 11.25, found C 38.32 H 4.13 N 11.57 w-%.

HR-MS: calcd. 607.9972, found 607.9978 g/mol [M - $H^+$].

[Oxalato-κ*O*$^1$,κ*O*$^2$(2-chloro-9-methyl-9H-purin-6-amine-κ*N*$^7$)(η$^6$-*p*-cymene)ruthenium(II)]: **3a-l**

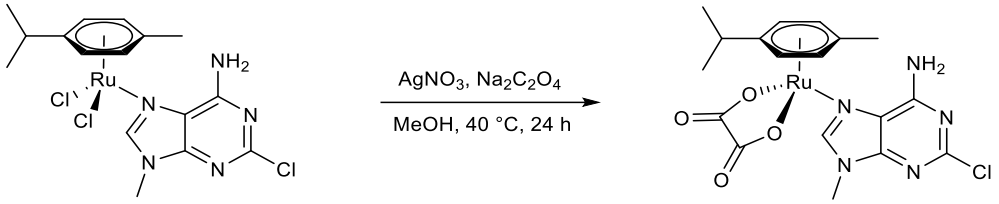


**2a** **3a-l**

[Dichlorido(2-chloro-9-methyl-9H-purin-6-amine-κ*N*$^7$)(η$^6$-*p*-cymene)ruthenium(II)] **2a** (0.050 g, 0.102 mmol, 1 eq.) and $AgNO_3$ (0.0347 g, 0.204 mmol, 2 eq.) were suspended in 2 mL methanol and stirred for 30 min under exclusion of light. Subsequently, the sodium oxalate (0.014 g, 0.107 mmol, 1.05 eq.) was added. The mixture was stirred overnight at 40 °C under light exclusion, whereby the color of the suspension changed from orange to yellow. On the following day, the mixture was filtered over celite, and the solvent was removed under reduced pressure. The crude product was dissolved in DCM and precipitated with hexane. After removing the solvents under reduced pressure, the ocher product was dried in vacuum at 40 °C and obtained in very good yield (0.086 g, 83%).

$^1$H-NMR (700.40 MHz, MeOD) δ = 8.32 (s, 1H, H5), 5.90 (s, 1H, Hd), 5.88 (s, 1H, Hd), 5.62 (s, 1H, Hc), 5.56 (s, 1H, Hc), 3.86 (s, 3H, H6), 2.88 (hept, *J* = 6.8 Hz, 1H, Hf), 1.97 (s, 3H, Ha), 1.33 (d, *J* = 6.9 Hz, 6H, Hg) ppm.

$^{13}$C-NMR (176.12 MHz, MeOD) δ = 167.6 ($C_q$, CI/II), 166.6 ($C_q$, CI/II), 156.7 ($C_q$, C1), 156.3 ($C_q$, C2), 152.1 ($C_q$, C3), 146.9 (CH, C5), 117.7 ($C_q$, C4), 103.7 ($C_q$, Ce), 98.9 ($C_q$, Cb), 83.4 (CH, Cd), 83.3 (CH, Cd), 81.0 (CH, Cc), 32.0 (CH, Cf), 30.8 ($CH_3$, C6), 22.5 ($CH_3$, Cg), 17.7 ($CH_3$, Ca) ppm.

HR-MS: calcd. 506.0169, found 506.0175 g/mol [M - H$^+$].

Solubility (PBS, pH 7.4, 1% DMSO): 50 mg/mL, 98 mM.

[Oxalato-κ$O^1$,κ$O^2$((2R,3R,4S,5R)-5-(6-amino-2-chloropurin-9-yl)-4-fluoro-2(hydroxymethyl) oxolan-3-ol- κ$N^7$)(η$^6$-*p*-cymene)ruthenium(II)]: **3b-l**

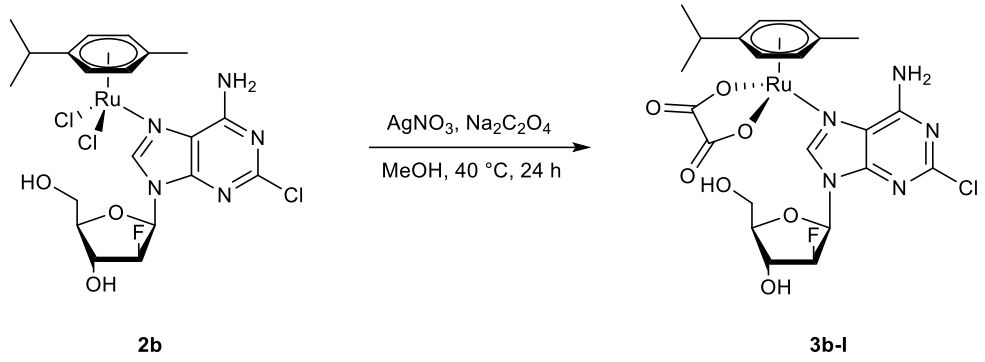


**2b** **3b-l**

A mixture of [dichlorido((2R,3R,4S,5R)-5-(6-amino-2-chloropurin-9-yl)-4-fluoro-2(hydroxy-methyl)oxolan-3-ol-κ$N^7$)(η$^6$-*p*-cymene)ruthenium(II)] **2b** (0.050 g, 0.082 mmol, 1 eq.) and $AgNO_3$ (0.028 g, 0.164 mmol, 2 eq.) was suspended in 2 mL of methanol and stirred for 30 minutes at 40 °C under exclusion of light. Next, the sodium oxalate (0.012 g, 0.086 mmol, 1.05 eq.) was added to the mixture, continuing stirring overnight under light exclusion at 40°C. Throughout this time period, the color of the suspension shifted from orange to yellow. The mixture was filtered using celite and the solvent was removed under reduced pressure. The resulting crude product was dissolved in methanol and precipitated by adding DCM. Afterwards, the solvents were removed under reduced pressure and the product was dried in vacuum at 40 °C. The ocher product was obtained in excellent yield (0.093 g, 90%).

$^1$H-NMR (700.40 MHz, DMSO d-6) δ = 8.27 (d, *J* = 1.9 Hz, 1H, H5), 7.88 (s, 2H, 1-$NH_2$), 6.32 (dd, *J* = 13.8, 4.7 Hz, 1H, H6), 6.01 (d, *J* = 6.2 Hz, 2H, Hd), 5.95 (d, *J* = 5.4 Hz, 1H, 8-OH), 5.89 (d, *J* = 6.5 Hz, 2H, Hc), 5.22 (dt, *J* = 52.5, 4.3 Hz, 1H, H7), 5.07 (t, *J* = 5.7 Hz, 1H, 10-OH), 4.42 (ddd, *J* = 18.9, 9.2, 5.2 Hz, 1H, H8), 3.84 (q, *J* = 4.8 Hz, 1H, H9), 3.71 – 3.60 (m, 2H, H10), 2.77 (hept, *J* = 6.9 Hz, 1H, Hf), 2.13 (s, 3H, Ha), 1.28 – 1.23 (m, 6H, Hg) ppm.

$^{13}$C-NMR (176.12 MHz, DMSO d-6) δ = 166.8 ($C_q$, Cl/II), 164.3 ($C_q$, Cl/II), 156.8 ($C_q$; C1), 153.2 ($C_q$, C2), 150.1 ($C_q$, C3), 140.0 (CH, C5), 117.3 ($C_q$, C4), 104.7 ($C_q$, Ce), 99.5 ($C_q$, Cb), 95.9 (CH, C7), 94.8 (CH, C7), 86.6 (CH, Cd), 85.6 (CH, Cc), 83.5 (CH, C9), 83.5 (CH, C9), 81.5 (CH, C6), 81.4 (CH, C6), 72.6 (CH, C8), 72.4 (CH, C8), 60.3 ($CH_2$, C10), 30.4 (CH, Cf), 22.0 ($CH_3$, Cg), 17.2 ($CH_3$, Ca), 17.1 ($CH_3$, Ca) ppm.

HR-MS: calcd. 650.0368, found 650.0362 g/mol [M + $Na^+$].

Solubility (PBS, pH 7.4, 1% DMSO): 50 mg/mL, 80 mM.

# 5 Conclusion and Outlook

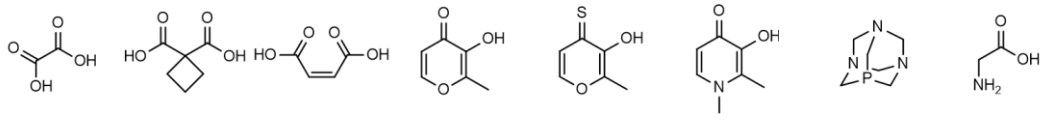

| | I | II | III | IV | V | VI | VII | VIII |
|---|---|---|---|---|---|---|---|---|
| Synthesis | ✓ | × | × | ✓ | × | × | × | × |
| Purification | ~ | × | × | × | × | × | × | × |

*Figure 34: Overview of the eight ligands tested, with a summary of synthesis and purification outcomes.*

In conclusion, this thesis attempted the synthesis and characterization of novel clofarabine-bearing organometallic ruthenium complexes, building on precursor complexes with adenine derivatives and clofarabine as ligands, previously developed by a previous master's student. A series of new ruthenium complexes was attempted to be synthesized using ligand exchange techniques, in which eight different ligands were tested.

Of the eight tested ligands, only two complexes – with maltolate (**IV**) and oxalate (**I**) ligands – were successfully synthesized with the model adenine derivatives (Figure 34). However, only the oxalate complex could be purified, albeit not to a level of elemental-analysis purity. The partial success in synthesizing the oxalate complex prompted the further synthesis of the corresponding clofarabine complex. Characterization of the synthesized complexes via NMR spectroscopy and mass spectrometry confirmed the successful formation of the two oxalate complexes with the adenine derivative and clofarabine, respectively. Stability studies revealed that the two semi-purified complexes remained stable in aqueous solutions for at least 24 hours, indicating a potential for biological applications. The other seven ligands failed to form viable complexes with the adenine model ligand and were therefore not pursued for further synthesis with clofarabine.

Throughout the synthesis and purification processes, several challenges emerged. In many cases, the desired complexes did not form as anticipated, often resulting in mixtures of compounds, as seen with the glycine (**VIII**) or cbdca (**II**) ligands, or ligand detachment during reactions, as observed with PTA (**VII**). Even after successful synthesis, purification proved problematic, particularly with the maltolate complex. Attempts to further purify the maltolate complex by re-dissolving it in various solvents led to the degradation of the complex. The oxalate complex was the exception, displaying both high solubility and stability, although only partial purification was achieved. In this case, precipitation was the only viable purification method, as MPLC methods proved ineffective. The difficulties regarding the

purification steps can likely be attributed to the underlying instability of the O,O-coordination in the oxalate and maltol bidentate ligands.

Despite the challenges in purification, the results of this work provide new insights into the development of ruthenium-based anticancer drugs. Future work is required to explore alternative purification strategies to achieve a higher level of purity, which are essential for conducting biological assays, such as assessing the complexes' activity on cancer cell lines. The knowledge gained provides a solid foundation for further research and, with additional refinement, these complexes may have the potential to make a significant contribution to cancer therapy.

# 6 References


(1) *Cancer*. WHO. https://www.who.int/news-room/fact-sheets/detail/cancer (accessed 2024-07-24).

(2) Bray, F.; Laversanne, M.; Weiderpass, E.; Soerjomataram, I. The Ever-increasing Importance of Cancer as a Leading Cause of Premature Death Worldwide. *Cancer* **2021**, *127* (16), 3029–3030. https://doi.org/10.1002/cncr.33587.

(3) *Global Burden of Disease 2021: Findings from the GBD 2021 Study.* Institute for Health Metrics and Evaluation (IHME).

(4) Bennett, J. E.; Kontis, V.; Mathers, C. D.; Guillot, M.; Rehm, J.; Chalkidou, K.; Kengne, A. P.; Carrillo-Larco, R. M.; Bawah, A. A.; Dain, K.; Varghese, C.; Riley, L. M.; Bonita, R.; Kruk, M. E.; Beaglehole, R.; Ezzati, M. NCD Countdown 2030: Pathways to Achieving Sustainable Development Goal Target 3.4. *The Lancet* **2020**, *396* (10255), 918–934. https://doi.org/10.1016/S0140-6736(20)31761-X.

(5) *Worldwide cancer data*. World Cancer Research Fund International. https://www.wcrf.org/cancer-trends/worldwide-cancer-data/ (accessed 2024-04-24).

(6) Bray, F.; Laversanne, M.; Sung, H.; Ferlay, J.; Siegel, R. L.; Soerjomataram, I.; Jemal, A. Global Cancer Statistics 2022: GLOBOCAN Estimates of Incidence and Mortality Worldwide for 36 Cancers in 185 Countries. *CA. Cancer J. Clin.* **2024**, *74* (3), 229–263. https://doi.org/10.3322/caac.21834.

(7) Hanahan, D.; Weinberg, R. A. The Hallmarks of Cancer. *Cell* **2000**, *100* (1), 57–70. https://doi.org/10.1016/S0092-8674(00)81683-9.

(8) Hanahan, D. Hallmarks of Cancer: New Dimensions. *Cancer Discov.* **2022**, *12* (1), 31–46. https://doi.org/10.1158/2159-8290.CD-21-1059.

(9) *Hallmarks of Cancer*. Rockland Immunochemicals. https://www.rockland.com/resources/hallmarks-of-cancer/ (accessed 2024-08-14).

(10) *Treatment Types*. American Cancer Society. https://www.cancer.org/cancer/managing-cancer/treatment-types.html (accessed 2024-07-25).

(11) *Radiation therapy to treat cancer*. National Cancer Institute. https://www.cancer.gov/about-cancer/treatment/types/radiation-therapy (accessed 2024-07-26).

(12) *Immunotherapy In-Depth*. CRI - Cancer Research Institute. https://www.cancerresearch.org/what-is-immunotherapy (accessed 2024-07-26).

(13) *Targeted Therapy*. American Cancer Society. https://www.cancer.org/cancer/managing-cancer/treatment-types/targeted-therapy/what-is.html (accessed 2024-07-26).

(14) *Die Chemotherapie*. Krebsgesellschaft Deutschland, ONKO Internetportal. https://www.krebsgesellschaft.de/onko-internetportal/basis-informationen-krebs/therapieformen/chemotherapie.html (accessed 2024-07-26).

(15) Löbermann, M.; Boršo, D.; Hilgendorf, I.; Fritzsche, C.; Zettl, U. K.; Reisinger, E. C. Immunization in the Adult Immunocompromised Host. *Autoimmun. Rev.* **2012**, *11* (3), 212–218. https://doi.org/10.1016/j.autrev.2011.05.015.

(16) Holland, J. F.; Frei, E.; Kufe, D. W. Alkylating Agents. In *Cancer Medicine*; BC Decker Inc., Hamilton, Ont, 2003.

(17) *LiverTox: Clinical and Research Information on Drug-Induced Liver Injury; Alkylating Agents*. National Library of Medicine. https://www.ncbi.nlm.nih.gov/books/NBK547849/ (accessed 2024-07-24).

(18) Fischer, D. S. Cancer Chemotherapeutic Agents. *Encycl. Toxicol.* **2005**, No. 2, 384–401. https://doi-org.uaccess.univie.ac.at/10.1016/B0-12-369400-0/10018-3.

(19) Schultz, M.; Dutta, S.; Tew, K. D. Inhibitors of Glutathione S-Transferases as Therapeutic Agents. *Adv. Drug Deliv. Rev.* **1997**, *26* (2–3), 91–104. https://doi.org/10.1016/S0169-409X(97)00029-X.

(20) Liu, D. Q.; Sun, M.; Kord, A. S. Recent Advances in Trace Analysis of Pharmaceutical Genotoxic Impurities. *J. Pharm. Biomed. Anal.* **2010**, *51* (5), 999–1014. https://doi.org/10.1016/j.jpba.2009.11.009.

(21) Puyo, S.; Montaudon, D.; Pourquier, P. From Old Alkylating Agents to New Minor Groove Binders. *Crit. Rev. Oncol. Hematol.* **2014**, *89* (1), 43–61. https://doi.org/10.1016/j.critrevonc.2013.07.006.

(22) Gao, Y.; Shang, Q.; Li, W.; Guo, W.; Stojadinovic, A.; Mannion, C.; Man, Y.; Chen, T. Antibiotics for Cancer Treatment: A Double-Edged Sword. *J Cancer* **2020**, *11* (17), 5135–5149. https://doi.org/10.7150/jca.47470.

(23) Wang, Y.; Fu, M.; Liu, J.; Yang, Y.; Yu, Y.; Li, J.; Pan, W.; Fan, L.; Li, G.; Li, X.; Wang, X. Inhibition of Tumor Metastasis by Targeted Daunorubicin and Dioscin Codelivery

Liposomes Modified with PFV for the Treatment of Non-Small-Cell Lung Cancer. *Int J Nanomedicine* **2019**, 4071–4090. https://doi.org/10.2147%2FIJN.S194304.

(24) Al-Aamri, H. M.; Ku, H.; Irving, H. R.; Tucci, J.; Meehan-Andrews, T.; Bradley, C. Time Dependent Response of Daunorubicin on Cytotoxicity, Cell Cycle and DNA Repair in Acute Lymphoblastic Leukaemia. *BMC Cancer* **2019**, *19* (1), 179. https://doi.org/10.1186/s12885-019-5377-y.

(25) Chandraprasad, M. S.; Dey, A.; Swamy, M. K. Introduction to Cancer and Treatment Approaches. In *Paclitaxel*; Elsevier, 2022; pp 1–27. https://doi.org/10.1016/B978-0-323-90951-8.00010-2.

(26) Parker, W. B. Enzymology of Purine and Pyrimidine Antimetabolites Used in the Treatment of Cancer. *Chem. Rev.* **2009**, *109* (7), 2880–2893. https://doi.org/10.1021/cr900028p.

(27) Dhyani, P.; Quispe, C.; Sharma, E.; Bahukhandi, A.; Sati, P.; Attri, D. C.; Szopa, A.; Sharifi-Rad, J.; Docea, A. O.; Mardare, I.; Calina, D.; Cho, W. C. Anticancer Potential of Alkaloids: A Key Emphasis to Colchicine, Vinblastine, Vincristine, Vindesine, Vinorelbine and Vincamine. *Cancer Cell Int.* **2022**, *22* (1), 206. https://doi.org/10.1186/s12935-022-02624-9.

(28) Ngo, Q. A.; Roussi, F.; Cormier, A.; Thoret, S.; Knossow, M.; Guénard, D.; Guéritte, F. Synthesis and Biological Evaluation of Vinca Alkaloids and Phomopsin Hybrids. *J. Med. Chem.* **2009**, *52* (1), 134–142. https://doi.org/10.1021/jm801064y.

(29) Khalid, E. B.; Ayman, E.-M. E.-K.; Rahman, H.; Abdelkarim, G.; Najda, A. Natural Products against Cancer Angiogenesis. *Tumor Biol.* **2016**, *37* (11), 14513–14536. https://doi.org/10.1007/s13277-016-5364-8.

(30) Shahpar, S.; Mhatre, P. V.; Oza, S. Rehabilitation. In *The Breast*; Elsevier, 2018; pp 1031-1038.e3. https://doi.org/10.1016/B978-0-323-35955-9.00083-0.

(31) Turunen, B. J.; Ge, H.; Oyetunji, J.; Desino, K. E.; Vasandani, V.; Güthe, S.; Himes, R. H.; Audus, K. L.; Seelig, A.; Georg, G. I. Paclitaxel Succinate Analogs: Anionic and Amide Introduction as a Strategy to Impart Blood–Brain Barrier Permeability. *Bioorg. Med. Chem. Lett.* **2008**, *18* (22), 5971–5974. https://doi.org/10.1016/j.bmcl.2008.09.103.

(32) Martino, E.; Della Volpe, S.; Terribile, E.; Benetti, E.; Sakaj, M.; Centamore, A.; Sala, A.; Collina, S. The Long Story of Camptothecin: From Traditional Medicine to Drugs. *Bioorg. Med. Chem. Lett.* **2017**, *27* (4), 701–707. https://doi.org/10.1016/j.bmcl.2016.12.085.

(33) *Cytostatic Drugs as a Weapon against Cancer*. Therapy Select. https://www.therapyselect.de/en/blog/cytostatic-drugs-weapon-against-cancer (accessed 2024-07-27).

(34) Kostova, I. Platinum Complexes as Anticancer Agents. *Recent Patents Anticancer Drug Discov.* **2006**, *1* (1), 1–22. https://doi.org/10.2174/157489206775246458.

(35) Kühn, F. E.; Schmidt, A. Metallkomplexe als Antikrebsmittel: Konzepte in der Tumorforschung und Wirkmechanismen. *Chem. Unserer Zeit* **2017**, *51* (2), 86–95. https://doi.org/10.1002/ciuz.201600756.

(36) Ott, I.; Gust, R. Medizinische Chemie der Platinkomplexe: Besonderheiten anorganischer Zytostatika. *Pharm. Unserer Zeit* **2006**, *35* (2), 124–133. https://doi.org/10.1002/pauz.200500161.

(37) Oun, R.; Wheate, N. J. Platinum Anticancer Drugs. In *Encyclopedia of Metalloproteins*; Springer, New York, NY; pp 1710–1714.

(38) Adhikari, S.; Nath, P.; Das, A.; Datta, A.; Baildya, N.; Duttaroy, A. K.; Pathak, S. A Review on Metal Complexes and Its Anti-Cancer Activities: Recent Updates from in Vivo Studies. *Biomed. Pharmacother.* **2024**, *171*, 116211. https://doi.org/10.1016/j.biopha.2024.116211.

(39) Zhang, C.; Xu, C.; Gao, X.; Yao, Q. Platinum-Based Drugs for Cancer Therapy and Anti-Tumor Strategies. *Theranostics* **2022**, *12* (5), 2115–2132. https://doi.org/10.7150/thno.69424.

(40) Ali, I.; A. Wani, W.; Saleem, K.; Haque, A. Platinum Compounds: A Hope for Future Cancer Chemotherapy. *Anticancer Agents Med. Chem.* **2013**, *13* (2), 296–306. https://doi.org/10.2174/1871520611313020016.

(41) Lucaciu, R. L.; Hangan, A. C.; Sevastre, B.; Oprean, L. S. Metallo-Drugs in Cancer Therapy: Past, Present and Future. *Molecules* **2022**, *27* (19), 6485. https://doi.org/10.3390/molecules27196485.

(42) *Definition von antineoplastic*. https://www.collinsdictionary.com/de/worterbuch/englisch/antineoplastic#:~:text=An%20antineoplastic%20is%20any%20drug,and%20spread%20of%20cancerous%20cells. (accessed 2024-07-31).

(43) Alberto, M. E.; Lucas, M. F. A.; Pavelka, M.; Russo, N. The Second-Generation Anticancer Drug Nedaplatin: A Theoretical Investigation on the Hydrolysis Mechanism. *J. Phys. Chem. B* **2009**, *113* (43), 14473–14479. https://doi.org/10.1021/jp9056835.

(44) McKeage, M. J. Lobaplatin: A New Antitumour Platinum Drug. *Expert Opin. Investig. Drugs* **2001**, *10* (1), 119–128. https://doi.org/10.1517/13543784.10.1.119.

(45) Wheate, N. J.; Walker, S.; Craig, G. E.; Oun, R. The Status of Platinum Anticancer Drugs in the Clinic and in Clinical Trials. *Dalton Trans.* **2010**, *39* (35), 8113. https://doi.org/10.1039/c0dt00292e.

(46) Jj, F.; Dj, K.; Aa, A.; Ka, F.; Jr, H. W. Platinum-Containing Cytostatic Drugs. **2006**.

(47) Collery, P.; Keppler, B.; Madoulet, C.; Desoize, B. Gallium in Cancer Treatment. **2002**.

(48) Van Rijt, S. H.; Sadler, P. J. Current Applications and Future Potential for Bioinorganic Chemistry in the Development of Anticancer Drugs. *Drug Discov. Today* **2009**, *14* (23–24), 1089–1097. https://doi.org/10.1016/j.drudis.2009.09.003.

(49) Wilke, N. L.; Abodo, L. O.; Frias, C.; Frias, J.; Baas, J.; Jakupec, M. A.; Keppler, B. K.; Prokop, A. The Gallium Complex KP46 Sensitizes Resistant Leukemia Cells and Overcomes Bcl-2-Induced Multidrug Resistance in Lymphoma Cells via Upregulation of Harakiri and Downregulation of XIAP in Vitro. *Biomed. Pharmacother.* **2022**, *156*, 113974. https://doi.org/10.1016/j.biopha.2022.113974.

(50) *Research Topics - Institute of Inorganic Chemistry*. Universität Wien. https://anorg-chemie.univie.ac.at/research/bioinorganic-chemistry/research-focus/.

(51) Schilling, T.; Keppler, K. B.; Heim, M. E.; Niebch, G.; Dietzfelbinger, H.; Rastetter, J.; Hanauske, A.-R. Clinical Phase I and Pharmacokinetic Trial of the New Titanium Complex Budotitane. *Invest. New Drugs* **1995**, *13* (4), 327–332. https://doi.org/10.1007/BF00873139.

(52) Keppler, B. K.; Friesen, C.; Moritz, H. G.; Vongeriehten, H.; Vogel, E. Tumor-Inhibiting Bis(13-Diketonato) Metal Complexes. Budotitane, Cis-Diethoxybis(1- Phenylbutane-1,3-Dionato)Titanium (IV).

(53) Tiekink, E. R. T. Gold Derivatives for the Treatment of Cancer. *Crit. Rev. Oncol. Hematol.* **2002**, *42* (3), 225–248. https://doi.org/10.1016/S1040-8428(01)00216-5.

(54) Ilari, A.; Baiocco, P.; Messori, L.; Fiorillo, A.; Boffi, A.; Gramiccia, M.; Di Muccio, T.; Colotti, G. A Gold-Containing Drug against Parasitic Polyamine Metabolism: The X-Ray Structure of Trypanothione Reductase from Leishmania Infantum in Complex with Auranofin Reveals a Dual Mechanism of Enzyme Inhibition. *Amino Acids* **2012**, *42* (2–3), 803–811. https://doi.org/10.1007/s00726-011-0997-9.

(55) Paprocka, R.; Wiese-Szadkowska, M.; Janciauskiene, S.; Kosmalski, T.; Kulik, M.; Helmin-Basa, A. Latest Developments in Metal Complexes as Anticancer Agents. *Coord. Chem. Rev.* **2022**, *452*, 214307. https://doi.org/10.1016/j.ccr.2021.214307.

(56) Enzo Alessio; Giovanni Mestroni; Alberta Bergamo; Gianni Sava. Ruthenium Antimetastatic Agents. *Curr. Top. Med. Chem.* **2004**, *4* (15), 1525–1535. https://doi.org/10.2174/1568026043387421.

(57) Gransbury, G. K.; Kappen, P.; Glover, C. J.; Hughes, J. N.; Levina, A.; Lay, P. A.; Musgrave, I. F.; Harris, H. H. Comparison of KP1019 and NAMI-A in Tumour-Mimetic Environments. *Metallomics* **2016**, *8* (8), 762–773. https://doi.org/10.1039/C6MT00145A.

(58) Berger, M. R.; Garzon, F. T.; Keppler, B. K.; Schmähl, D. Efficacy of New Ruthenium Complexes against Chemically Induced Autochthonous Colorectal Carcinoma in Rats. *Anticancer Res* **1989**, *9* (3), 761–765.

(59) Meier-Menches, S. M.; Gerner, C.; Berger, W.; Hartinger, C. G.; Keppler, B. K. Structure–Activity Relationships for Ruthenium and Osmium Anticancer Agents – towards Clinical Development. *Chem. Soc. Rev.* **2018**, *47* (3), 909–928. https://doi.org/10.1039/C7CS00332C.

(60) Cetinbas, N.; Webb, M. I.; Dubland, J. A.; Walsby, C. J. Serum-Protein Interactions with Anticancer Ru(III) Complexes KP1019 and KP418 Characterized by EPR. *JBIC J. Biol. Inorg. Chem.* **2010**, *15* (2), 131–145. https://doi.org/10.1007/s00775-009-0578-5.

(61) Trondl, R.; Heffeter, P.; Kowol, C. R.; Jakupec, M. A.; Berger, W.; Keppler, B. K. NKP-1339, the First Ruthenium-Based Anticancer Drug on the Edge to Clinical Application. *Chem Sci* **2014**, *5* (8), 2925–2932. https://doi.org/10.1039/C3SC53243G.

(62) Blazevic, A.; Hummer, A. A.; Heffeter, P.; Berger, W.; Filipits, M.; Cibin, G.; Keppler, B. K.; Rompel, A. Electronic State of Sodium Trans-[Tetrachloridobis(1H-Indazole)Ruthenate(III)] (NKP-1339) in Tumor, Liver and Kidney Tissue of a SW480-Bearing Mouse. *Sci. Rep.* **2017**, *7* (1), 40966. https://doi.org/10.1038/srep40966.

(63) Lizardo, M. M.; Morrow, J. J.; Miller, T. E.; Hong, E. S.; Ren, L.; Mendoza, A.; Halsey, C. H.; Scacheri, P. C.; Helman, L. J.; Khanna, C. Upregulation of Glucose-Regulated Protein 78 in Metastatic Cancer Cells Is Necessary for Lung Metastasis Progression. *Neoplasia* **2016**, *18* (11), 699–710. https://doi.org/10.1016/j.neo.2016.09.001.

(64) Gifford, J. B.; Huang, W.; Zeleniak, A. E.; Hindoyan, A.; Wu, H.; Donahue, T. R.; Hill, R. Expression of GRP78, Master Regulator of the Unfolded Protein Response, Increases

Chemoresistance in Pancreatic Ductal Adenocarcinoma. *Mol. Cancer Ther.* **2016**, *15* (5), 1043–1052. https://doi.org/10.1158/1535-7163.MCT-15-0774.

(65) *BOLD-100*. bold therapeutics. https://www.bold-therapeutics.com/technology (accessed 2024-08-03).

(66) Baier, D.; Mendrina, T.; Schoenhacker-Alte, B.; Pirker, C.; Mohr, T.; Rusz, M.; Regner, B.; Schaier, M.; Sgarioto, N.; Raynal, N. J.; Nowikovsky, K.; Schmidt, W. M.; Heffeter, P.; Meier-Menches, S. M.; Koellensperger, G.; Keppler, B. K.; Berger, W. The Lipid Metabolism as Target and Modulator of BOLD-100 Anticancer Activity: Crosstalk with Histone Acetylation. *Adv. Sci.* **2023**, No. 10, 2301939. https://doi.org/10.1002/advs.202301939.

(67) Gasser, G.; Ott, I.; Metzler-Nolte, N. Organometallic Anticancer Compounds. *J. Med. Chem.* **2011**, *54* (1), 3–25. https://doi.org/10.1021/jm100020w.

(68) Clarke, M. J.; Zhu, F.; Frasca, D. R. Non-Platinum Chemotherapeutic Metallopharmaceuticals. *Chem. Rev.* **1999**, *99* (9), 2511–2534. https://doi.org/10.1021/cr9804238.

(69) Murray, B. S.; Babak, M. V.; Hartinger, C. G.; Dyson, P. J. The Development of RAPTA Compounds for the Treatment of Tumors. *Coord. Chem. Rev.* **2016**, *306*, 86–114. https://doi.org/10.1016/j.ccr.2015.06.014.

(70) Novakova, O.; Chen, H.; Vrana, O.; Rodger, A.; Sadler, P. J.; Brabec, V. DNA Interactions of Monofunctional Organometallic Ruthenium(II) Antitumor Complexes in Cell-Free Media. *Biochemistry* **2003**, *42* (39), 11544–11554. https://doi.org/10.1021/bi034933u.

(71) Yan, Y. K.; Melchart, M.; Habtemariam, A.; Sadler, P. J. Organometallic Chemistry, Biology and Medicine: Ruthenium Arene Anticancer Complexes. *Chem. Commun.* **2005**, No. 38, 4764. https://doi.org/10.1039/b508531b.

(72) Scolaro, C.; Chaplin, A. B.; Hartinger, C. G.; Bergamo, A.; Cocchietto, M.; Keppler, B. K.; Sava, G.; Dyson, P. J. Tuning the Hydrophobicity of Ruthenium(Ii)–Arene (RAPTA) Drugs to Modify Uptake, Biomolecular Interactions and Efficacy. *Dalton Trans.* **2007**, No. 43, 5065. https://doi.org/10.1039/b705449a.

(73) Kilpin, K. J.; Cammack, S. M.; Clavel, C. M.; Dyson, P. J. Ruthenium(II) Arene PTA (RAPTA) Complexes: Impact of Enantiomerically Pure Chiral Ligands. *Dalton Trans* **2013**, *42* (6), 2008–2014. https://doi.org/10.1039/C2DT32333H.

(74) Dyson, P. J.; Sava, G. Metal-Based Antitumour Drugs in the Post Genomic Era. *Dalton Trans.* **2006**, No. 16, 1929. https://doi.org/10.1039/b601840h.

(75) Hodgson, J. ADMET—Turning Chemicals into Drugs. *Nat. Biotechnol.* **2001**, *19* (8), 722–726. https://doi.org/10.1038/90761.

(76) Renfrew, A. K. Transition Metal Complexes with Bioactive Ligands: Mechanisms for Selective Ligand Release and Applications for Drug Delivery. *Metallomics* **2014**, *6* (8), 1324–1335. https://doi.org/10.1039/C4MT00069B.

(77) Rautio, J.; Kumpulainen, H.; Heimbach, T.; Oliyai, R.; Oh, D.; Järvinen, T.; Savolainen, J. Prodrugs: Design and Clinical Applications. *Nat. Rev. Drug Discov.* **2008**, *7* (3), 255–270. https://doi.org/10.1038/nrd2468.

(78) Steel, T. R.; Walsh, F.; Wieczorek-Błauż, A.; Hanif, M.; Hartinger, C. G. Monodentately-Coordinated Bioactive Moieties in Multimodal Half-Sandwich Organoruthenium Anticancer Agents. *Coord. Chem. Rev.* **2021**, *439*, 213890. https://doi.org/10.1016/j.ccr.2021.213890.

(79) Ghanem, H.; Kantarjian, H.; Ohanian, M.; Jabbour, E. The Role of Clofarabine in Acute Myeloid Leukemia. *Leuk. Lymphoma* **2013**, *54* (4), 688–698. https://doi.org/10.3109/10428194.2012.726722.

(80) Parker, W. B.; Gandhi, V. Clofarabine: Structure, Mechanism of Action, and Clinical Pharmacology. In *Chemotherapy for Leukemia*; Springer, Singapore, 2017; pp 261–286.

(81) Zhenchuk, A.; Lotfi, K.; Juliusson, G.; Albertioni, F. Mechanisms of Anti-Cancer Action and Pharmacology of Clofarabine. *Biochem. Pharmacol.* **2009**, *78* (11), 1351–1359. https://doi.org/10.1016/j.bcp.2009.06.094.

(82) Jörg, M. Novel Adenosine A2A Receptor Ligands: A Synthetic, Functional and Computational Investigation of Selected Literature Adenosine A2A Receptor Antagonists for Extending into Extracellular Space. *Bioorg Med Chem Lett* **2013**.

(83) Xu, Z.; Huang, J.; Kong, D.; Yang, Y.; Guo, L.; Jia, X.; Zhong, G.; Liu, Z. Potent Half-Sandwich Ru(Ⅱ) N^N (Aryl-BIAN) Complexes: Lysosome-Mediated Apoptosis, in Vitro and in Vivo Anticancer Activities. *Eur. J. Med. Chem.* **2020**, *207*, 112763. https://doi.org/10.1016/j.ejmech.2020.112763.

# 7 Appendix

## 7.1 List of Figures

## 7.2 List of Schemes

## 7.3 NMR Spectra

### Compound **a**

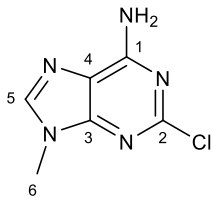


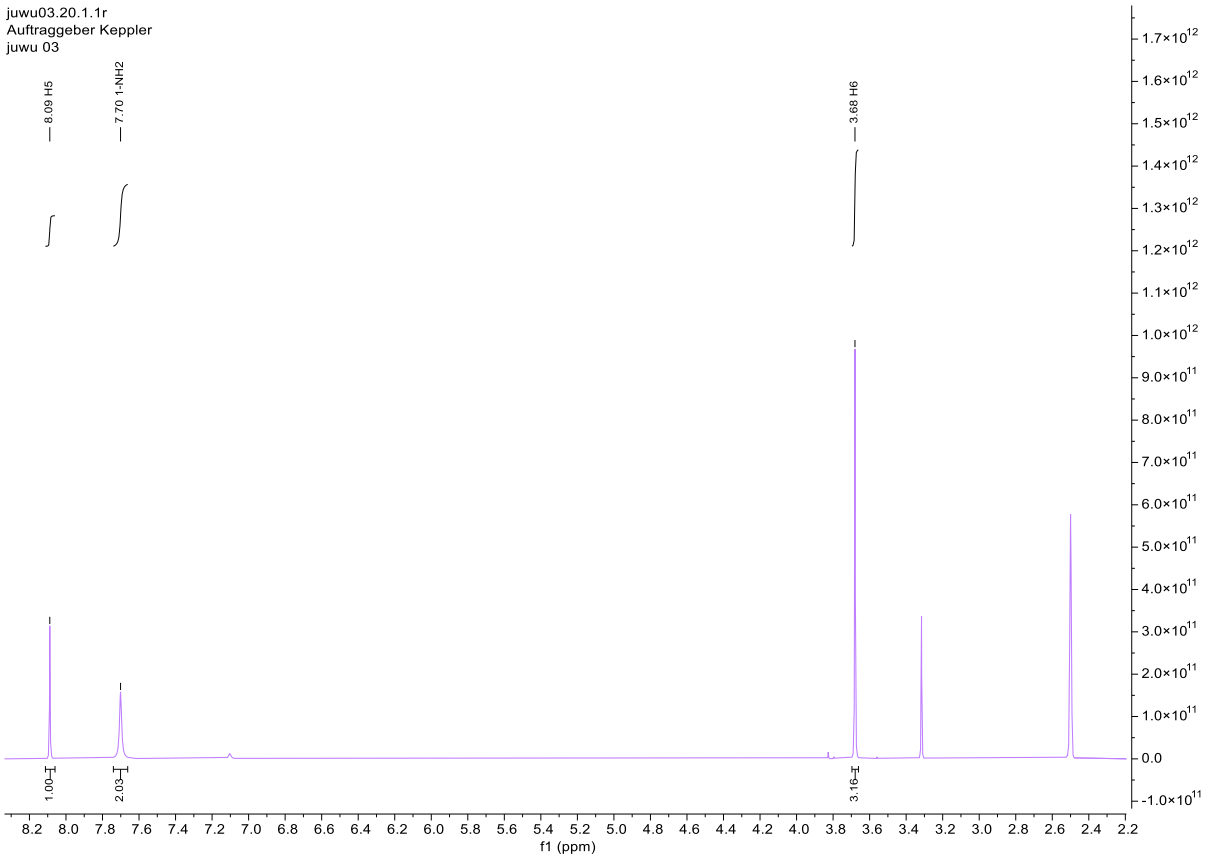


*Figure 35: $^{1}$H-NMR spectrum of compound **a** in DMSO d-6.*

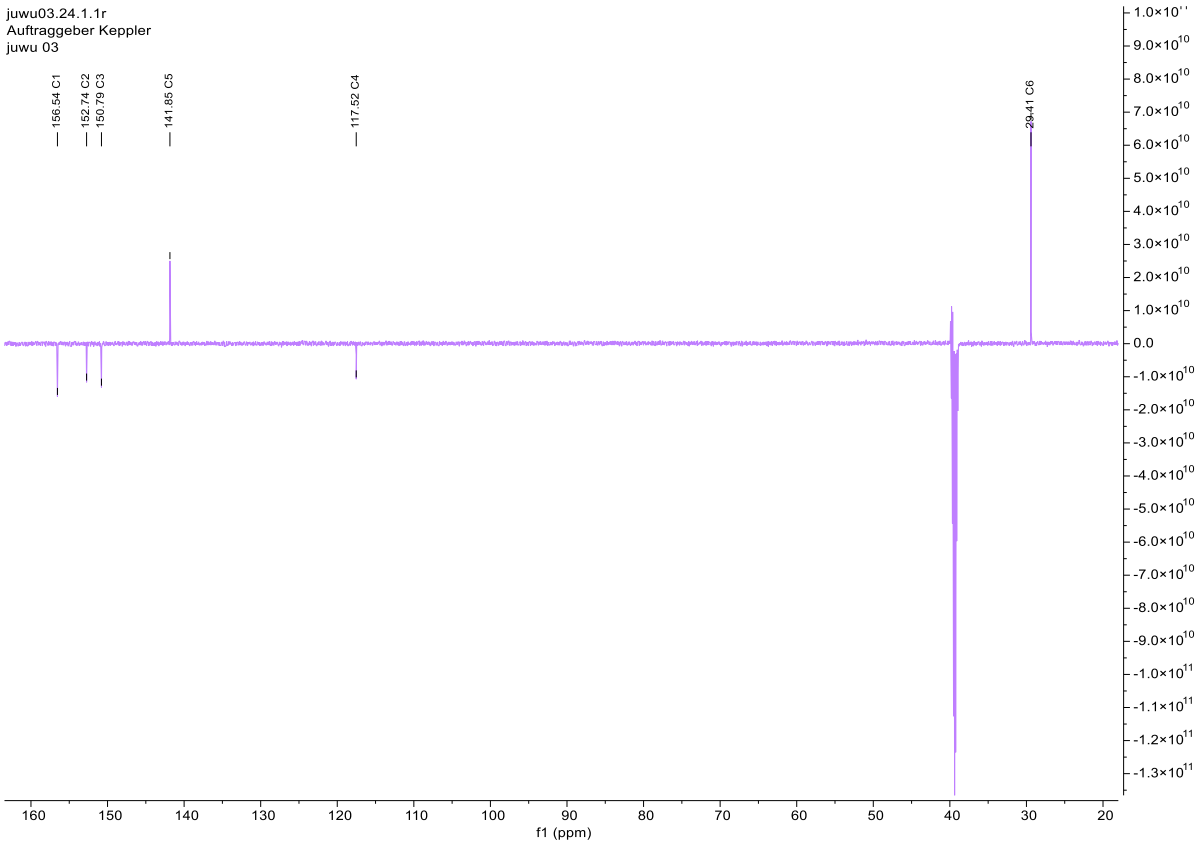


*Figure 36: $^{13}$C-NMR spectrum of compound **a** in DMSO d-6.*

Compound **1**

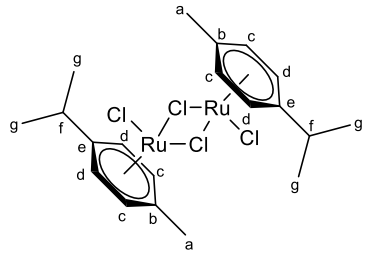


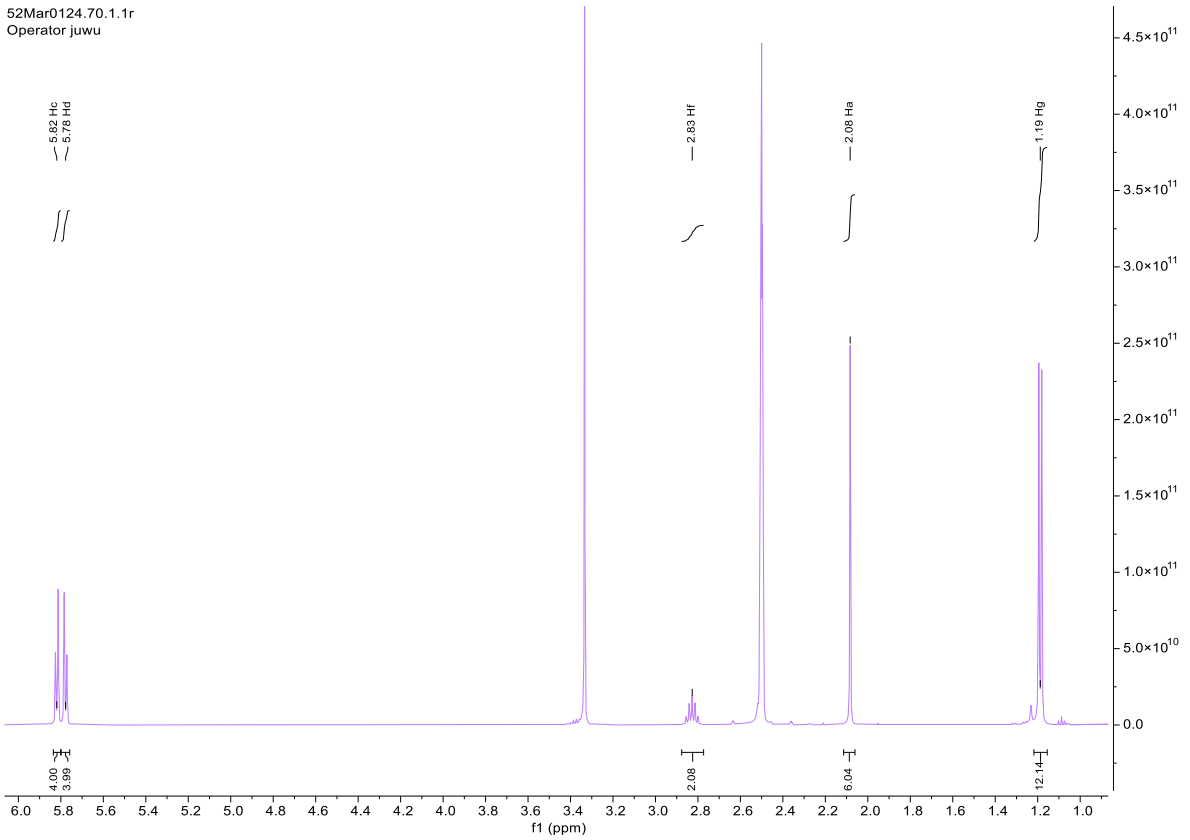


*Figure 37: [1]H-NMR spectrum of compound **1** in DMSO d-6.*

Compound **2a**

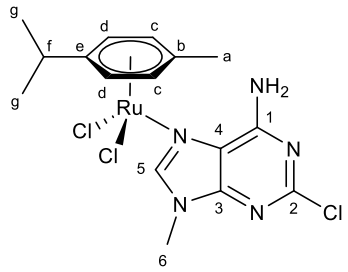


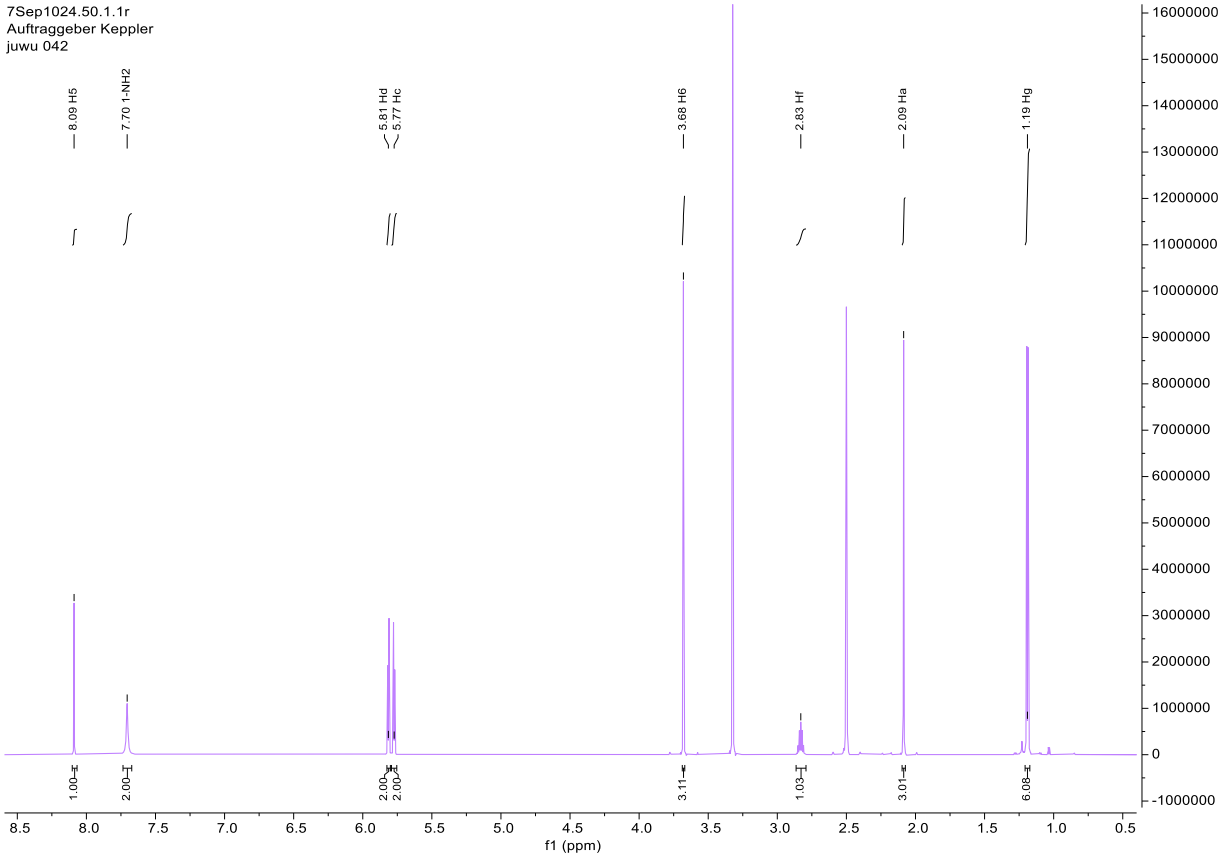


*Figure 38: [1]H-NMR spectrum of compound **2a** in DMSO d-6.*

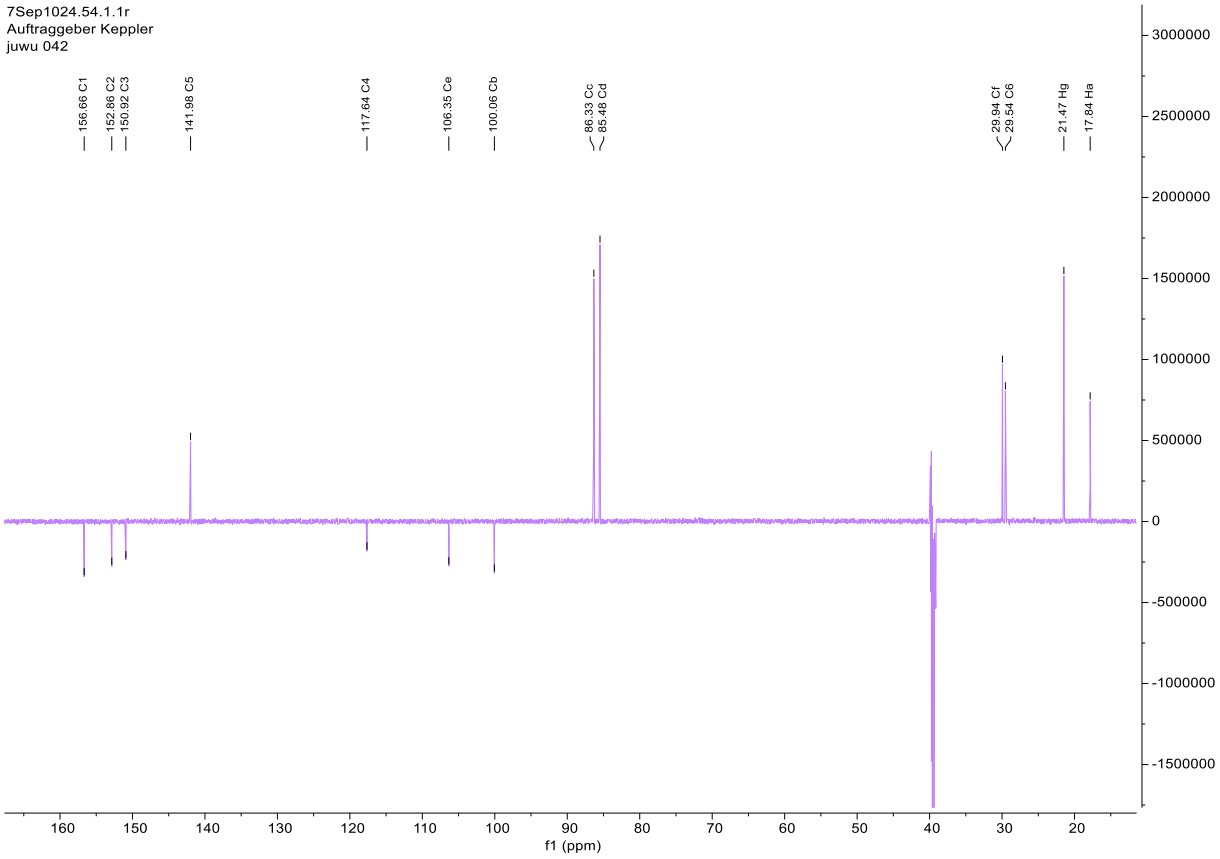


*Figure 39: $^{13}$C-NMR spectrum of compound **2a** in DMSO d-6.*

Compound **2b**

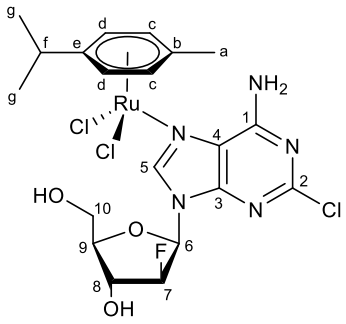


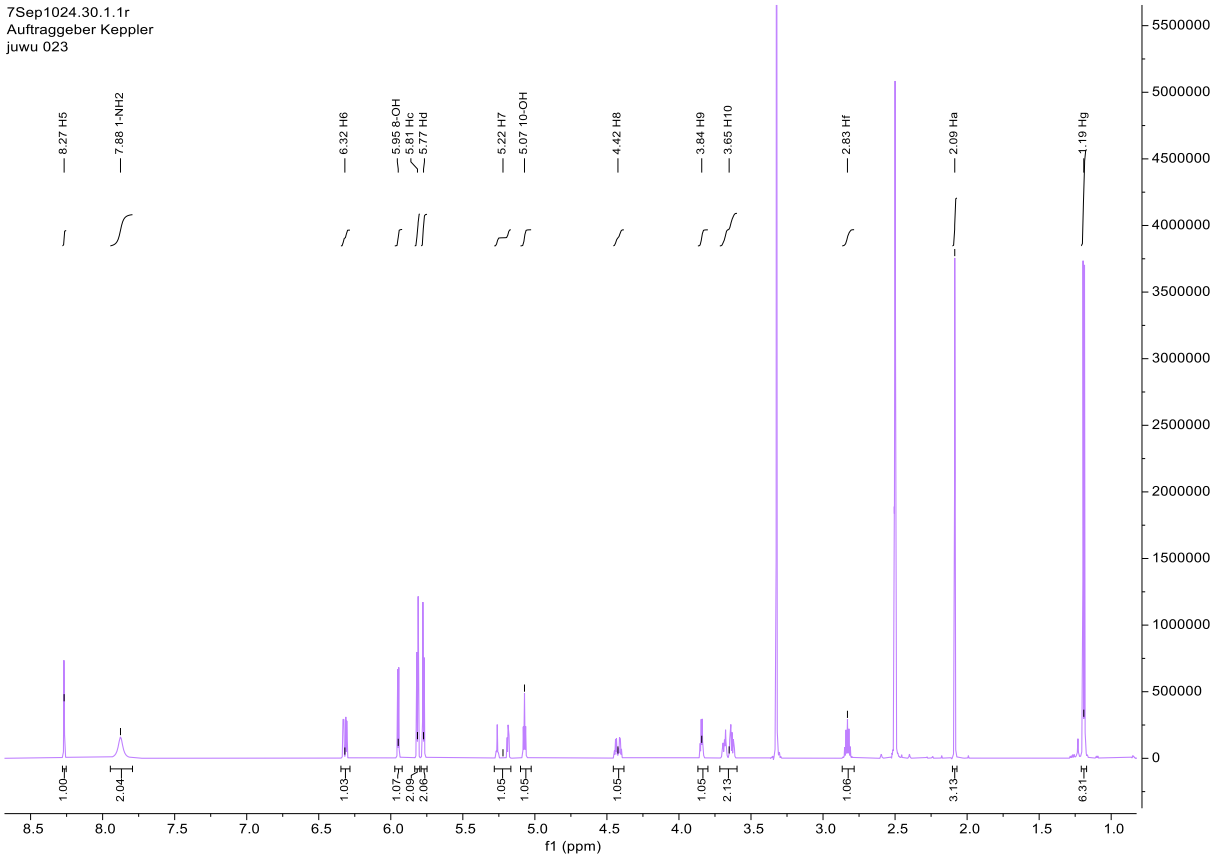


*Figure 40: [1]H-NMR spectrum of compound **2b** in DMSO d-6.*

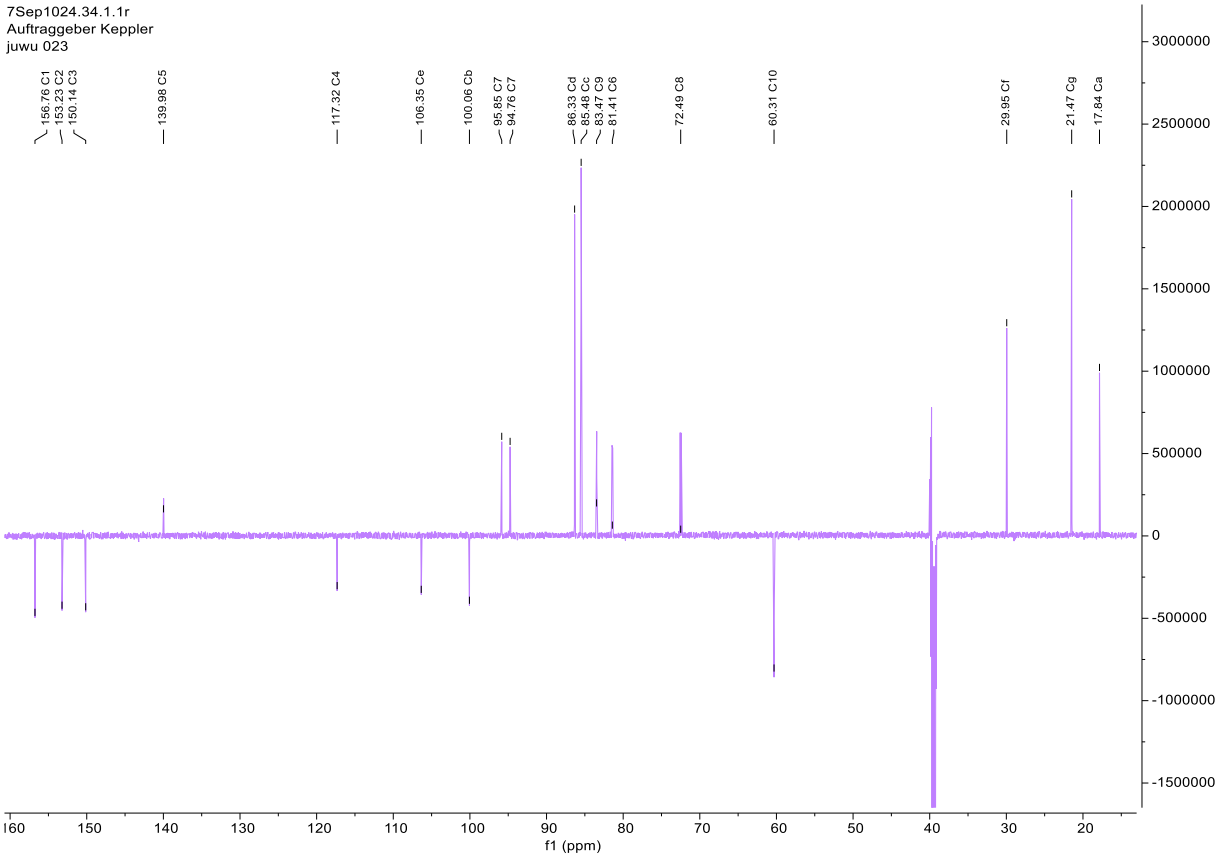


*Figure 41: $^{13}$C-NMR spectrum of compound **2b** in DMSO d-6.*

Compound **3a-l**

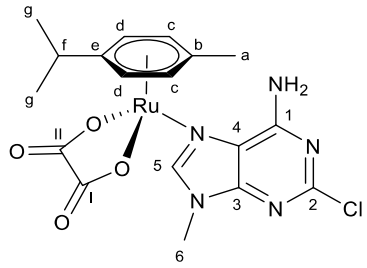


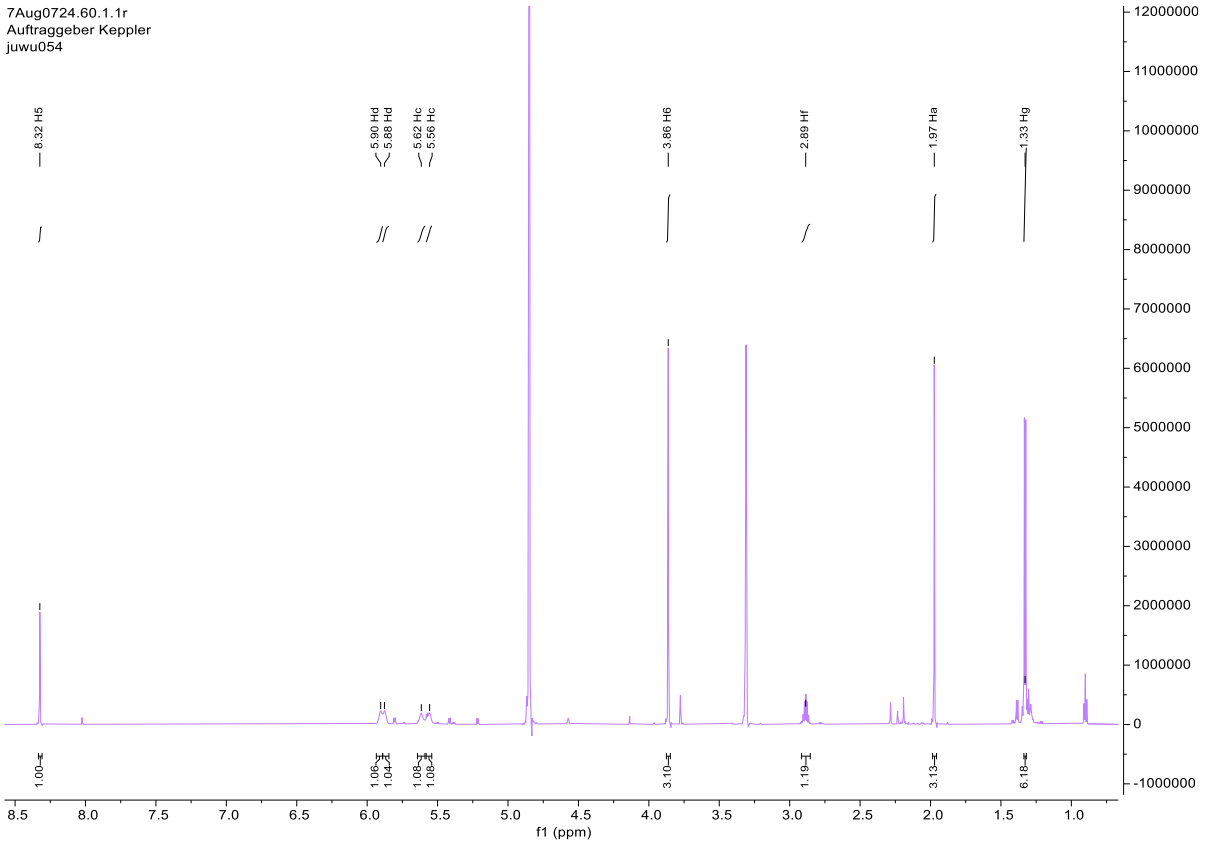


*Figure 42: [1]H-NMR spectrum of compound **3a-l** in MeOD.*

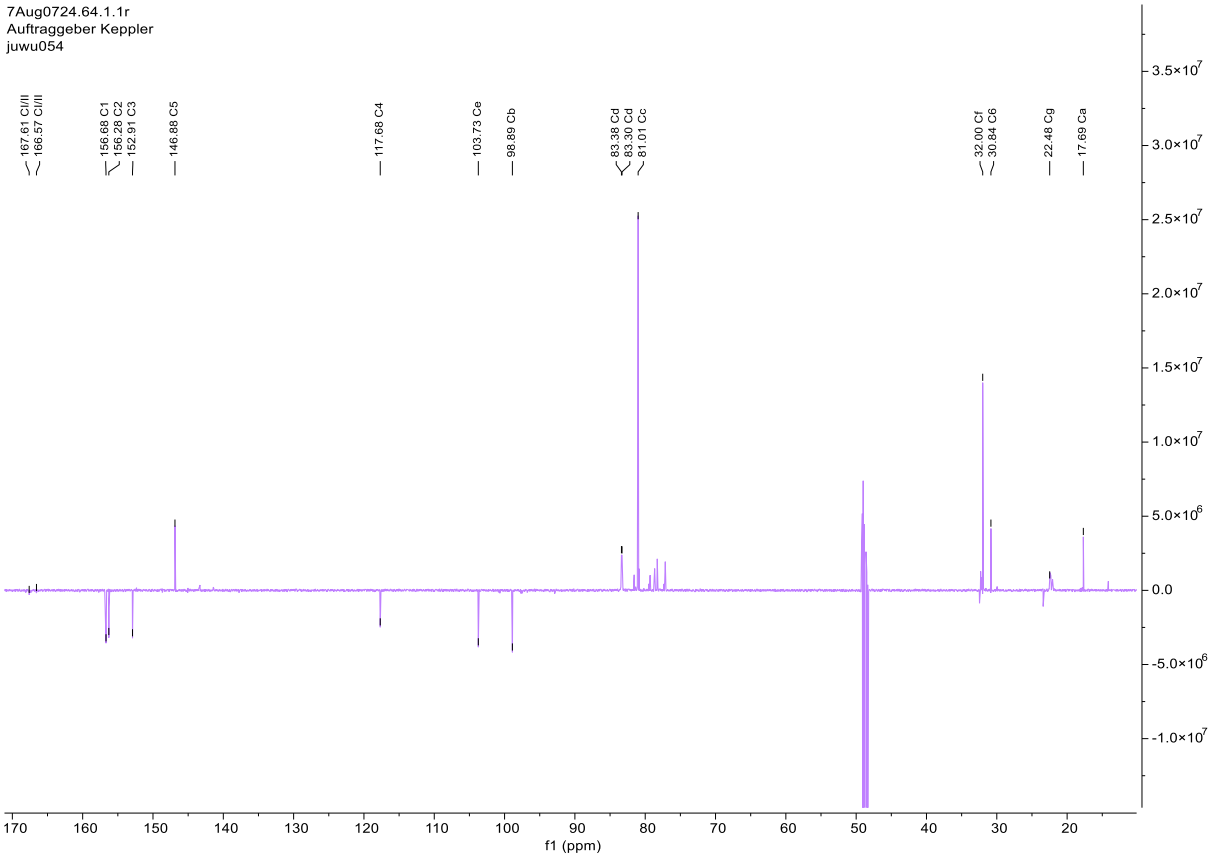


*Figure 43: $^{13}$C-NMR spectrum of compound **3a-l** in MeOD.*

Compound **3b-l**

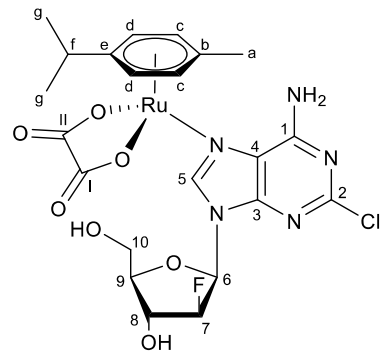


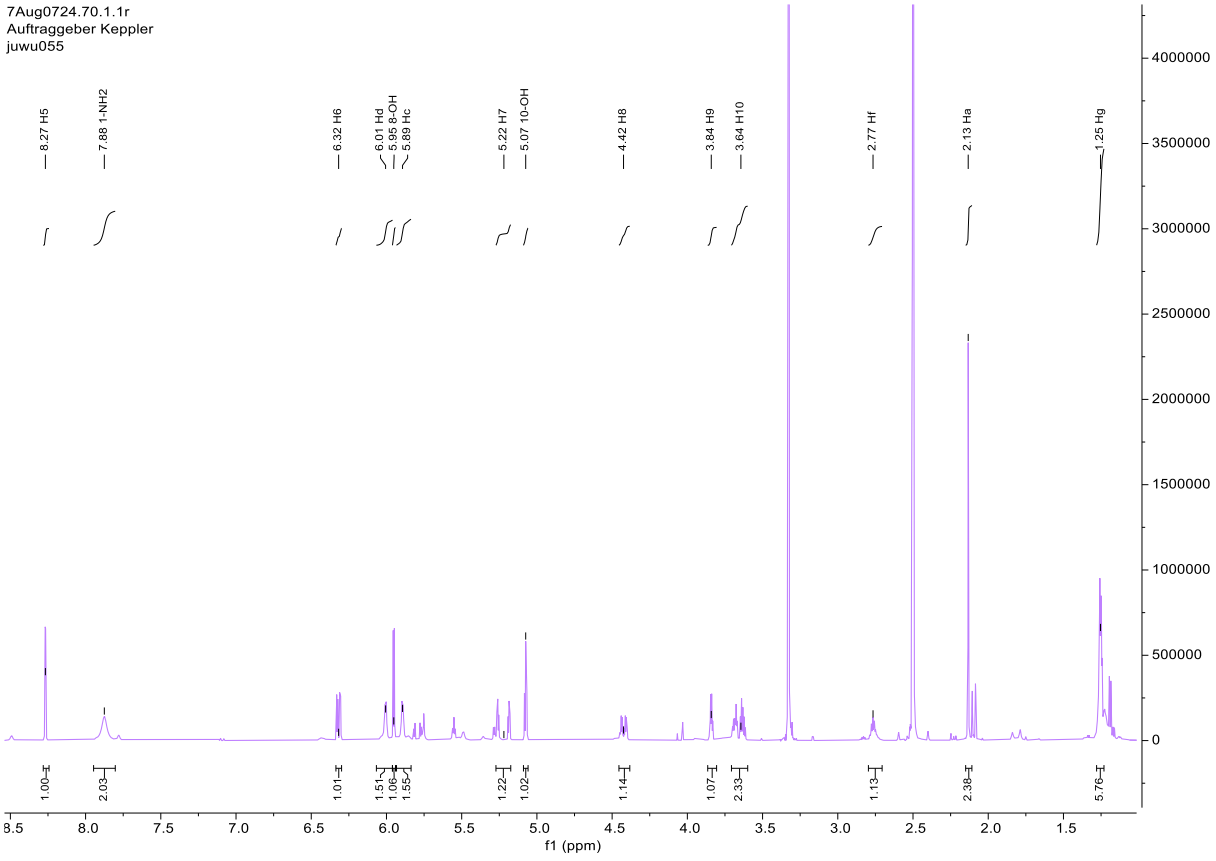


*Figure 44: [1]H-NMR spectrum of compound **3b-l** in DMSO d-6.*

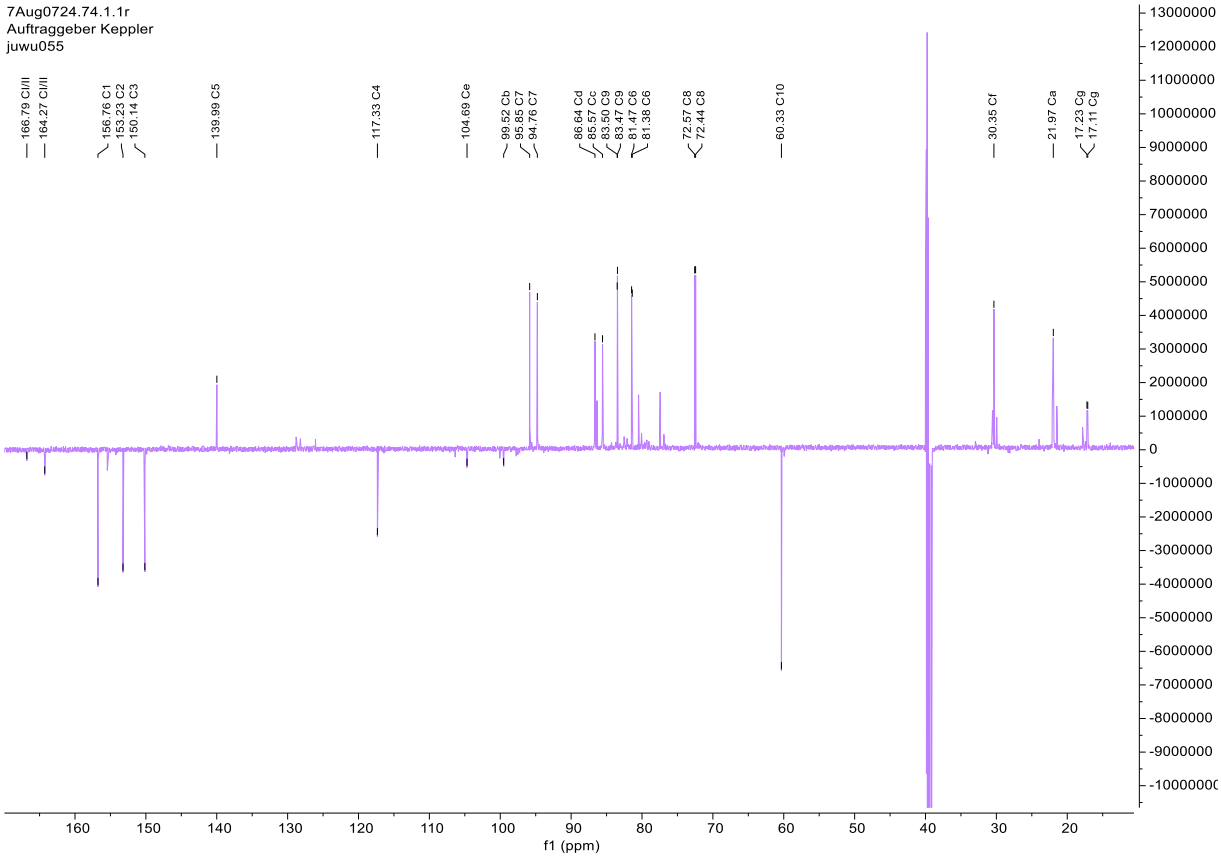


*Figure 45: $^{13}$C-NMR spectrum of compound **3b-l** in DMSO d-6.*

## 7.4 Mass Spectra

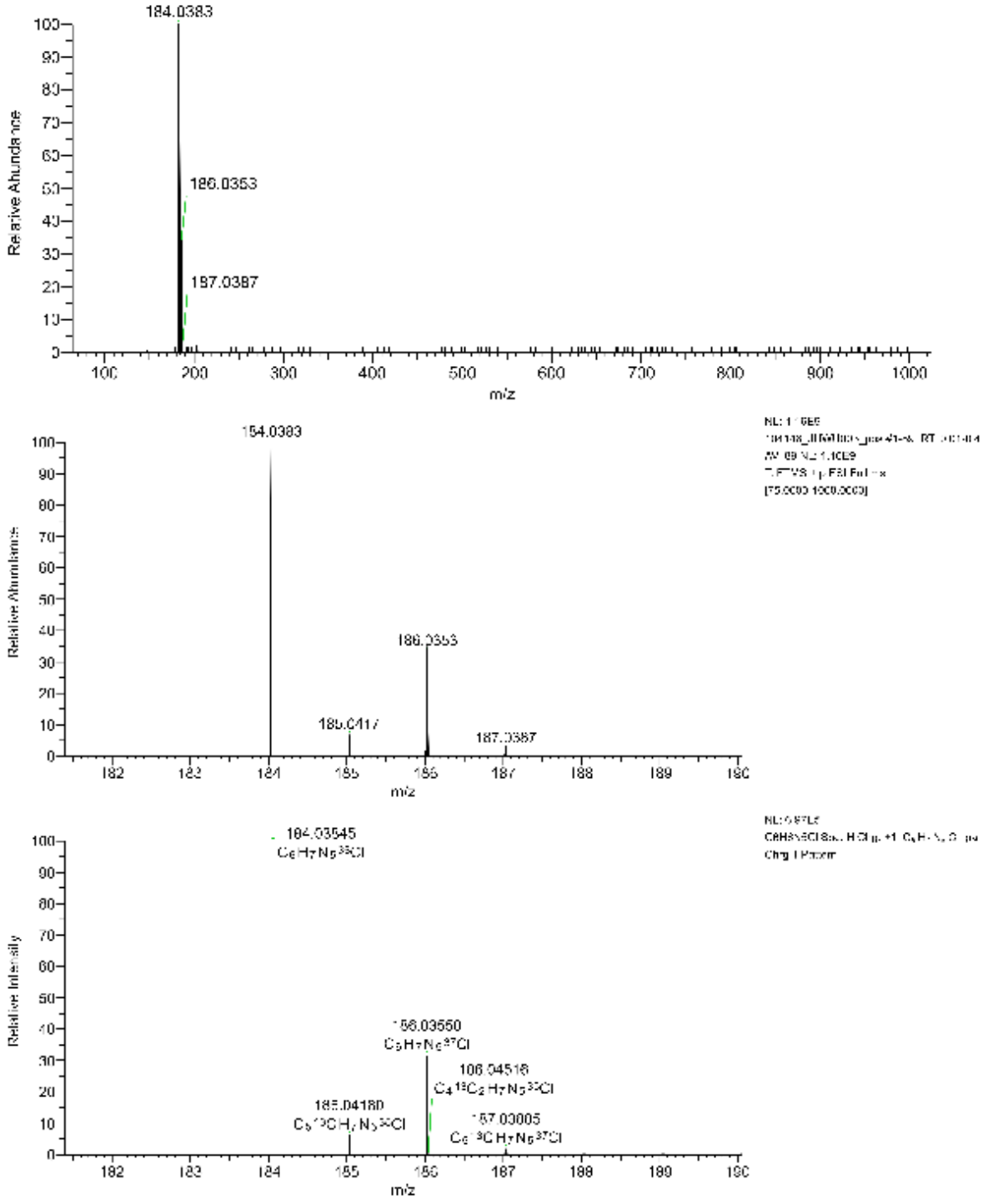


*Figure 46: HR mass spectrum of compound **a**.*

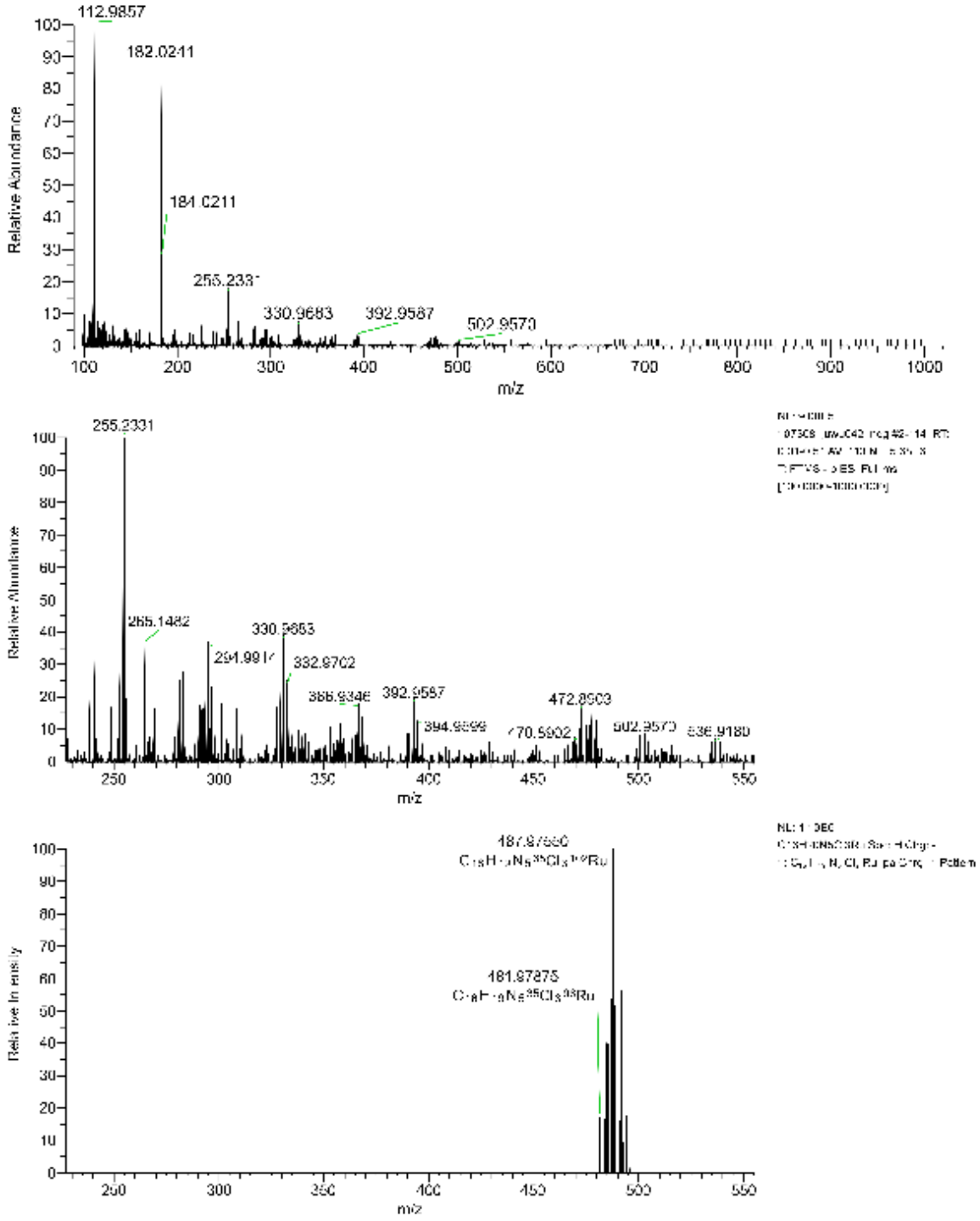


*Figure 47: HR mass spectrum of complex **2a**.*

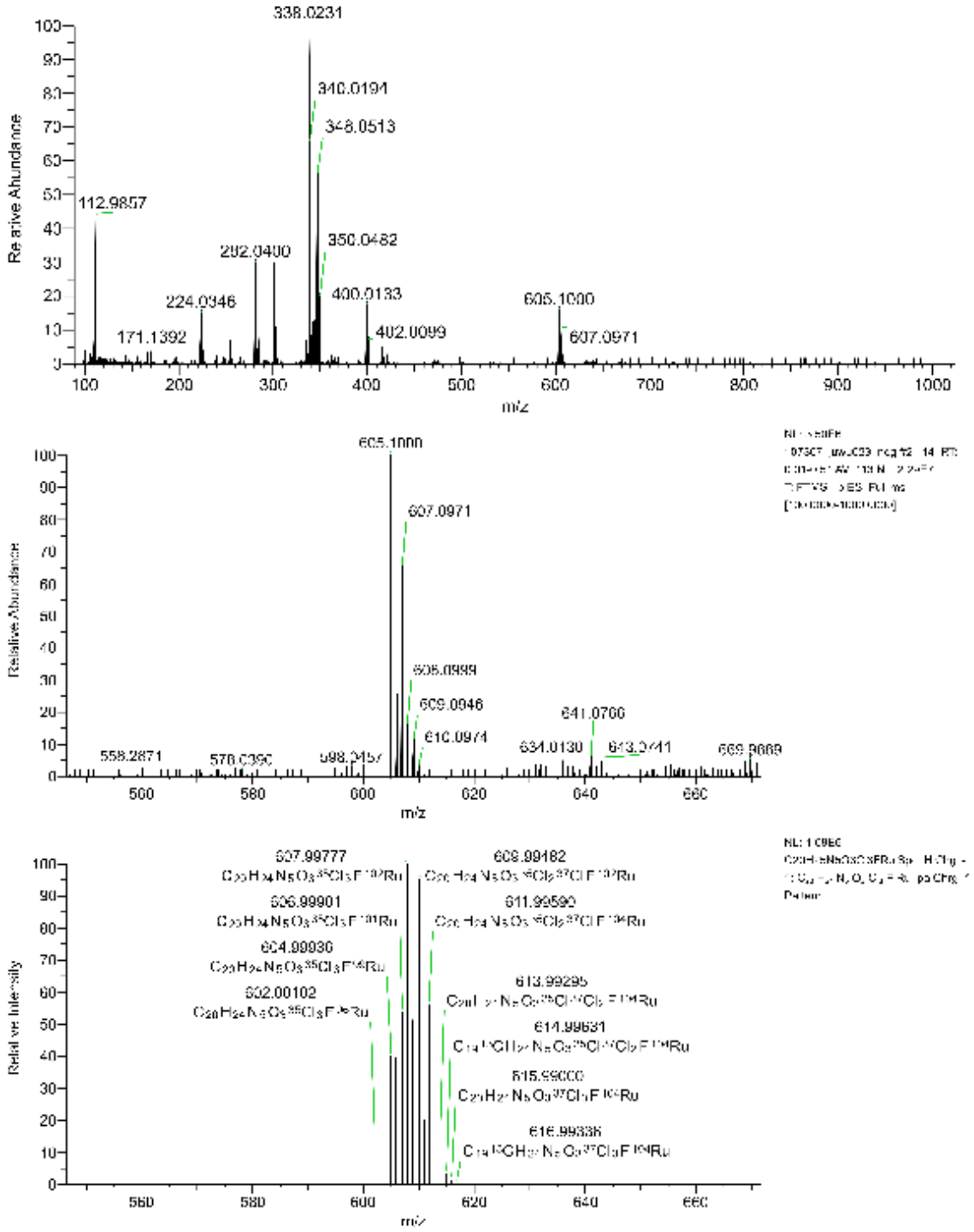


*Figure 48: HR mass spectrum of complex **2b**.*

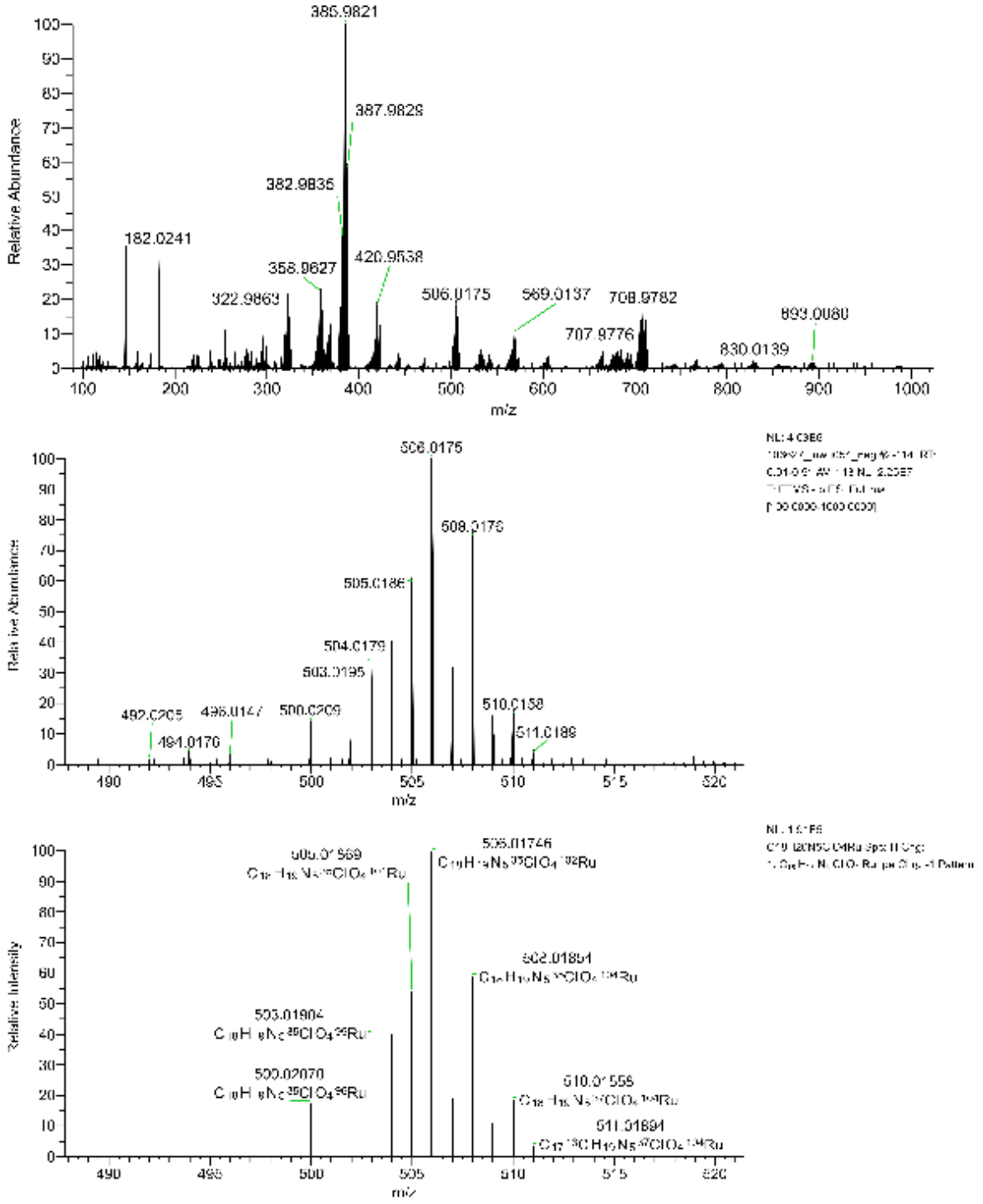


*Figure 49: HR mass spectrum of complex **3a-l**.*

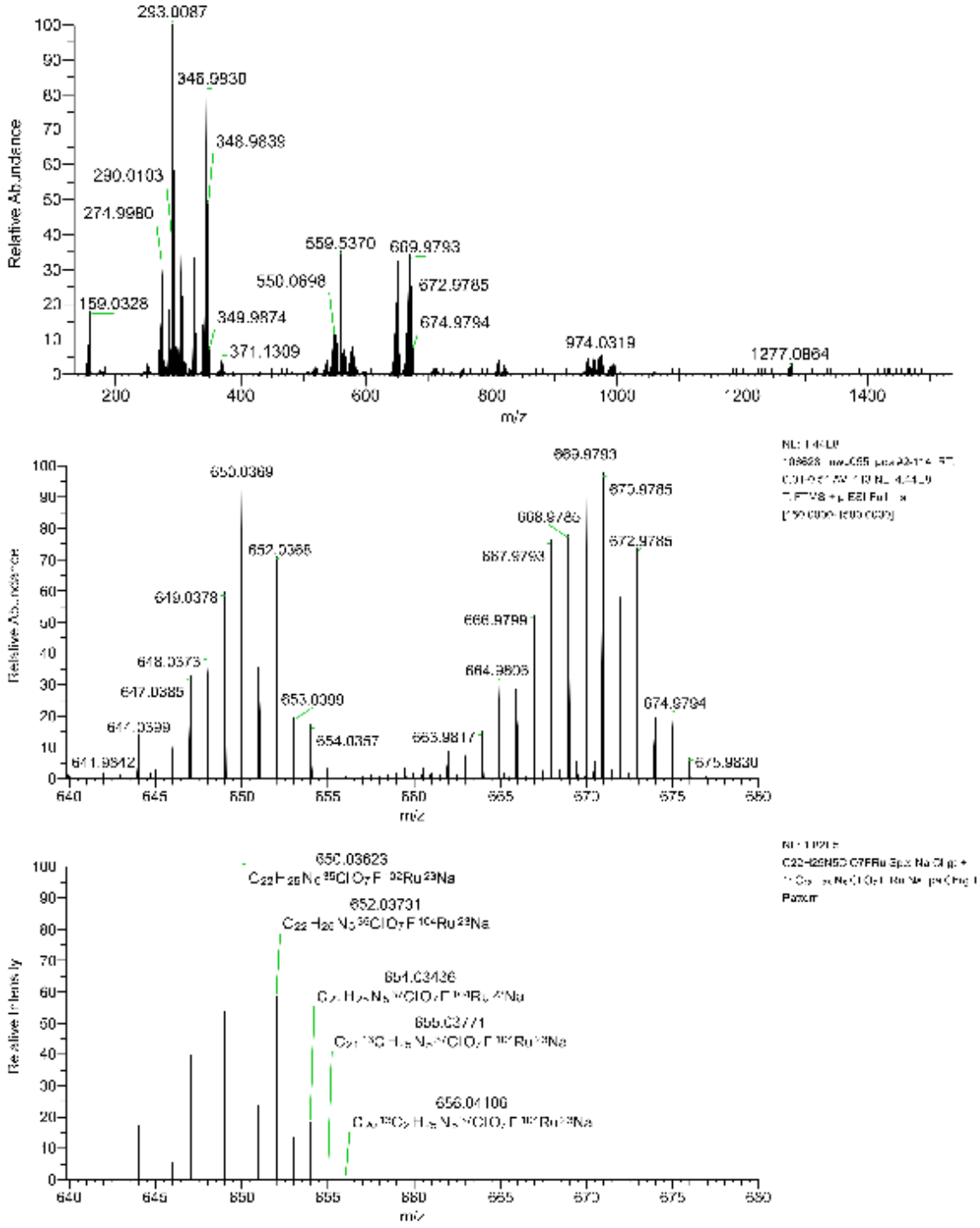


*Figure 50: HR mass spectrum of complex **3b-I**.*